A Study of Water and Carbonated Water Injection with Constant Pressure Boundaries

by

© Huan Yang

A Thesis submitted to the School of Graduate Studies in partial fulfillment of the requirements for the degree of

Master of Engineering

Faculty of Engineering and Applied Science

Memorial University of Newfoundland

May 2014

St. John's Newfoundland

Abstract

The Buckley-Leverett theory for one-dimensional constant fluid velocity is widely used in the oil and gas industry. However, given a changing fluid velocity with fixed pressure boundary conditions, limitations arise. This work is based on an existing extension of the Buckley-Leverett theory in a water-oil system with fixed pressure boundary conditions. This allows the Buckley-Leverett theory to be applied to situations of injecting water at a constant bottom-hole pressure and producing oil at a fixed bottom-hole pressure. Based on mass conservation, numerical simulation is performed in Matlab® using the Implicit Pressure Explicit Satuation (IMPES) method for two-phase flow. The numerical solution is compared to the recently developed analytical solution for different case studies. The comparison is also used to illustrate the effect of numerical dispersion and round-off errors. This extension of the Buckley-Leverett theory has significant consequences in its applicability to more realistic operating scenarios and computational savings through analytical solutions.

Carbonated water injection is studied numerically based on the validated water injection model. In carbonated water injection, CO_2 is dissolved in water phase before injection. After injection, the properties of reservoir fluids will change due to the partitioning of CO_2 between both the water and oil phases. Therefore, the reduction of oil viscosity and oil-water interfacial tension would be the main factors affecting the oil recovery. However, there is minimal research on carbonated water flooding combining both thermodynamics and reservoir simulation models. This research aims to study the effect

for oil recovery in carbonated water injection based on both physical and numerical perspectives.

Acknowledgements

I would like to take this opportunity to express my sincere appreciation to my supervisors, Dr. Lesley James and Dr. Thormod Johansen. Thank you for your outstanding technical guidance that inspires me to work on this thesis. Your patience takes me through every difficulty that I have encountered during my study. I am grateful for your support and encouragement that motivate me to accomplish this project.

I also want to thank Norah Hyndman. Thank you for helping with my writing.

Thanks also to my research colleagues: Hashem Nekouie, Jie Cao, Nan Zhang, Xiaolong Liu, Ali Souri Laki, Xiaoyan Tang, Mahsa Moayed, Eskandari Saeed. Thanks for their suggestions and help during my research. I really enjoyed the time that we were working together.

My thanks also go to my dear friend Weiyun Lin. Thanks to the friendship that makes me feel lucky and happy.

Last but not least, I would like to express my deeply thanks to my parents and my fiancé Yi Li. To my parents, I could not complete my study without all the sacrifice that you have made. Your selfless giving is my best treasure in my life. Thanks to my fiancé Yi Li. Because of his caring and concerning I always feel warm and secure. Thanks to my little cat Tiger, for his company in every working night.

Table of Contents

List of Tables

List of Figures

Nomenclature

A_c	Cross section area, m^2
$c^o_{co_2}, c^w_{co_2}$	CO_2 mass concentrations in oil, water phases
c	Compressibility
c_{pv}	Rock compressibility
E_t	Total sweep efficiency
E_a	Areal sweep efficiency
E_v	Vertical sweep efficiency
E_m	Microscope sweep efficiency
f_w	Fraction flow function
$\overline{F}$	Mass flux, $kg/(m^3 \cdot s)$
K	Formation permeability, m^2
K_o, K_w	Permeability of oil, water, m^2
k_{ro}, k_{rw}	Relative permeability of oil, water
$k^o_{co_2}, k^w_{co_2}$	Equilibrium coefficients of CO_2 mole fraction in oil, water phases
$\overline{k}^o_{co_2}, \overline{k}^w_{co_2}$	Equilibrium coefficients of CO_2 mass concentration in oil, water phases
L	Length, m
MW_o, MW_{co_2}	Molecular weight of oil, gas

m_{co_2}	Molality of CO_2 (mol/kg)
p	Pressure, Pa
p_c	Capillary pressure, Pa
p_b	Bubble point pressure, Pa
Q	Volumetric flow rate, m^3/s
$\widetilde{Q}$	Mass flow rate, kg/s
$\tilde{q}$	Mass flow rate per unit volume, $kg/(m^3 \cdot s)$
R	Universal gas constant
S	Saturation
$\overline{S}$	Average saturation
S_{or}	Residual oil saturation
S_{wc}	Irreducible water saturation
S_{wf}	Front water saturation
t_{BT}	Time of breakthrough, s
t	Time, s
T	Temperature, ℃
u_t	Total fluid velocity, m/s
u_w, u_o	Velocity of water, oil, m/s
V	Volume, m^3
V_b	Bulk volume, m^3

v_f	Front velocity, m/s
$x^o_{co_2}, x^w_{co_2}$	CO_2 mole fraction in oil, water phases
y_{co_2}	CO_2 mole fraction in the gas phase
α_{co_2}	Activity coefficient
β_o, β_w	Formation volume factor of oil, water
γ	Partition coefficient
γ_o	Oil specific gravity
φ_{co_2}	CO_2 fugacity coefficient
ρ_{oi}	Initial oil density, kg/m^3
ϕ	Porosity
λ	Mobility
ω	Mass concentration in bulk volume, kg/m^3
μ_o, μ_w	Viscosity of oil, water phases, Pa·s
$\mu^{l(0)}_{co_2}$, $\mu^{v(0)}_{co_2}$	Standard liquid and gas chemical potential in ideal conditions, J/kg
ρ	Density, kg/m^3
ρ^*_o, ρ^*_w	Density ratio between stock tank condition and reservoir condition
σ_{ow}	Water-oil interfacial tension, N/m

Abbreviation

EOR	Enhance Oil Recovery
IFT	Interfacial Tension
IMPES	Implicit Pressure, Explicit Saturation
WI	Water Injection
CWI	Carbonated Water Injection
CFL	Friedrichs-Lewy Condition
MMP	Minimal Miscible Pressure
WAG	Water Alternating with Gas
NGL	Natural Gas Liquid
GA	Genetic Algorithm
RF	Recovery Factor

Chapter 1 Introduction

1.1 The Overview of Global Oil Production and Consumption

Energy demand has grown significantly worldwide since the late 1970s and early 1980s. Hydrocarbon fluids are considered as one of the major sources of energy. As a fundamental resource, oil has been providing heat, light and power as well as non-energy products like chemicals and lubricants (Roorda, 1979). The demand or consumption of oil is affected by many aspects such as population, economic activity, government policies, international oil prices and technological advances etc. (Jordan, 1998). East Asia has been rapidly expanding oil markets due to the population and economic development in the 1990s (Davies, 1994). However, a rapid decline of oil production has been observed from many oil fields worldwide with many more fields transitioning into decline each year. The total world oil production stopped expanding in approximately mid-2004 (Höök *et al*., 2009). According to Andrew Gould, CEO of Schlumberger, although an accurate average decline rate is hard to estimate, an overall figure of 8% is not an unreasonable assumption (Schlumberger, 2005). In order to meet the growing oil demand, exploiting new oil fields continues. However, it is difficult to justify the development of new oil reservoirs that are generally located in remote, isolated or harsh off-shore areas (Stahl *et al*., 1987). Efficient recovery from already discovered oil fields becomes a matter of improved and enhanced oil recovery economics factoring in capital costs of directional and multilateral wells, advanced wells, and including operating costs

for different injection strategies such as polymer, CO_2, water-alternating-gas (WAG), etc. along with the need for an additional separation and treatment capacities.

1.2 The Background of Oil Recovery

Typically, only a fraction of the total resources in place can be recovered from a reservoir. The fraction of oil ultimately produced from a given field depends on the geology of the field, the recovery mechanisms, and economic conditions (Lake, 1989).

1.2.1 Primary Oil Recovery

During the primary recovery stage, initial production flow by the pressure difference between the reservoir and the well flowing pressure. Operating with a constant reservoir and well flowing pressure, albeit for a finite period of time, can be mathematically considered as constant pressure boundary conditions. This will be discussed in Section 3.5. Artificial lift can be used if the pressure is not sufficient (Tzimas *et al*., 2005). However, due to the pressure depletion during production the reservoir oil eventually ceases to flow leaving considerable oil trapped in the pores of reservoir rock (Lake, 1989).

1.2.2 Secondary Oil Recovery

Secondary oil recovery is when gas or water is injected into the formation in order to maintain the reservoir pressure and forcing oil to flow towards production wells. Although a great amount of oil can be produced after applying a secondary oil recovery

strategy, in most reservoirs, 50-80% of the oil remains in the reservoir after the waterflood since water is immiscible with oil (Dullien, 1991).

1.2.3 Tertiary Oil Recovery

The purpose of tertiary or enhanced oil recovery (EOR) is to increase the extraction by changing the oil mobility. Examples include: gas injection, carbon dioxide flooding, polymer injection, hot water or steam injection, in-situ combustion, etc. The goal of thermal methods is to achieve a more mobile oil phase thermally by reducing the oil viscosity. In-situ combustion intends to crack the heavy oil molecules into a light (mobile) fractions and a heavy fuel fraction by combusting the oil in-situ with injected air. During the process the combustion front propagates through the reservoir. The carbon-rich product is formed by the thermal cracking and distillation of the residual oil near the combustion front which sustains the in-situ combustion (Mahinpey *et al*., 2007).

Immiscible solvent injection is another EOR process where chemicals can be injected into the reservoir in order to reduce oil viscosity and interfacial tension (IFT) between the water and oil. Natural gas, CO_2, and air can be injected immiscibly depending on the reservoir conditions and oil and gas compositions (Tunio *et al*., 2011). Polymer flooding is the most common way in immiscible injection with the goal of increasing the viscosity of the water phase, decreasing the mobility ratio and therefore increasing the sweep efficiency (Needham and Doe, 1987).

Gas injection or miscible tending flooding is presently the most commonly used approach in EOR. The miscible displacement process is adopted to maintain the reservoir

pressure and improve oil displacement by lowering IFT between gas and oil. Miscibility can develop between injection gas and oil phases depending on their injection composition, pressure and temperature (Rao and Lee, 2003). Gases used in the miscible process include: methane under high pressures, natural gas enriched with intermediate hydrocarbon, nitrogen under high pressures, and carbon dioxide (CO_2) under suitable temperature and pressure conditions etc. The most commonly used fluid during miscible flooding is CO_2 due to the lower cost, available supply and ability to achieve miscibility at lower pressure.

1.2.4 Current and Invested CO_2 EOR Project

According to a summary document recently released by The U.S. Department of Energy there are hundred CO_2-driven enhanced oil recovery projects operational in the United States (Dooley *et al*., 2009). The CO_2 used in the majority of existing EOR projects is captured from natural geologic deposits. However, in recent years a number of large industrial sources have also contributed to the use of CO_2 in EOR (Peter, 2010). The successful application of CO_2 in EOR over the last 35 years suggests that over the next ten years the incremental oil produced by CO_2 injection and the number of CO_2 flood projects will grow steadily (Melzer and Midland, 2012). Figure 1.1 shows the number of projects of CO_2 in EOR from 1984 to 2010. As indicated in the figure, the number of CO_2 related projects in EOR has grown from 1986 to 2010.

CO_2 is a widely used injection agent, in either free form or as a solvent for both secondary and tertiary oil recovery processes. Even under immiscible flood conditions oil

recovery is increased by changing the physical properties of the oil phase. Poor sweep efficiency has been reported (Patel *et al*., 1987) due to the high mobility of gas and gravity driven gas sometimes override leading to premature CO_2 breakthrough. The impact of poor sweep significantly reduces the contact between the CO_2 and oil. Carbonated water injection in where CO_2 is dissolved in water prior to injection may help alleviate the low sweep efficiency during CO_2 injection, as the CO_2 partitions to the oil phase upon water-oil contact. The physical properties of oil phase are changed by primarily altering the oil phase composition as a result of mixing with CO_2. Carbonated Water Injection (CWI) has three main advantages: 1) the CO_2 dissolved in the oil phase changes the oil viscosity and hence the mobility ratio; 2) experimentally the interfacial tension (IFT) between the water and oil phases is reduced (Mungan, 1964) resulting in an improved overall performance of CWI compared to water injection (Dong *et al*., 2011), and 3) significant swelling of oil was observed during CWI due to CO_2 dissolution in the oil phase. The disconnected oil ganglia left behind after conventional water flooding may reconnect as oil swells. The trapped oil then become remobilized and recovered due to the reconnection of the oil (Mungan, 1981). Carbon dioxide solvent flooding processes were initially investigated in laboratory flooding experiments where additional oil was recovered by the carbon dioxide solution drive (Holm, 1961). According to the results of experimental research (Siregar *et al*., 1999), an optimum oil recovery can be achieved by maximizing the CO_2 concentration in the water phase. A calculation method has been developed for CWI (Noel, 1964). The solution revealed the crucial effect of viscosity reduction and oil swelling using CWI. Compared to water injection (WI), the

experimental results showed a better oil recovery in both cases through the two different mechanisms discussed above (Sohrabi *et al*., 2009a).

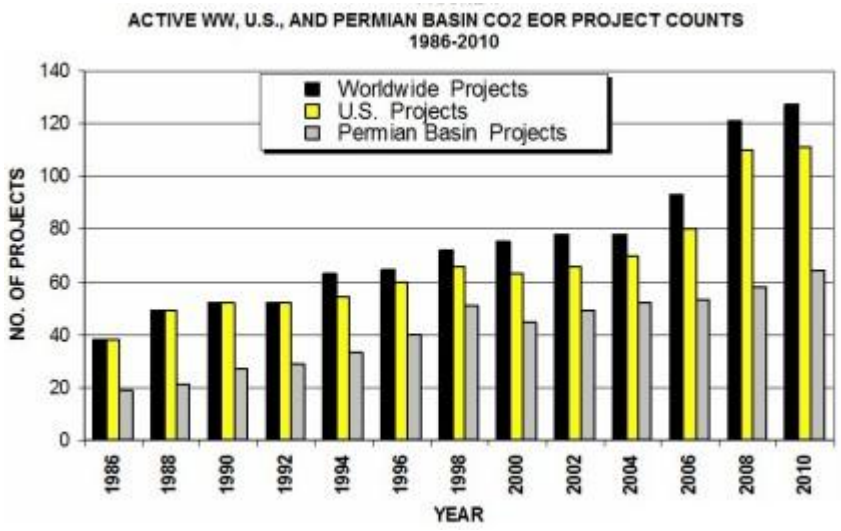

Figure 1.1 Number of CO_2 EOR Projects (Melzer and Midland, 2012)

1.3 Scope of Thesis

The various CO_2 EOR processes are reviewed in chapter 2. Both the secondary and tertiary (EOR) oil recovery processes have been studied regarding the fluid behavior underground and the efficiency of oil recovery.

As the most commonly used gas in EOR, CO_2 has been injected in either free form or as a solvent into oil reservoirs. In order to evaluate the performance of carbonated water injection (CWI) numerically, the scope of this thesis starts with a simple water injection process. In Chapter 3 the mathematical model of horizontal two-component two-phase

water flooding is formulated and discretized for constant pressure boundaries. This is the first study where the model is developed under constant pressure boundary conditions reflecting the more realistic operating scenario.

As the fundamental study for a horizontal three-component two-phase CWI, this one-dimensional numerical simulation for two-component two-phase WI is validated by the comparison of numerical solution with analytical solution. The numerical errors have been minimized.

As a third component, CO_2 is added to the simple water injection in Chapter 4. By combining both mathematical models and thermodynamics the performance of CWI is evaluated numerically in this chapter. Since WI is validated in Chapter 3 the CWI model here is also partly validated as mathematically it is a reasonably modest extension of validated WI model. The goal of CWI study is to:

1. Study the effects of oil viscosity and interfacial tension reduction on CWI.
2. Evaluate the performance of CWI by comparing it with WI.

The conclusions and further suggestions for a deeper study are given in Chapter 5. Figure 1.2 shows a summarized concept map regarding this thesis.

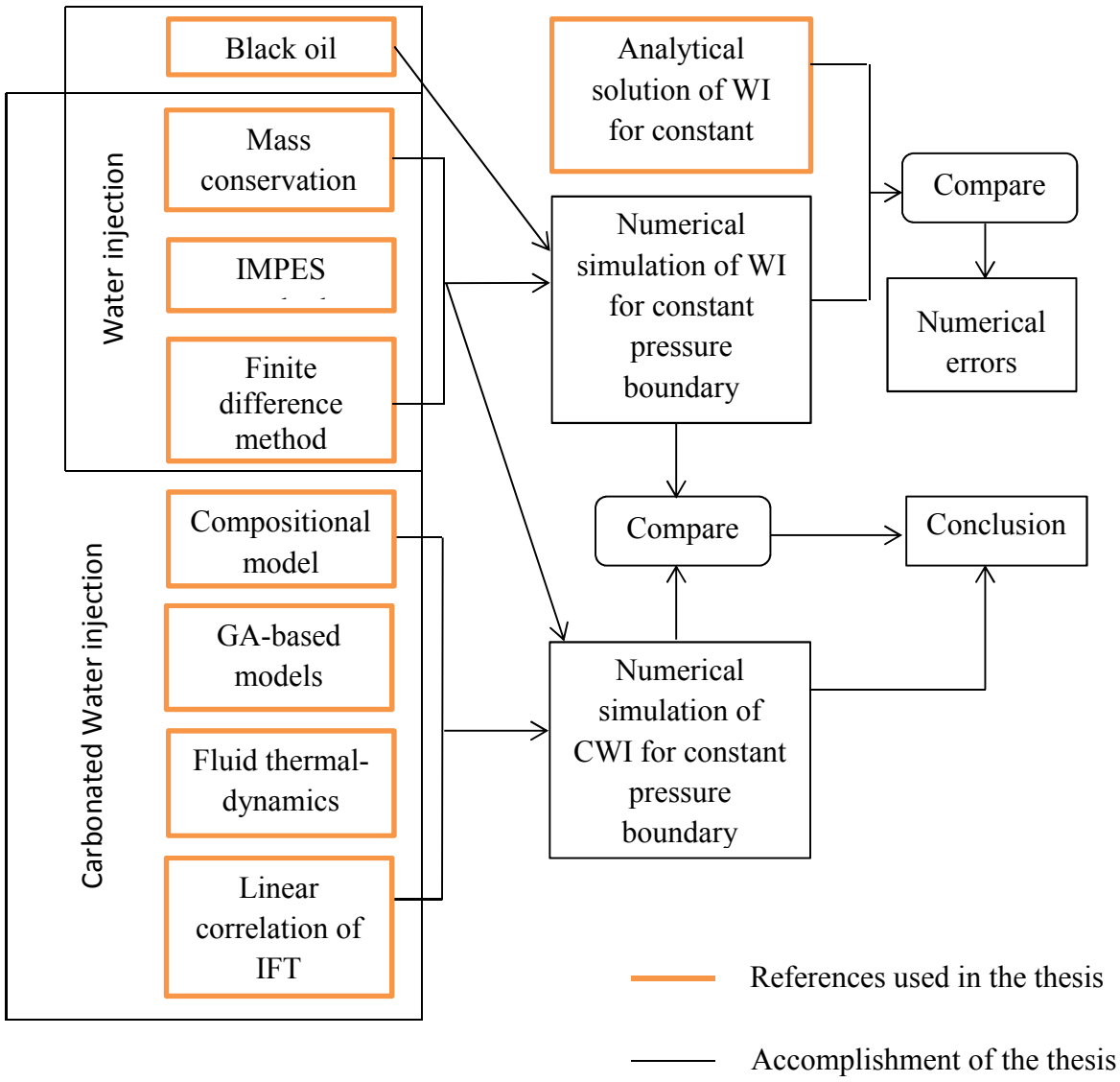

Figure 1.2 Summarized Concept Map of Thesis

Chapter 2 Literature Review of CO_2 Oil Recovery Process

2.1 Review of Buckley-Leverett Theory

The fractional flow theory, as developed by Buckley and Leverett (1942) is reviewed here both in its original form for constant flow rate and its extended form for constant pressure boundaries (Johansen and James, 2012).

In this study the displacement is only two components — oil and water, with negligible capillary pressure and incompressible fluids. The fractional flow (f_w) function can be written as (Buckley and Leverett, 1942):

$$f_w = \frac{u_w}{u_t} = \frac{1}{1 + \frac{k_{ro}(S_w)}{\mu_o}\frac{\mu_w}{k_{rw}(S_w)}} \quad . \tag{2.1}$$

As shown in equation (2.1), since the fluids are incompressible and therefore the viscosities are constant, it is clear that f_w is a unique function of water saturation S_w which can be expressed as $f_w(S_w)$.

The continuous equations for water and oil can be written as:

$$\phi\frac{\partial S_w}{\partial t} + \frac{\partial u_w}{\partial x} = 0\,, \tag{2.2}$$

$$\phi\frac{\partial S_o}{\partial t} + \frac{\partial u_o}{\partial x} = 0\,. \tag{2.3}$$

The summation of water and oil saturation equals to one, therefore, by adding equation (2.2) and equation (2.3) the expression of total fluid velocity is:

$$\frac{\partial}{\partial x}(u_x + u_o) = \frac{\partial u_t}{\partial x} = 0 . \tag{2.4}$$

The equation (2.2) then can be written as:

$$\phi \frac{\partial S_w}{\partial t} + \frac{\partial u_w}{\partial x} = \phi \frac{\partial S_w}{\partial t} + \frac{\partial \left(f_w \cdot u_t \right)}{\partial x} = 0 . \tag{2.5}$$

Due to the constant total flow rate along distance which is shown in equation (2.4), equation (2.5) can be rewritten as:

$$\phi \frac{\partial S_w}{\partial t} + u_t \frac{\partial \left[f_w(S_w) \right]}{\partial x} = 0 . \tag{2.6}$$

The fractional flow function, f_w depends only on S_w, therefore equation (2.6) can be also expressed by:

$$-\frac{df_w}{dS_w}\frac{\partial S_w}{\partial x} = \frac{\phi}{u_t}\frac{\partial S_w}{\partial t} . \tag{2.7}$$

The above equation (2.7) is known as the Buckley-Leverett equation.

The total fluid velocity here is treated as constant for any position at any time.

The front velocity (v_f) is given by:

$$v_f = \frac{u_t}{\phi}\frac{df_w}{dS_w}\bigg|_{S_w = S_{wf}} . \tag{2.8}$$

Clearly, this is directly related to the slope of tangent to the fractional flow curve. In a water injection process with a continuous injection the water front travels along the reservoir formation from the injecting point to the outlet boundary and the oil phase is partly displaced by the moving water. In order to obtain the uniqueness in water

saturation values at any location with propagation of time, a shock front which is also called water front is introduced to indicate an abrupt changing from front water saturation to the connate water saturation shown by Figure 2.1.

Figure 2.2 shows a typical fractional flow curve. As shown from the figure the fractional flow curve starts from zero at irreducible water saturation and ends at one with the maximum water saturation (1-S_{or}) which is 70% in this thesis.

The determination of the front velocity must follow both the entropy condition and velocity constraint. Entropy conditions state that the shock velocity ($\left.\frac{df_w}{dS_w}\right|_{S_w=S_{wf}}$) has to be larger than (or equal to) the downstream wave velocity ($\frac{df_w}{dS_w}$) but smaller than (or equal to) the upstream wave velocity ($\frac{df_w}{dS_w}$). Based on the velocity constraint the wave velocity should decrease monotonically from downstream to upstream. According to these conditions the shock velocity can be determined as shown in Figure 2.2.

In Figure 2.2 the straight line is the tangent of fractional flow curve and the water saturation at the tangent point is corresponding to the front saturation shown by Figure 2.1. Since, the term $\left.\frac{df_w}{dS_w}\right|_{S_w=S_{wf}}$ in equation (2.8) is the slope of the tangent to the curve at the front saturation, and the constant total fluid velocity is assumed known, the front velocity can be calculated analytically as depicted in Figure 2.2 for a constant total fluid velocity. The average water saturation in the reservoir ($\overline{S_w}$) can be obtained graphically by extending the tangent from the point of f_w (S_{wf}) to the upper limit where the y-value is

equal to one. The average water saturation then can be found by reading the value on the x-axis at the intersection point (Welge, 1952) shown in Figure 2.2.

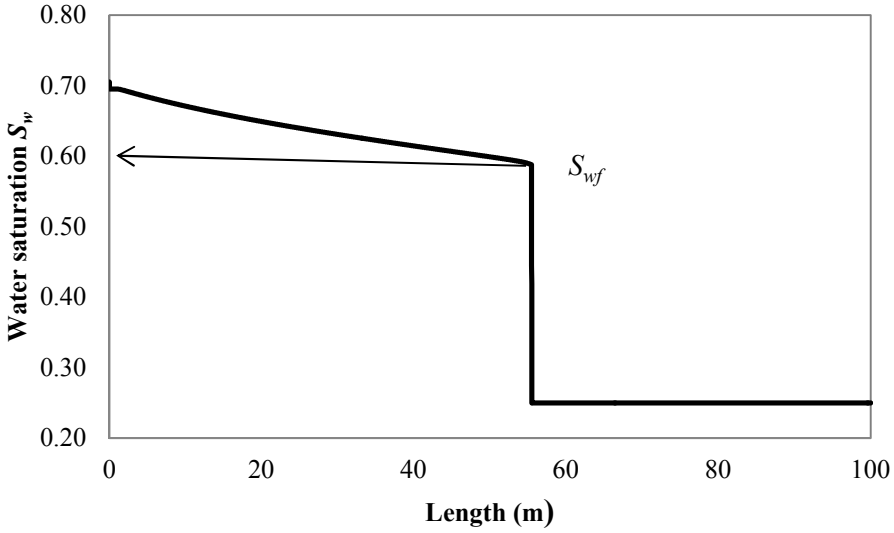

Figure 2.1 The Typical Water Saturation Profile

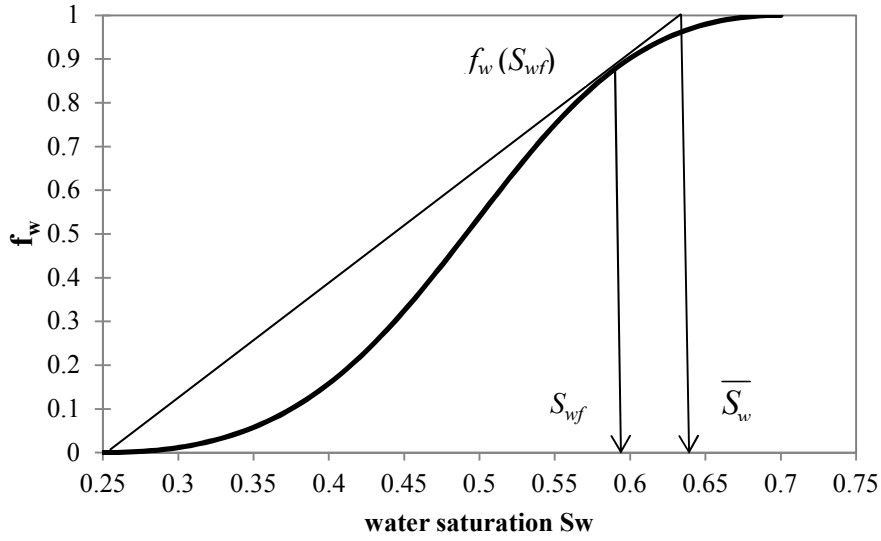

Figure 2.2 Fraction Flow Curve

2.1.1 Limitation of The Buckley-Leverett theory for a Constant Flow Rate

The previous discussion of the Buckley-Leverett theory is for a one-dimensional two-phase displacement with a constant total fluid velocity. According to equation (2.8), the constant total flow rate and the unique shape of the fractional flow curve result in the water front moving with a constant velocity. Hence the water breakthrough time can be easily determined by dividing the total length of the formation by the front velocity. However, in the fixed pressure boundary conditions case, Buckley-Leverett theory (under a constant flow rate) is no longer applicable (Johansen and James, 2012), since the flow rate is not constant (see Appendix B).

Due to this limitation, without an analytical solution the valuable information of water injection under the fixed pressure boundary conditions can only be generated by numerical simulation. However, a numerical simulation consumes a lot of computation time and creates numerical errors that may lead to a misunderstanding of the reservoir or result in a physically unrealistic situation. Moreover, in industry water is more likely to be injected at a constant pressure to displace oil at a fixed bottom-hole pressure. Therefore, for the sake of accuracy and time efficiency, an analytical solution is desirable.

2.1.2 Extension of the Buckley-Leverett Theory with Constant Pressure Boundaries

An analytical solution has been recently described (Johansen and James, 2012) which is an extension of the classical Buckley-Leverett theory. This analytical method is applicable for multi-component flow under the constant pressure boundary conditions. Using this analytical method the pressure at any location along the formation can be predicted as well as the water breakthrough time. The total flow rate can be calculated at any time before or after breakthrough during the displacement. The analytical method is provided in Appendix B.

In terms of time and accuracy, the analytical extension of Buckley-Leverett theory for constant pressure boundaries provides an efficient and reliable solution for multi-component problems with fixed pressure boundary conditions. In this section we focus on the waterflooding problem.

Based on this analytical method, the displacement time has been divided into two sections which are defined as before and after water breakthrough. For each section, the total velocity has different mathematical expressions.

Time less than or equal to the breakthrough time ($t \leq t_{BT}$)

Equation (2.9) predicts the total velocity prior and up to water breakthrough. The front position, breakthrough time, and pressure at the front position are described in equations (2.10) through (2.12).

Defining $\zeta = \int_{S_L}^{S^*} \frac{f''(S)}{\lambda_t(S)} dS$ and letting S^* and λ_o be the front water saturation and the oil

phase mobility, respectively, the total fluid velocity is given as:

$$u_t = \frac{\Delta p}{\sqrt{B^2 + 4ACt}}, \tag{2.9}$$

where, $A = 0.5\left(\frac{\zeta}{f'(S_{wf})} - \frac{1}{\lambda_o}\right)$, $B = \frac{L}{\lambda_o}$, $C = \frac{f'(S_{wf})}{\phi}\Delta p$.

The solution of front position (x_f) is:

$$x_f = \frac{-B + \sqrt{B^2 + 4ACt}}{2A}. \tag{2.10}$$

The water breakthrough time (t_{BT}) can be calculated by:

$$t_{BT} = \frac{AL^2 + BL}{C}. \tag{2.11}$$

The equation of front pressure can be calculated as:

$$p_f = p_{out} + \frac{u_t}{\lambda_o}\left(L - x_f\right). \tag{2.12}$$

The above calculations are applied when the time is less than or equal to the breakthrough time. After breakthrough different expressions apply to calculate the total fluid velocity and the pressure at the specific water saturation.

Time after water breakthrough ($t > t_{BT}$)

The water saturation at any location behind the front (along the formation) is larger than the front saturation. Assuming a specific water saturation that is larger than front saturation and smaller than injecting water saturation, i.e. $S_{inj} > S > S_{wf}$. Let t_{BT} denote the water breakthrough time and t_s is the time when this specific S reaches the outer boundary.

The position of S at the breakthrough time can be calculated by:

$$x(S,t_{BT})=\frac{f'(S)}{\phi}\psi(t_{BT}), \tag{2.13}$$

where, $\psi(t)=\int_0^t u_t(t)dt$.

The time for water saturation S to break through, t_s, can then be expressed as:

$$t_s = t_{BT} + \frac{\phi\left[L^2 - x(S,t_{BT})\right]\zeta(S)}{2\Delta p f'(S)^2}. \tag{2.14}$$

Applying equation (2.14) the corresponding value of total fluid velocity at t_s finally can be calculated as:

$$u_t^S = \phi\frac{L^2 - x(S,t_{BT})^2}{2Lf'(S)\left(t_s - t_{BT}\right)}. \tag{2.15}$$

The summarized procedure of this calculation is as follows: 1) Calculate t_s for the water saturation S breakthrough from equation (2.14), 2) and obtain the total velocity by equation (2.15).

Based on the previous discussion, this analytical solution is applicable to both before and after water breakthrough, under constant pressure boundary conditions.

In Chapter 3 the numerical solutions of WI is compared with this analytical solutions in order to validate the numerical approach used in this thesis.

2.2 Summary of CO_2 EOR Process

Carbon dioxide (CO_2) has been used for injection in enhanced oil recovery (EOR) since the 1970s. Carbon dioxide (CO_2) can be injected into a reservoir under different conditions. In this section the main strategies of CO_2 EOR are discussed.

2.2.1 CO_2 Gas Injection

In first contact miscible gas injection, the injection gas and reservoir oil form to a single phase under a sufficiently high pressure. It is not possible to form first-contact miscibility at all reservoir conditions or injected gas compositions, thus, multi-contact miscibility strategies are adopted in gas injection processes depending on reservoir conditions and properties. Vaporizing gas drive is one of multi-contact miscible flood methods. In this process the crude oil (I_2) is located in the right hand side of critical tangent, as opposite to injected gas (J_1) as shown in Figure 2.3. Lean injection gas vaporizes the intermediate components from the oil phase and creates a miscible transition zone. The gas front moves throughout the reservoir. By contacting the original reservoir oil, gas is enriched in intermediate components and eventually the composition of enriched gas is sufficiently rich in intermediate components that the enriched gas phase becomes miscible with the oil as shown in Figure 2.4. Condensing gas drive, the other mechanism, is when the crude oil (I_1) is on the left hand side of critical tangent line and the injected gas (J_2) is on the right hand side of this line shown in Figure 2.3. In condensing gas drive the intermediate components (C_2-C_6) transfer from the displacing gas to the oil phase. After multiple contacts, the oil and injected gas becomes miscible by enriching the

transition oil phase with C_2-C_6 generating a critical mixture at the displacing front shown in Figure 2.5.

In condensing-vaporizing gas drive the miscibility is developed by the combined condensing/vaporizing mechanism. In this condensing-vaporizing gas drive, gas is initially enriched by vaporization. This enriched gas is not rich enough to be miscible with the oil but it contains intermediate components (C_2-C_6) which generate the condensing gas drive mechanism with the original oil. The intermediate components then condense when the gas encounters the fresh oil which is very similar to the condensing gas drive mechanism.

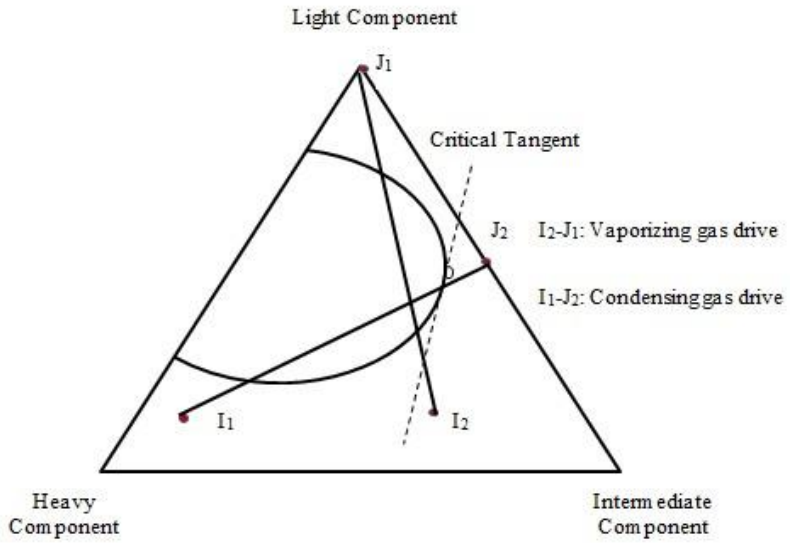

Figure 2.3 Developed Miscibility

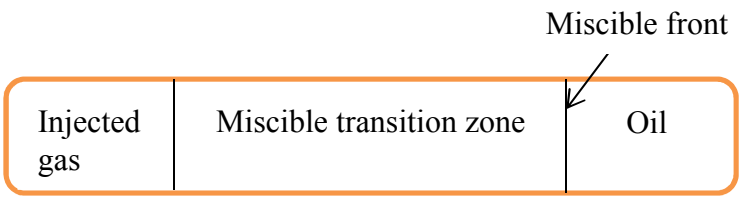

Figure 2.4 Vaporizing Gas Drive

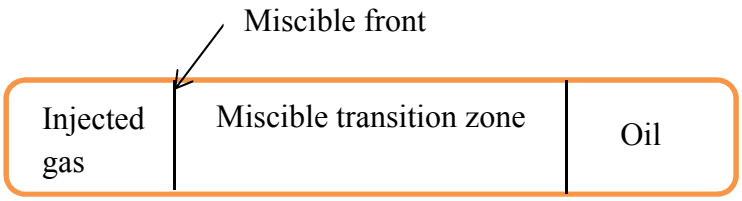

Figure 2.5 Condensing Gas Drive

CO_2 injection is a well-established technology for EOR. The main factor that affects the efficiency of gas injection (CO_2) EOR is the miscibility of CO_2 in the oil phase after injection. Once the pressure exceeds the minimum miscible pressure (MMP), CO_2 is miscible with the oil phase reducing the interfacial tension to zero, reducing oil viscosity and causing oil swelling. The oil trapped in the pore space can therefore be mobilized and flow through the rock, hence enhancing the oil recovery (Dullien, 1991).

The study of CO_2 injection in the Dulang field in Malaysia (Zain *et al*., 2001) at a reservoir temperature of 101 ℃ and a reservoir of pressure 12.41 MPa indicates that although the miscibility cannot be achieved under operating conditions, additional oil recovery is possible. Moreover, according to their test, CO_2 was capable of extracting the hydrocarbon components heavier than C_7.

In multi-contact miscible CO_2 gas injection the intermediate and high molecular weight hydrocarbons are extracted into the CO_2-rich phase. Under certain conditions, this CO_2-rich phase can reach a composition which is miscible with the original reservoir oil. Once this point is achieved, miscible or near-miscible conditions are established at the displacement front. A miscible or near-miscible CO_2 injection can result in a considerable oil recovery. However, low sweep efficiency has been reported due to high mobility of CO_2. Hence, different injection strategies have been proposed and used to alleviate this problem (Riazi, 2011).

2.2.2 Water Alternative Gas Injection

Water alternating gas (WAG) injection was developed to improve the mobility efficiency of high mobility gas overriding lower mobility reservoir fluid. In this process water injection and gas injection are conducted alternately for periods of time. As the evolutionary step in gas based EOR, WAG has been applied in both immiscible and miscible gas injection EOR (Rogers and Grigg, 2000). The injection gases in a WAG process are usually CO_2 mixed with natural gas liquid (NGL). The performance of WAG is affected by many factors, such as reservoir conditions, fluid properties, injection techniques and WAG parameters which include the WAG ratio and the slug size (Jiang *et al*., 2012).

A number of core flood experiments revealed that the timing of cyclic injections has direct impact on WAG performance. An untimely WAG injection will lead to low sweep efficiency (Nuryaningsih *et al*., 2010). The optimal time to inject CO_2 WAG is when the

flood front passes the middle of the core (Jiang *et al*., 2012). In other words, CO_2 WAG should be injected after half of the oil is produced by secondary water flooding.

The evaluation of CO_2 WAG oil recovery in heterogeneous porous media has been done using a compositional simulator. (Ghomian *et al*., 2008) listed the most to least influential factors regarding oil recovery as reservoir heterogeneity characteristics, combination of WAG ratio and slug size, and the slug size itself. This research has also pointed out that a higher oil recovery is expected under low heterogeneity with high WAG ratio and large CO_2 slug size.

Carbon dioxide (CO_2) WAG projects have been applied in the oil industry for the interest of additional oil recovery, however, the poor performance caused by the presence of water layers between isolated oil ganglia has been observed. This so-called water blocking effect prevents the contact between oil and CO_2 reducing the CO_2 solution in oil (Lin and Huang, 1990).

Due to the poor sweep efficiency of direct CO_2 injection and reduction of oil recovery by water-blocking in WAG, other alternative CO_2 injection approaches are being considered.

2.2.3 Carbonated Water Injection

Conventional CO_2 gas injections such as continuous CO_2 gas flooding and WAG injection require a large amount of CO_2 and may not achieve the desirable results due to poor sweep efficiency and water-blocking. In carbonated water injection (CWI), CO_2 is dissolved in the water or brine prior to injection. Due to the high solubility in oil, CO_2 will transfer from the water to the oil phase changing the reservoir fluid properties.

CWI was first introduced as an improved secondary oil recovery process. The first implementation of CWI was to enhance water flooding in the K&S project in Oklahoma. About 43% more oil was recovered compared to the original forecast and improved mobility ratio was also reported (Kechut *et al*., 2011).

Carbonated water injection can contact more reservoir oil since CO_2 is dissolved into water before injection rather than presenting as a free gas. As an EOR technique, CWI not only can reduce the oil viscosity and improve the mobility ratio, it can also reduce the IFT between the water and oil. The swelling effect caused by the dissolved CO_2 in the oil phase results in a reconnection of disconnected residual oil leading to additional oil recovery (Riazi *et al*., 2009).

2.3 Literature Review of Carbonated Water Injection (CWI)

2.3.1 Experimental Investigations of Carbonated Water Injection

CWI was first considered in early 1950s as a potential EOR strategy by conducting coreflood experiments. CWI was reported to reduce the initial oil saturation from 30% to 22%. In 1959, experimental core displacement tests were conducted to study the impact of CO_2 solvent flooding on oil recovery (Holm, 1959). They found that after solvent flooding, carbonated water flooding recovered more oil than using conventional water flooding. Carbonated water flooding showed a higher oil recovery compared to CO_2 slug injection driven by plain water.

High-pressure (pressure range from 600 to 2500 psig) direct flow micromodel experiments have been implemented to reveal the mechanisms of CWI from a pore-scale perspective (Sohrabi *et al*., 2009b). The experimental results showed additional oil recovery in both heavy and light oil via different mechanisms. The experiments revealed that the dominant mechanism of oil recovery by CWI in light oil is the oil swelling due to the reconnection of disconnected oil trapped in the pore space, whereas the reduction in the oil viscosity was the main contributor to increased oil recovery for more viscous oil resulting in improved mobility.

Kechut *et al*. (2011) carried out core flooding experiments to investigate the oil recovery and benefit of CO_2 storage. The experiments were carried out under 17.24 MPa, 37.8℃. The oil samples used in their tests were pure n-decane and stock tank oil with viscosity 0.158 Pa·s. The experimental results demonstrated an increased oil recovery in CWI under both secondary and tertiary oil recovery processes. More oil can be produced by CWI compared with WI. In terms of CO_2 storage, the study revealed that more than 46% of total volume of injected CO_2 was stored after CWI.

2.3.2 Numerical Modeling of Carbonated Water Injection

Noel (1964) introduced a mathematical model for carbonated water flooding based on a Buckley-Leverett linear flow model without dispersion and considering an incompressible fluid system. This method considered the effect of reduction of oil viscosity and the oil swelling due to carbon dioxide mixed with reservoir oil. The sample calculations showed that the increased oil recovery is mainly due to the decrease of oil

viscosity. Contrary to previous work, this calculation method was used to discuss a "slug" injection of carbonated water rather than a continuous injection with a constant fluid composition. A few conclusions can be summarized as follows:

1. Oil viscosity reduction due to dissolved CO_2 leads to higher oil recovery from carbonated water flooding than pure water flooding.
2. Improved sweep efficiency also contributes to higher oil recovery.
3. The CO_2 slug size and the concentration of CO_2 in the water injected also affect oil recovery.

(Ramesh and Dixon, 1972) developed a model to predict the performance of carbonated water flooding in a heterogeneous oil reservoir for a three-phase fluid system where the CO_2 is allowed to exist in the gas state. The mathematical model was based on the transport equation with two dimensions and a three-phase simultaneous flow system in a heterogeneous reservoir. The numerical solution predicted the transfer of one phase to the adjacent blocks too soon compared with experimental results. To minimize the error, an arbitrary cut-off saturation was specified at which the transmissibility of the displacement phase was set to zero. An adequate application of this model was validated by experimental results.

The above numerical studies only incorporate the reservoir numerical models and ignored the change of fluid properties such as IFT. In this thesis carbonated water injection (CWI) is studied by combining both thermodynamics and reservoir simulation models with the goal to better understand the effects on oil recovery from both physical and numerical perspectives.

2.4 Variation of Fluid Properties with Dissolved CO_2

Due to the presence of CO_2 in the liquid phase, the properties of oil and water are variable during carbonated water flooding. The reduction of oil viscosity and oil swelling are major mechanisms that affect the oil recovery in CWI; hence, a better understanding of the change in fluid properties is essential in CWI. In recent years, the Genetic Algorithm-based (GA-based) technique (Emera and Sarma, 2006) has been used to provide the correlations to predict CO_2 solubility, CO_2-oil swell factor, CO_2-oil density and CO_2-oil viscosity for both dead and live oils. The models were developed and tested based on the experimental data (Jarba and Anazi, 2009). Unlike other correlations which are applicable in a limited range of conditions, the GA-based correlations can be applied over a wide range of conditions. These correlations have been validated with published experimental data. In this study, the GA-based correlations are used to calculate the oil fluid properties with dissolved CO_2 shown in the next sections.

The dissolved CO_2 in the water phase also results in a variation of water properties. Increasing the amount of dissolved CO_2 in the water and oil phase is expected to reduce the IFT during the CO_2 flooding process.

2.4.1 Change in Fluid Viscosity

Oil viscosity decreases significantly due to increasing amount of CO_2 in the oil phase. A graphical correlation was built to predict the oil viscosity after CWI as a function of pressure and initial oil viscosity, (Welker, 1963). However, this correlation was

established based on dead oil at a temperature of 26.67 ℃ and a pressure of 800 psia thus; failing to be applicable over a wide range of reservoir conditions.

A correlation (Lohrenz *et al*., 1964) was proposed to calculate the decrease in oil viscosity when gases are dissolved in oil phases. The calculation was based on the composition of the fluid; hence the results were greatly affected by the fluid density. Since the correlation was mainly applied to light oil samples; it is not applicable for the case of heavy oil recovery.

Beggs and Robinson (1975) developed a CO_2-oil viscosity calculation method based on reservoir temperature and CO_2 solubility. In this method, the impact of pressure on oil viscosity was neglected. (Chang *et al*., 1998) found that the dissolved CO_2 in the water phase has minimal effect on water viscosity. The water viscosity was calculated at the reservoir conditions (temperature, pressure, and the salinity of water). However, the CO_2 solubility was neglected (Kestin *et al*., 1978).

A GA-based CO_2-oil viscosity correlation (Emera and Sarma, 2006) was developed based on CO_2 solubility, initial oil viscosity (Pa·s), pressure (MPa), temperature (℃) and oil specific gravity under SI unit. This correlation is applicable for both dead and live oil for pressures in the range from 0.1 MPa to 34.5 MPa, and temperature in the range from 21.1℃ to 140 ℃. Compared with other correlations more accurate results have been observed by the comparison with experimental data.

The correlation for oil viscosity used here is the GA-based model (Emera and Sarma, 2006):

$$\mu_o = y\mu_{oi} + A\left(\frac{x^o_{co_2}}{\mu_{oi}}\right), \tag{2.16}$$

where

$$y = X^B,$$

$$X = \left[C\mu_{oi}\left(\frac{p}{1.8T+32}\right)^D\right]^{\left(\gamma_o x^o_{co_2}\right)},$$

where *A*, *B*, *C* and *D* are dimensionless constants provided in Table 2.1.

Table 2.1 Coefficients used to calculate oil viscosity for both live and dead oils

Oil type	*A*	*B*	*C*	*D*
Live	0	-0.587	305.873	1.15
Dead	-9.5	-0.732	3.14129	0.23

2.4.2 Change in Fluid Density

The CO_2-oil density for both dead and live oil can be calculated based on the Genetic Algorithm-based (GA-based) correlations (Emera and Sarma, 2006), which account for the reservoir pressure (MPa) and temperature (℃), oil specific gravity (γ_o) and the initial oil density (ρ_{oi}, g/cm^3) at bubble point pressure (MPa) under the defined temperature (℃) and a specific oil composition.

The density correlation in the GA-based model (Emera and Sarma, 2006) for SI unit is:

$$\rho_o = \rho_{oi} - 0.10276y^{0.608} + 0.1407y^{0.6133}, \tag{2.17}$$

where

$$y = \frac{\gamma_o \rho_{oi} \left(p - p_b\right)^{1.25}}{1.8T + 32}.$$

The density of carbonated water can be updated by applying an existing correlation based on the relation of pressure, volume, temperature and concentration of solvent (Rowe Jr and Chou, 1970).

In this study, the model for water density over a range of pressures and given reservoir temperature is generated by **PVTsim™** Calcep simulator.

2.4.3 CO_2 Oil Swelling

The oil swelling in CO_2 flooding is considered as one of the important factors directly affecting the recovery of efficiency.

In the 1960s, the relationship between swelling factor, mole fraction of dissolved CO_2 and molecular size was studied (Simon and Graue, 1965).

The GA-based correlation for the oil swelling factor (*SF*) as a function of CO_2 solubilty (*Sol*, mole fraction), oil molecular weight (*MW*) and oil specific gravity (γ_o) has been proposed by Emera and Sarma (2006) :

$$SF = 1 + 0.48411y - 0.9928y^2 + 1.6019y^3 - 1.2773y^4 + 0.48267y^5 - 0.06671y^6, \quad (2.18)$$

where

$$y = 1000\left(\frac{\gamma_o Sol^2}{MW}\right)^{\exp\left(\frac{\gamma_o}{MW}\right)}.$$

According to Figure 2.6, (Jarba and Anazi, 2009) the GA-based correlation gives a more accurate result compared to previous work.

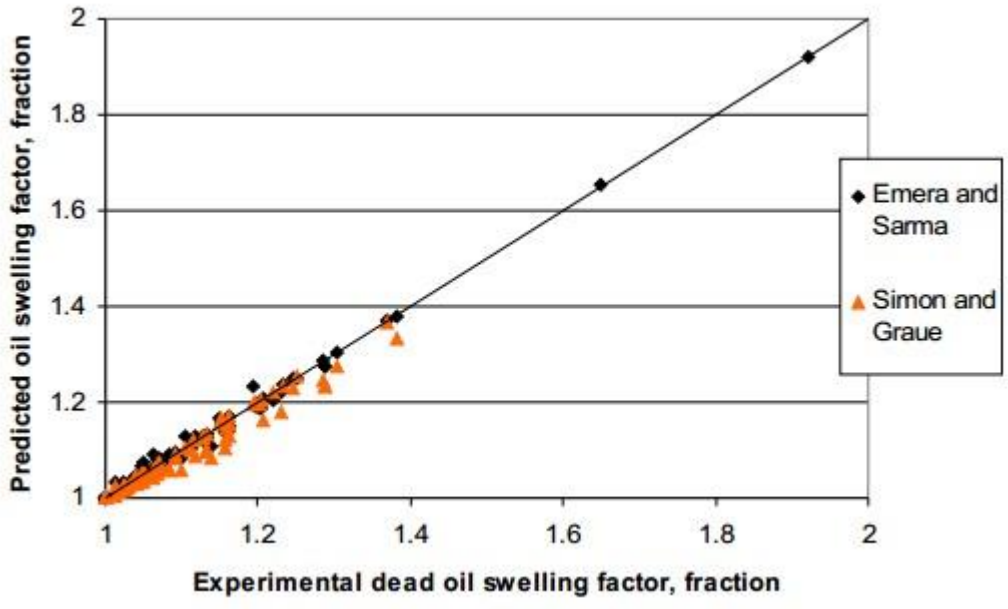

Figure 2.6 Comparison Results between Emera and Sarma (2006) and Simon and Graue (1965) Oil Swelling Factor (due to CO_2) Correlations Prediction Results (Jarba and Anazi, 2009).

2.4.4 Oil-Water Interfacial Tension

As mentioned previously, additional oil recovery in carbonated water flooding can be attributed to the reduction of oil viscosity, oil swelling as well as the decrease of interfacial tension between water and oil when sufficient CO_2 has been dissolved in oil phase.

According to experimental CO_2 flooding results at ambient temperature for effluent oil cuts (Zekri *et al*., 2007), after injection of 0.25 pore volume of CO_2 the maximum drop in

IFT between oil and water was 85%. Figure 2.7 (Zekri *et al*., 2007) shows the relationship of IFT between crude oil and brine as a function of CO_2 pore volume injected. The reduced IFT is expected to reduce the residual oil saturation. However, based on the previous work of (Torabzadey, 1984), the residual oil saturation was not affected under high IFT (IFT > 20 mN/m); but a significant drop of residual oil was obeserved under low IFT fluid system (IFT < 0.2 mN/m).

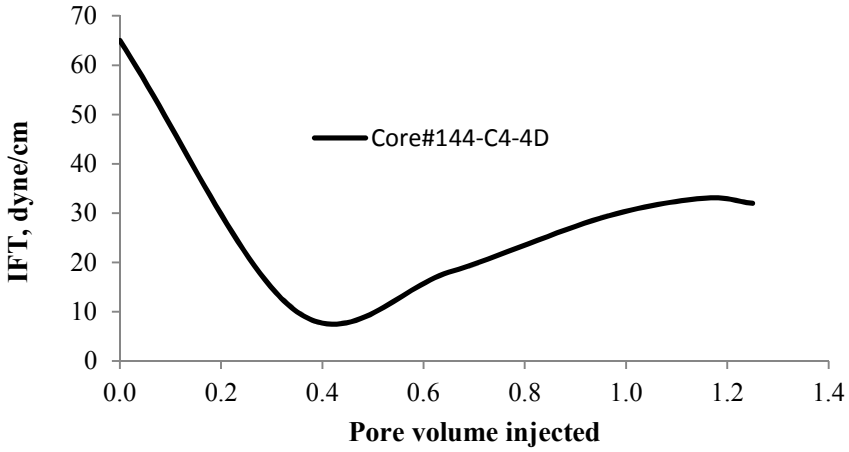

Figure 2.7 Oil-Water Interfacial Tension as Function of CO_2 Injected (Zekri *et al.*, 2007)

Chapter 3 Water Injection under Constant Pressure Boundary Condition

In any injection process the breakthrough time is one of the most important variables that need to be estimated by reservoir engineers. An early breakthrough time usually indicates poor sweep efficiency and an uneconomic recovery strategy. The water breakthrough time under constant pressure boundaries is, therefore, predicted in this study both numerically and analytically. The numerical model is validated by the comparing the numerical and analytical solutions. The numerical errors are minimized in this study.

3.1 Mathematical Model

The movement of fluids through porous media in the subsurface is governed by the conservation of mass, and momentum and energy. The governing equations model a physical system. The behavior of the whole system is complex; hence, the primary task in modeling is to choose a set of equations that can accurately describe the complex fluid system. The most widely used equations in reservoir simulation are built upon the laws of conservation, which for isothermal system consist of 1) the mass balance, and 2) the momentum balance (Darcy's law).

3.1.1 The Continuity Equation

Given a control volume (V) that fluid can flow through, the conservation of mass states that the rate of change of mass in V is equal to the mass flux across the boundary of V

plus any mass injected (source) or removed (sink).

The change of mass in this control volume V, in a unit time can be written as:

$$\frac{\partial}{\partial t}\iiint_V \frac{\text{Mass of component in} V}{\text{Bulk volume of } V} dV . \tag{3.1}$$

The conservation of mass in the volume V can be described using the "Gauss" theorem:

$$\frac{\partial}{\partial t}\iiint_V \frac{\text{mass of component in } V}{\text{Bulk volume of } V} dV = -\iiint_V \left(\nabla \cdot \vec{F}\right) dV + \iiint_V \tilde{q} dV , \tag{3.2}$$

where $\vec{F}$ is the mass flux into the medium and $\tilde{q}$ is the mass flow rate per unit volume injected or produced within V.

If we define

$$\omega = \frac{\text{Mass of component in } V}{\text{Bulk volume of } V}, \tag{3.3}$$

then, since V is an arbitrary control volume, the following equation holds at any point

$$\frac{\partial \omega}{\partial \text{t}} + \nabla \cdot \vec{F} - \tilde{q} = 0 . \tag{3.4}$$

3.1.2 Darcy's Law for a Single Phase

Based on Darcy's law, for a single phase horizontal flow, the volumetric flow rate Q through a horizontal porous medium with length L and cross sectional area A can be written as:

$$Q = \frac{KA}{\mu}\frac{\Delta p}{L}, \tag{3.5}$$

where K is permeability describing the ability of the rock to transfer the amount of fluid, μ is the fluid viscosity and Δp is the pressure difference between inlet and outlet.

For a flow in only one direction (x) Darcy's law can also be expressed in the following

differential form:

$$u = \frac{Q}{A} = -\frac{K}{\mu}\frac{\partial p}{\partial x}. \tag{3.6}$$

Applying Darcy's Law for one dimensional horizontal flow, equation (3.4) becomes:

$$\frac{1}{\partial x}\left(\rho \cdot \frac{K}{\mu} \cdot \frac{\partial p}{\partial x}\right) + \tilde{q} = \frac{\partial \omega}{\partial t}. \tag{3.7}$$

3.2 One-Dimensional Horizontal Water Flooding

3.2.1 Introduction

The displacement of oil by either water or gas is commonly investigated using reservoir simulation. In a water-oil system, we assume that there is no mass transfer between the two phases. The void volume of the porous medium is occupied by the two phases (oil and water), i.e.

$$S_w + S_o = 1. \tag{3.8}$$

In a water-oil system, water is usually the wetting phase which wets the porous medium more than oil. Due to the curvature of the interface between water and oil in the microscopic pores, the pressure in the oil (p_o) is higher than the pressure in the water (p_w). This pressure difference is the capillary pressure, p_c:

$$p_c = p_o - p_w. \tag{3.9}$$

When water and oil flow simultaneously through a porous medium, each of the two phases interferes with the other. Hence, the permeability of each phase is less than or

equal to the permeability for single phase flow.

If the permeability for oil and water are K_o and K_w respectively, then the relative permeability of these two phases (k_{ro} , k_{rw}) can be defined as:

$$k_{ro} = \frac{K_o}{K} \le 1 \,, \qquad k_{rw} = \frac{K_w}{K} \le 1 \,. \tag{3.10}$$

The relative permeabilities are unique functions of the phase saturations.

3.2.2 The Black Oil Model

A simplified model, the "black oil" model, was introduced for describing the equilibrium of a hydrocarbon system at temperature well below critical temperature. In this model the assumption is made that no mass transfer occurs between water/gas and water/oil. In a water-oil system, both components (oil and water) are defined at the standard condition on the surface called "stock tank oil" and "stock tank water", however, the mass balance of these components is performed at reservoir conditions. A parameter is introduced called "formation volume factor (FVF)" denoted as β:

$$\beta = \frac{V^{RC}}{V^{ST}}, \tag{3.11}$$

where, V^{RC} is the volume of a phase under reservoir condition and V^{ST} is the volume of the same phase under stock tank condition.

In a water-oil system, the mass of water component per bulk volume is defined as:

$$\omega_w = \frac{\text{Mass of component in } V}{\text{Bulk volume of } V} = \frac{\rho_w^{ST} V_w^{ST}}{V_{bulk}} = \frac{\rho_w^{ST} V_w^{RC}}{V_{bulk}\beta_w} = \frac{\rho_w^{ST}\phi S_w V_{bulk}}{V_{bulk}\beta_w} = \frac{\rho_w^{ST}\phi S_w}{\beta_w(p_w)}, \tag{3.12}$$

$$\omega_o = \frac{\text{Mass of component } V}{\text{Bulk volume } V} = \frac{\rho_o^{STC} V_o^{STC}}{V_{bulk}} = \frac{\rho_o^{STC} V_o^{RC}}{V_{bulk}\beta_o} = \frac{\rho_o^{STC}\phi S_o V_{bulk}}{V_{bulk}\beta_o} = \frac{\rho_o^{STC}\phi S_o}{\beta_o(p_o)}, \quad (3.13)$$

where, S is phase saturation and ϕ is the porosity.

The mass influx (F) can be expressed as:

$$F = \rho^{RC} u = \frac{\rho^{ST}}{\beta(p)} u . \quad (3.14)$$

Equation (3.4) can then be rewritten for water and oil components:

Water:

$$\frac{\partial}{\partial t}\left(\frac{\phi S_w}{\beta_w(p_w)}\right) + \nabla \cdot \left(\frac{u_w}{\beta_w(p_w)}\right) = \frac{\tilde{q}_w}{\rho_w^{ST}} = q_w . \quad (3.15)$$

Oil:

$$\frac{\partial}{\partial t}\left(\frac{\phi S_o}{\beta_o(p_o)}\right) + \nabla \cdot \left(\frac{u_o}{\beta_o(p_o)}\right) = \frac{\tilde{q}_o}{\rho_o^{ST}} = q_o , \quad (3.16)$$

where,

$$\begin{aligned} u_w &= -\frac{K_w}{\mu_w}\left(\frac{\partial p}{\partial x}\right) = -\frac{K k_{rw}}{\mu_w}\left(\frac{\partial p}{\partial x}\right), \\ u_o &= -\frac{K_o}{\mu_o}\left(\frac{\partial p}{\partial x}\right) = -\frac{K k_{ro}}{\mu_o}\left(\frac{\partial p}{\partial x}\right). \end{aligned} \quad (3.17)$$

Using equation (3.8) and equation (3.9) for horizontal one-dimensional water flooding case, the governing system of equations can be written as:

$$\frac{\partial}{\partial t}\left(\frac{\phi S_w}{\beta_w(p_w)}\right)+\frac{\partial}{\partial x}\left(\frac{u_w}{\beta_w(p_w)}\right)=q_w \ ,$$

$$\frac{\partial}{\partial t}\left(\frac{\phi S_o}{\beta_o(p_o)}\right)+\frac{\partial}{\partial x}\left(\frac{u_o}{\beta_o(p_o)}\right)=q_o \ ,$$

$$u_w=-\frac{Kk_{rw}(S_w)}{\mu_w}\left(\frac{\partial p_w}{\partial x}\right) \ ,$$

$$u_o=-\frac{Kk_{ro}(S_o)}{\mu_o}\left(\frac{\partial p_o}{\partial x}\right) \ , \qquad (3.18)$$

$$S_w+S_o=1 \ ,$$

$$p_c=p_o-p_w \ .$$

The system of equations can be simplified by assuming that there is no source or sink terms in the 1-D reservoir and that capillary pressure can be neglected ($p=p_o=p_w$). The system of equations (3.18) then becomes:

$$\frac{\partial}{\partial t}\left(\frac{\phi S_w}{\beta_w(p)}\right)+\frac{\partial}{\partial x}\left(\frac{u_w}{\beta_w(p)}\right)=0 \ ,$$

$$\frac{\partial}{\partial t}\left(\frac{\phi S_o}{\beta_o(p)}\right)+\frac{\partial}{\partial x}\left(\frac{u_o}{\beta_o(p)}\right)=0 \ ,$$

$$u_w=-\frac{Kk_{rw}(S_w)}{\mu_w}\left(\frac{\partial p}{\partial x}\right) \ , \qquad (3.19)$$

$$u_o=-\frac{Kk_{ro}(S_o)}{\mu_o}\left(\frac{\partial p}{\partial x}\right) \ ,$$

$$S_w+S_o=1 \ .$$

In the above system of equations there are five unknowns (S_w, S_o, u_w, u_o, p) and five equations. Therefore, by applying certain boundary conditions this system can be solved at any location at any point in time.

3.2.3 Numerical Model

In this section, the numerical solution for one-dimensional horizontal water injection is developed.

Defining water mobility as:

$$\lambda_w = \frac{Kk_{rw}(S_w)}{\mu_w \beta_w}, \tag{3.20}$$

the water continuity equation becomes:

$$\frac{\partial}{\partial t}\left(\frac{\phi S_w}{\beta_w(p)}\right) = \frac{\partial}{\partial x}\left(\lambda_w \frac{\partial p}{\partial x}\right). \tag{3.21}$$

After expansion the equation can be reorganized as:

$$\phi S_w \left(c_{pv} + c_w\right)\frac{\partial p}{\partial t} + \phi \frac{\partial S_w}{\partial t} = \beta_w \frac{\partial}{\partial x}\left(\lambda_w \frac{\partial p}{\partial x}\right), \tag{3.22}$$

where, $c = -\frac{1}{\beta}\frac{d\beta}{dp}$ and $c_{pv} = \frac{1}{\phi}\frac{d\phi}{dp}$ are fluid and rock compressibility, respectively.

By the same procedure, the oil phase continuity equation can be obtained:

$$\phi S_o \left(c_{pv} + c_w\right)\frac{\partial p}{\partial t} + \phi \frac{\partial S_o}{\partial t} = \beta_o \frac{\partial}{\partial x}\left(\lambda_o \frac{\partial p}{\partial x}\right). \tag{3.23}$$

As was previously discussed, the summation of oil and water saturation is equal to one, hence by adding equation (3.22) and equation (3.23) the oil saturation S_o cancels out:

$$\phi\left(c_{pv}+S_w c_w+c_o-S_w c_o\right)\frac{\partial p}{\partial t}=\beta_w\frac{\partial}{\partial x}\left(\lambda_w\frac{\partial p}{\partial x}\right)+\beta_o\frac{\partial}{\partial x}\left(\lambda_o\frac{\partial p}{\partial x}\right). \tag{3.24}$$

3.2.3.1 Implicit pressure and Explicit Saturation (IMPES)

Equation (3.24) indicates that a system of two-phase immiscible flow through 1D porous media is governed by a nonlinear time-dependent partial differential equation. Two types of discretization numerical schemes can be applied to solve this type of equation, the fully implicit and the implicit-explicit. In this case, the Implicit Pressure Explicit Saturation (IMPES) approach has been adopted. The IMPES method was introduced to solve a partial differential coupled system for two-phase flow in a porous medium (Sheldon *et al*., 1959; Stone and Garder Jr, 1961). The main idea of this classical method is to separate the computation of pressure from that of saturation. Using this method, the coupled system is split into two separate equations for pressure and saturation. The saturation and pressure equations are solved using explicit and implicit time approximation approaches, respectively. This method can be set up easily and efficiently implemented for two-phase immiscible flow. However, the IMPES method is conditionally stable and converges if and only if the time step is selected carefully according to the classical Courant-Friedrichs-Lewy condition (CFL) (Courant *et al*., 1928). In the current case, the CFL condition expresses that the time step must ensure that change of mass in each control volume is less than the mass of one pore volume of the cell per time step. In other words,

$$\Delta t<\frac{\phi\Delta L}{u_t}, \tag{3.25}$$

where L is the length of the grid block.

Discretization of the flow equations

The block-centered finite difference method with constant size of grid blocks is used to solve the numerical problem in this work.

Figure 3.1 indicates three blocks (x_{i-1}, x_i and x_{i+1}), each with a constant length Δx. The value (y_i) in position x_i can be approximated by:

$$y_i = \frac{y_{i-1/2} + y_{i+1/2}}{2} \tag{3.26}$$

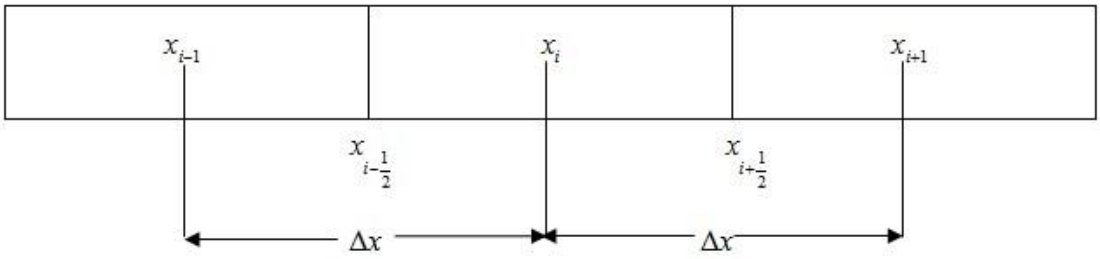

Figure 3.1 Block-Centered Finite Difference Model

For a general differential equation as:

$$\frac{\partial}{\partial x}\left(\alpha \frac{\partial p}{\partial x}\right) = \frac{\partial p}{\partial t}, \tag{3.27}$$

the discretization can be expressed as:

$$\begin{aligned} \frac{\partial}{\partial x}\left(\alpha \frac{\partial p}{\partial x}\right)_i &\cong \frac{1}{\Delta x}\left[\alpha_{i+1/2}\left(\frac{\partial p}{\partial x}\right)_{i+1/2} - \alpha_{i-1/2}\left(\frac{\partial p}{\partial x}\right)_{i-1/2}\right] \\ &= \frac{1}{\Delta x}\left(\alpha_{i+1/2}\frac{p_{i+1}-p_i}{\Delta x_{i+1/2}} - \alpha_{i-1/2}\frac{p_i - p_{i-1}}{\Delta x_{i-1/2}}\right). \end{aligned} \tag{3.28}$$

Applying IMPES, equation (3.28) becomes:

$$\frac{\partial}{\partial x}\left(\alpha\frac{\partial p}{\partial x}\right)=\frac{1}{\Delta x}\left[\alpha^{n}_{i+1/2}\left(\frac{\partial p}{\partial x}\right)^{n+1}_{i+1/2}-\alpha^{n}_{i-1/2}\left(\frac{\partial p}{\partial x}\right)^{n+1}_{i-1/2}\right]$$
$$=\frac{1}{\Delta x}\left(\alpha^{n}_{i+1/2}\frac{p^{n+1}_{i+1}-p^{n+1}_{i}}{\Delta x_{i+1/2}}-\alpha^{n}_{i-1/2}\frac{p^{n+1}_{i}-p^{n+1}_{i-1}}{\Delta x_{i-1/2}}\right). \tag{3.29}$$

In the above equation only pressure is solved implicitly and α^{n} is the coefficient from the last time step n, i.e. $t=n\Delta t$. Therefore, the scheme for solving a general partial differential equation (refer to equation (3.27)) can be written as:

$$\frac{1}{\Delta x}\left(\alpha^{n}_{i+1/2}\frac{p^{n+1}_{i+1}-p^{n+1}_{i}}{\Delta x_{i+1/2}}-\alpha^{n}_{i-1/2}\frac{p^{n+1}_{i}-p^{n+1}_{i-1}}{\Delta x_{i-1/2}}\right)=\frac{p^{n+1}_{i}-p^{n}_{i}}{\Delta t}. \tag{3.30}$$

Pressure distribution in a water-oil system

Based on equation (3.28), the water term on the right hand side of the equation (3.24) becomes:

$$\beta_{w}\frac{\partial}{\partial x}\left(\lambda_{w}\frac{\partial p}{\partial x}\right)=\frac{\beta_{wi}}{\Delta x}^{n}\left(\lambda_{w}{}^{n}_{i+1/2}\frac{p^{n+1}_{i+1}-p^{n+1}_{i}}{\Delta x_{i+1/2}}-\lambda_{w}{}^{n}_{i-1/2}\frac{p^{n+1}_{i}-p^{n+1}_{i-1}}{\Delta x_{i-1/2}}\right). \tag{3.31}$$

Leting

$$\delta_{w_{i+1/2}}=\frac{\lambda_{w_{i+1/2}}}{\Delta x_{i+1/2}}, \tag{3.32}$$

and

$$\delta_{w_{i-1/2}}=\frac{\lambda_{w_{i-1/2}}}{\Delta x_{i-1/2}}, \tag{3.33}$$

and defining,

$$A_{w_i}=\frac{\beta_{w_i}}{\Delta x_i}\delta_{w_{i+1/2}}, \tag{3.34}$$

$$B_{w_i} = \frac{\beta_{w_i}}{\Delta x_i}\delta_{w_{i-1/2}}, \tag{3.35}$$

$$C_{w_i} = -A_{w_i} - B_{w_i}, \tag{3.36}$$

equation (3.31) can be rewritten as:

$$\frac{\partial}{\partial x}\left(\lambda_w \frac{\partial p}{\partial x}\right) = A_{wi}{}^{n} p_{i+1}^{n+1} + C_{wi}{}^{n} p_i^{n+1} + B_{wi}{}^{n} p_{i-1}^{n+1}. \tag{3.37}$$

Repeating the same procedure for the oil term on the right hand side of equation (3.24):

$$\frac{\partial}{\partial x}\left(\lambda_o \frac{\partial p}{\partial x}\right) = A_{oi}{}^{n} p_{i+1}^{n+1} + C_{oi}{}^{n} p_i^{n+1} + B_{oi}{}^{n} p_{i-1}^{n+1}. \tag{3.38}$$

The expansion of the left hand side of equation (3.24) can be obtained by:

$$\phi\left(c_{pv} + S_w c_w + c_o - S_w c_o\right)\frac{\partial p}{\partial t} = \left[\phi\left(c_{pv} + S_w c_w + c_o - S_w c_o\right)\right]_i^n \frac{p_i^{n+1} - p_i^n}{\Delta t}. \tag{3.39}$$

Leting

$$E_i^n = \frac{\left[\phi\left(c_{pv} + S_w c_w + c_o - S_w c_o\right)\right]_i^n}{\Delta t}, \tag{3.40}$$

equation (3.39) becomes:

$$\phi\left(c_{pv} + S_w c_w + c_o - S_w c_o\right)\frac{\partial p}{\partial t} = E_i^n\left(p_i^{n+1} - p_i^n\right). \tag{3.41}$$

Substituting equations (3.37), (3.38) and (3.41) into equation (3.24), the final expression consisting of both water and oil appears as:

$$\left(A_w + A_o\right)_i^n p_{i+1}^{n+1} + \left(C_w + C_o - E\right)_i^n p_i^{n+1} + \left(B_w + B_o\right)_i^n p_{i-1}^{n+1} = -E_i^n p_i^n. \tag{3.42}$$

The above linear equation can be solved for p^{n+1} under certain boundary and initial reservoir conditions. Based on the block centered method, the coefficients shown in

equation (3.42) are approximated by the value in the center of the grid block and the flux is approximated on the edge of each grid block.

3.3.3.2 Saturation Profile

Once the pressure difference is solved implicitly, the saturation value can then be updated explicitly at each point in the medium.

By applying the explicit finite difference approach equation (3.22) is arranged as:

$$\frac{S_i^{n+1}-S_i^n}{\Delta t}=\frac{\beta_{wi}{}^n}{\phi}\left\{\frac{\partial}{\partial x}\left[\left(\lambda_w\right)_i^n\frac{\partial p}{\partial x}\right]-\left[S_w\phi\left(c_{pv}+c_w\right)\right]_i^n\frac{\partial p}{\partial t}\right\}. \tag{3.43}$$

Applying the pressure distribution that was solved implicitly, equation (3.43) becomes:

$$S_i^{n+1}=S_i^n+\frac{\beta_{wi}{}^n\cdot\Delta t}{\phi}\cdot\left\{\begin{array}{c}\frac{\delta_{w_{i+1/2}}}{\Delta x_i}\left(p_{i+1}^{n+1}-p_i^{n+1}\right)-\frac{\delta_{w_{i-1/2}}}{\Delta x_i}\left(p_i^{n+1}-p_{i-1}^{n+1}\right)\\ -\left[S_w\phi\left(c_{pv}+c_w\right)\right]_i^n\left(p_i^{n+1}-p_i^n\right)\end{array}\right\}. \tag{3.44}$$

The water saturation profile can then be updated at time step $n+1$ from time step n and pressure p_i^{n+1} .

3.3 Numerical Simulation and Analysis

The numerical model was developed and executed in Matlab®. The numerical model is easily modified for different reservoir properties, conditions or extra calculations.

The simulation procedures consist of four major steps:

1. Computation of the pressure distribution
2. Updating of the saturation profile
3. Calculation of the total fluid velocity
4. Generation of the main graphics (figures)

The fluid properties are specified prior to simulation; hence the pressure distribution is a unique function of time and position under the given boundary conditions. The saturation profile and total fluid velocity can then be calculated based on the distribution of pressure at any time and position. Graphical representations of the results are presented in the last step for better observation and analysis.

3.3.1 Data Preparation

The aim of the simulation study is to better understand the fluid behavior in the reservoir. The data selection is important for a realistic comprehension of fluid performance in the reservoir. The three property sets that need to be defined are the fluid, reservoir, and rock properties plus the reservoir boundary conditions.

3.3.1.1 Fluid Properties

The initial fluid properties can be selected from various resources. The reservoir fluid properties are functions of pressure, fluid composition and temperature; hence the fluid properties will vary according to the change of the fluid itself and the reservoir conditions. The simulations in this study are based on the "black oil model" and the reservoir temperature is constant, therefore, the fluid properties are considered to be functions only of pressure. The pressure distribution is function of time; hence the fluid properties need to be recalculated and updated at each computational time step during water flooding.

Formation volume factor (β)

The volume of both water and oil in the reservoir is inversely proportional to pressure ($\beta \propto p^{-1}$). In many simulation studies, a linear correlation is adopted as a simplification

to estimate the coefficients that are used during the computation. In the case study we assume the fluid is incompressible and β is assumed to be 1.

Fluid compressibility (c_o, c_w)

The compressibility coefficient of oil (c_o) and water (c_w) is defined as the absolute ratio between the amount of volume change per unit change in pressure and initial volume. In general, the volume of single phase petroleum fluid decreases with increasing pressure under constant reservoir temperature. Since the fluid is assumed incompressible the fluid compressibility equals to zero in this study.

Viscosity (μ_o, μ_w)

Pressure has been shown to have an insignificant effect on the viscosity of a liquid, except under extremely high pressure conditions. In this study the impact of pressure on fluid viscosity is neglected.

3.3.1.2 Reservoir Properties

Reservoir permeability (K)

Permeability is a parameter which quantifies the ability of rock to pass and receive flowing fluid. In the petroleum industry, permeability (K) is measured in Darcy. However, to maintain the consistency during the calculation all the units are converted into SI unit.

Relative permeability (k_{ro}, k_{rw})

Corey's model is introduced for calculating the relative permeability in this work. The expressions for water and oil in this study are chosen as:

$$k_{rw} = 0.2\left(\frac{S_w - S_{wc}}{1 - S_{wc} - S_{or}}\right)^2, \tag{3.45}$$

$$k_{ro} = 0.8\left(\frac{1 - S_w - S_{or}}{1 - S_{wc} - S_{or}}\right)^2, \tag{3.46}$$

where, S_{wc} is reservoir irreducible water saturation and S_{or} is the residual oil saturation. The typical relative permeability curves are shown by Figure 3.2.

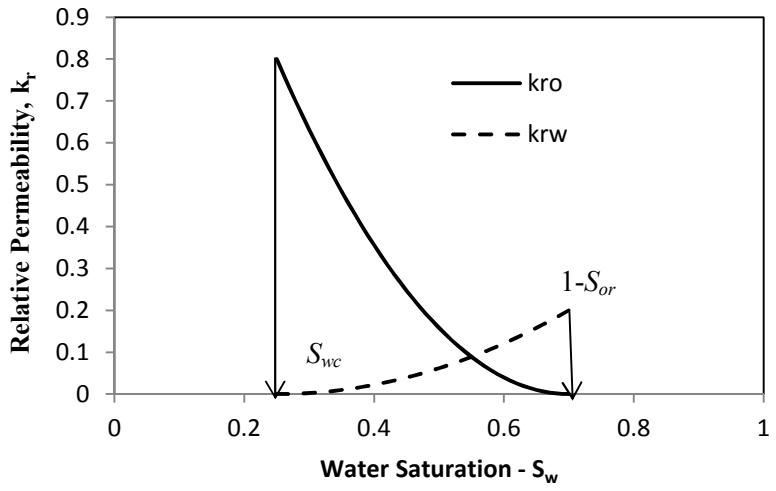

Figure 3.2 Typical relative permeability curves of water and oil

Porosity (ϕ)

Porosity is defined as the fraction of void volume of over the total bulk volume. In this study a constant porosity, ϕ=0.18, is used.

Initial formation water and oil saturation (S_w^0, S_o^0)

Initial formation saturation has to be defined in order to start the calculation. The initial water saturation is 0.25 in this study.

Pore volume compressibility (c_{pv})

Due to the porosity the pore space in the formation tends to change under different pressure conditions. The constant porosity is adopted in this study i.e. effect on change of pore volume is neglected, i.e. $c_{pv} = 0$.

3.3.1.3 Boundary Conditions

In order to solve the pressure equation shown in equation (3.42) the specified boundary conditions have to be applied.

For a secondary oil recovery process the water is injected to drive the oil to the surface. The injection pressure (p_{in}), 21 MPa, will be fixed as well as the outlet pressure (p_{out}), 17 MPa. Since most of void space is occupied by the water phase at the point of injection the injection water saturation (S_{in}) is equal to $1-S_{or}$ which is 0.7 in this case.

3.3.2 Computation of Finite Difference Equation

3.3.2.1 Pressure Distribution

Having defined the reservoir properties, fluid properties and boundary conditions; the pressure distribution can be obtained by solving the finite difference equation (3.42):

$$\left(A_w + A_o\right)_i^n p_{i+1}^{n+1} + \left(C_w + C_o - E\right)_i^n p_i^{n+1} + \left(B_w + B_o\right)_i^n p_{i-1}^{n+1} = -E_i^n p_i^n . \qquad (3.42)$$

For a system with M grid blocks, M equations can be developed corresponding to each block which are shown below:

$$
\begin{aligned}
&\left(B_w+B_o\right)_1^n p_{in}^{n+1}+\left(C_w+C_o-E\right)_1^n p_1^{n+1}+\left(A_w+A_o\right)_1^n p_2^{n+1}=-E_1^n p_1^n \\
&\left(B_w+B_o\right)_2^n p_1^{n+1}+\left(C_w+C_o-E\right)_2^n p_2^{n+1}+\left(A_w+A_o\right)_2^n p_3^{n+1}=-E_2^n p_2^n \\
&\left(B_w+B_o\right)_3^n p_2^{n+1}+\left(C_w+C_o-E\right)_3^n p_3^{n+1}+\left(A_w+A_o\right)_3^n p_4^{n+1}=-E_3^n p_3^n \qquad (3.47) \\
&\cdots\cdots\cdots\cdots\cdots\cdots\cdots\cdots\cdots\cdots\cdots\cdots\cdots\cdots\cdots\cdots\cdots\cdots\cdots\cdots\cdots\cdots\cdots\cdots \\
&\left(B_w+B_o\right)_m^n p_{m-1}^{n+1}+\left(C_w+C_o-E\right)_m^n p_m^{n+1}+\left(A_w+A_o\right)_m^n p_{out}^{n+1}=-E_m^n p_m^n \ .
\end{aligned}
$$

The above system of equations (3.47) can be organized into matrix form as:

$$
\begin{pmatrix}
\left(C_w+C_o-E\right)_1^n & \left(A_w+A_o\right)_1^n & & \\
 & \vdots & & \\
 & \left(B_w+B_o\right)_m^n & \left(C_w+C_o-E\right)_m^n
\end{pmatrix}
\begin{pmatrix} \\ p_i^{n+1} \\ \\ \end{pmatrix}=
\begin{pmatrix}
-\left(Ep\right)_1^n-\left(B_w+B_o\right)_1^n p_{in}^{n+1} \\
-\left(Ep\right)_i^n \\
-\left(Ep\right)_m^n-\left(A_w+A_o\right)_m^n p_{out}^{n+1}
\end{pmatrix}. \qquad (3.48)
$$

In this equation, the constant matrix consists of three diagonals. The main diagonal is sitting on the diagonal of the matrix adjacent to an upper diagonal and a lower diagonal. The rest of the elements of this matrix are zero. The pressure in each grid block can be easily calculated by computing the matrix solution in Matlab®.

3.3.2.2 Saturation Profile and Total Fluid Velocity

Saturation profile

As discussed previously, equation (3.44), the saturation profile along the cell, can be updated by applying the values of p^{n+1} that were solved from pressure profile (linear system in equation (3.48)).

Total fluid velocity

In order to assess the oil production from the economic perspective the estimation of water breakthrough time becomes crucial in the process. To achieve a better understanding of water breakthrough, the total fluid velocity is necessary. This value is

calculated as follows:

The total fluid velocity can be written as:

$$u_t = u_w + u_o , \tag{3.49}$$

Applying Darcy's Law, equation (3.49) becomes:

$$u_{t,i+1/2} = (\frac{Kk_{rw}}{\mu_w} + \frac{Kk_{ro}}{\mu_o}) \cdot (\frac{p_i - p_{i+1}}{\Delta x}) . \tag{3.50}$$

The saturation distribution is used to determine the relative permeability calculated by the Corey's model (equations (3.45) and (3.46)) in equation (3.50). Therefore, once saturation and pressure are solved the total fluid velocity can be easily calculated along the distance for each time level. The programming procedures can be summarized by Figure 3.3:

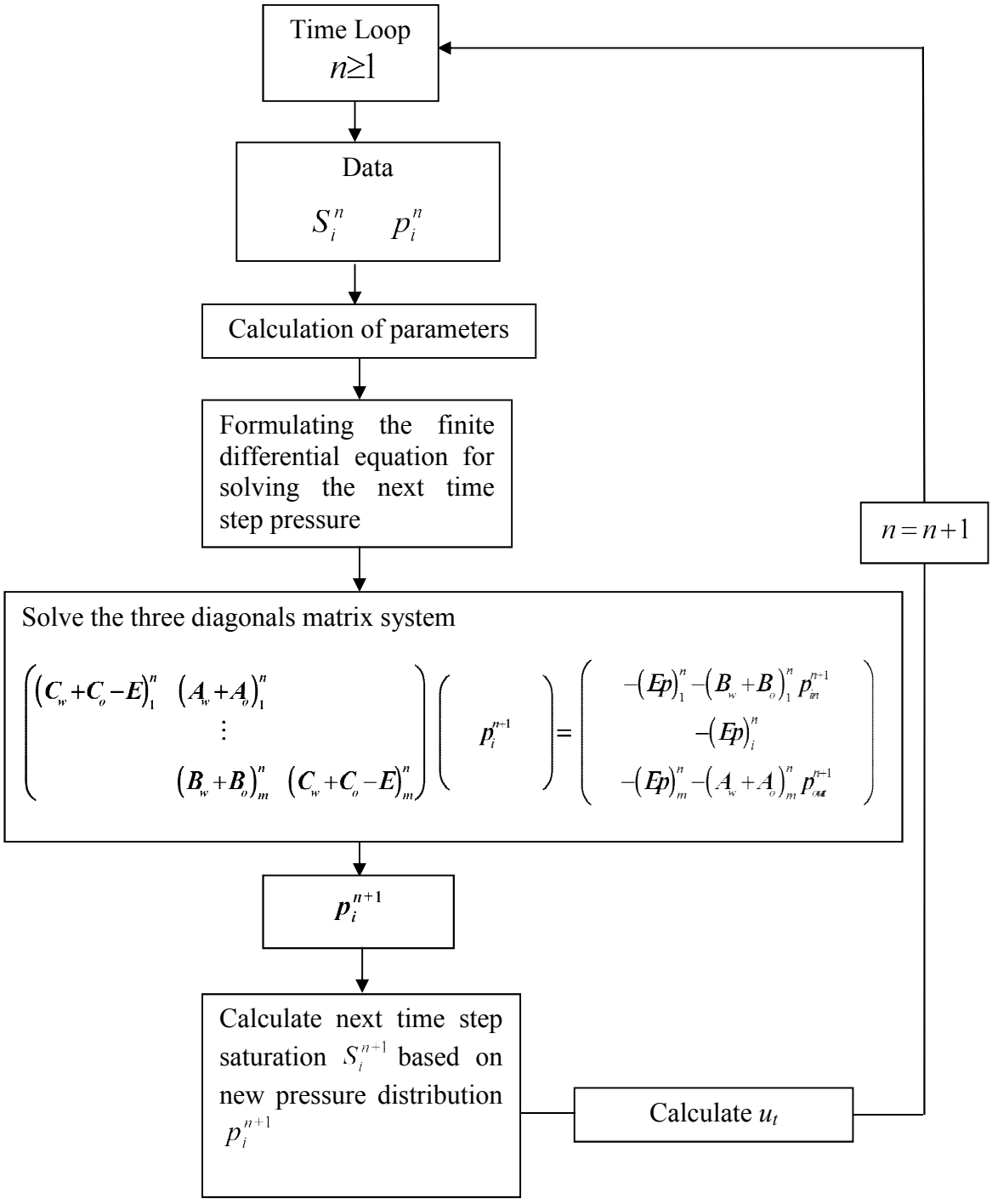

Figure 3.3 Summarized by The Flow Chart for Solving One-Dimension Water Flooding

3.4 Case Study under the Constant Pressure Boundary Conditions

In this section we compare the results of two cases developed for water flooding including breakthrough time, saturation profile, and pressure distribution. The numerical solutions will be presented graphically and discussed from a physical point of view. The conditions used to generate the numerical simulation are from the text book "PVT and Phase Behaviour of Petroleum Reservoir Fluids" by Danesh (1998)

Assumptions

Assumptions of the model include:

1) The model is for one-dimension horizontal flow.
2) Capillary pressure is negligible.
3) The fluids are incompressible.
4) No mass transfer occurres between the water and oil phases.
5) Viscosities of both liquids are assumed constant and independent of pressure.
6) Reservoir formation will not be deformed during the depletion, $c_{pv} = 0$.

3.4.1 Input Parameters

Water is continuously injected into the reservoir at constant injecting pressure (21 MPa) during water flooding. The outlet pressure is fixed to 17 MPa which is equal to the initial reservoir pressure. At the injection point, the formation rock is saturated by 70% water and 30% residual oil. Initially, the reservoir water saturation is 25% and the oil saturation is 75%. The reservoir formation is 100 meters long with a porosity of 0.18 and a

permeability of 1 Darcy. All values are shown in Table 3.1.

3.4.2 Case Studies

1) In the first case oil is the least mobile phase compared with water. The viscosity of oil is 20 cP which is 20 times larger than water, 1cP.
2) In the second case water is assumed to be much more viscous than oil, having a viscosity of 20 cP with the oil viscosity is equal to 1cP.

Table 3.1 Parameters used in case study

Data	Unit	Case 1	Case 2
μ_o	Pa·s	0.02	0.001
μ_w	Pa·s	0.001	0.02
μ_o / μ_w	-	20	0.05
L	m	100	
ϕ	-	0.18	
P_{in}	Pa	2.1×10^7	
P_{res}^0	Pa	1.7×10^7	
P_{out}	Pa	1.7×10^7	
S_{or}	-	0.3	
S_{wc}	-	0.25	
K	m^2	1×10^{-12}	
β_o	-	1	
β_w	-	1	
k_{rw}	-	$0.2\cdot(\frac{S_w - S_{wc}}{1 - S_{wc} - S_{or}})^2$	
k_{ro}	-	$0.8\cdot(\frac{1 - S_w - S_{or}}{1 - S_{wc} - S_{or}})^2$	

3.4.3 Results

3.4.3.1 Saturation Profile and Pressure Distribution

Under continuous injection, the water front travels along the reservoir formation from the injection point to the outlet boundary displacing the oil phase. The water breakthrough time is calculated numerically for case 1 ($\mu_o / \mu_w = 20$) and case 2 (($\mu_o / \mu_w = 0.05$) and is found to be 27 and 120 days, respectively. Figure 3.4 shows the water front propagation corresponding to four different times (0.25, 0.5, 0.75, 1of breakthrough time) for the two cases. As illustrated by Figure 3.4 the front is located at different positions along the formation at different times. As shown in Figure 3.5, the shape of fractional flow curve behaves differently according to different fluid systems. The values of water saturation at the front from Figure 3.4 are approximately 0.43 and 0.68 for case 1 ($\mu_o / \mu_w = 20$) and case 2 (($\mu_o / \mu_w = 0.05$), respectively and this can be also observed from Figure 3.5. Under constant pressure injection the reservoir pressure will increasing with time. The distribution of pressure, therefore, is different at each time step. Figure 3.6 shows the pressure profiles at 0.25 and 0.75 of breakthrough time in both cases. The higher injection pressure inlet is responsible for the fluid flow and the pressure profile moves from left to right (injection to production) with time.

Since discontinuity appears in shock front, the pressure does not vary smoothly along the reservoir formation. As shown by Figure 3.6, the break point has been observed in the pressure profile. The shape of pressure profile changes at the same location point as the oil-water shock as illustrated in Figure 3.7.

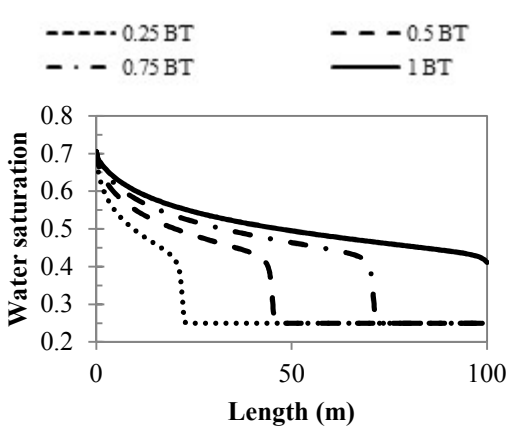

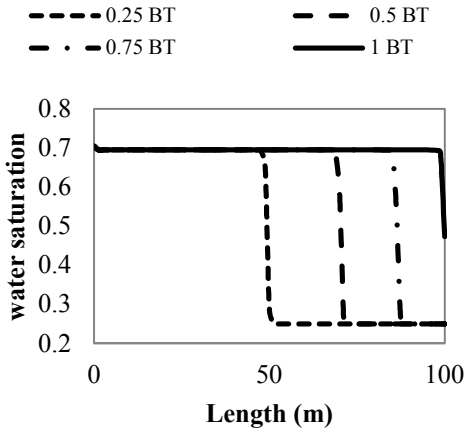

3.4a (case 1 $\mu_o > \mu_w$)

3.4b (case 2 $\mu_o < \mu_w$)

Figure 3.4 Saturation Profile at Water Breakthrough Time 0.25, 0.5, 0.75, 1

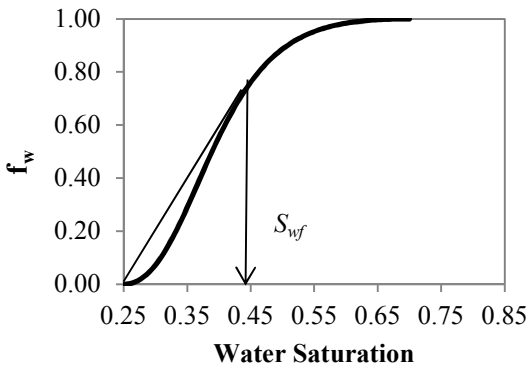

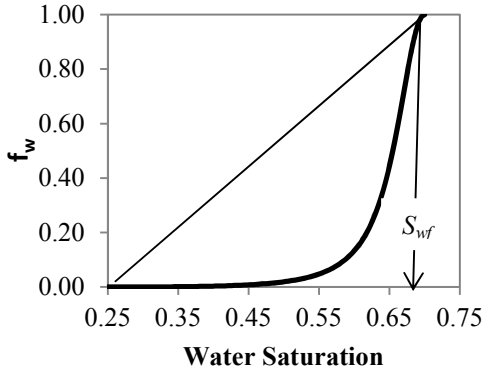

3.5a (case 1 $\mu_o > \mu_w$)

3.5b (case 2 $\mu_o < \mu_w$)

Figure 3.5 Fractional flow curve of case 1 ($\mu_o > \mu_w$) and case 2 ($\mu_o < \mu_w$)

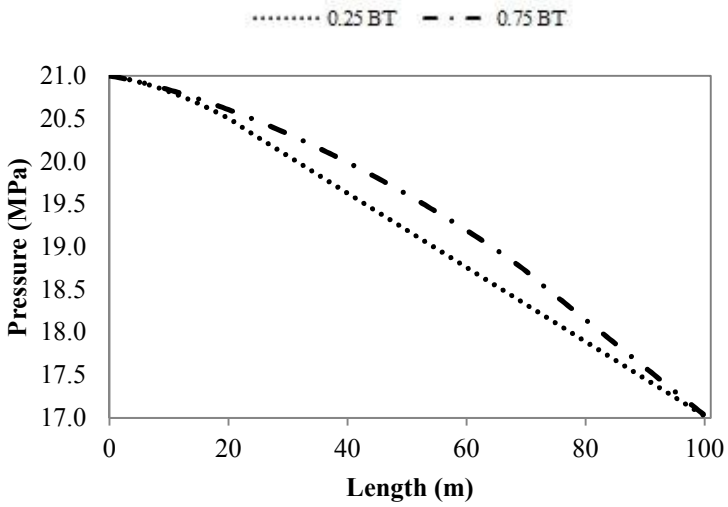

3.6a (case 1 $\mu_o > \mu_w$)

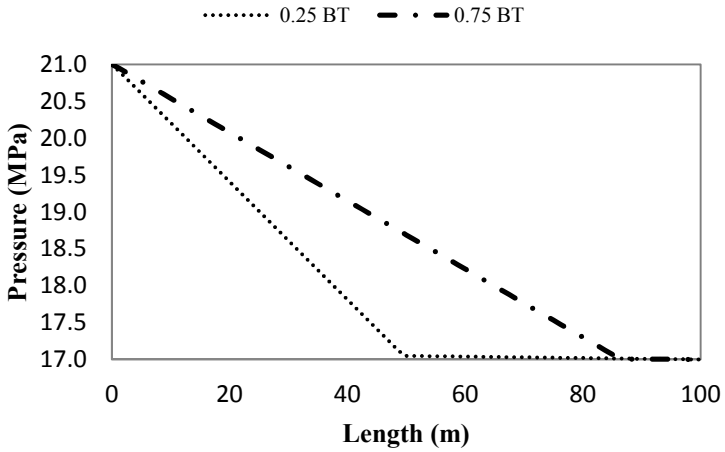

3.6b (case 2 $\mu_o < \mu_w$)

Figure 3.6 Pressure Distribution at Water Breakthrough Time 0.25, 0.75

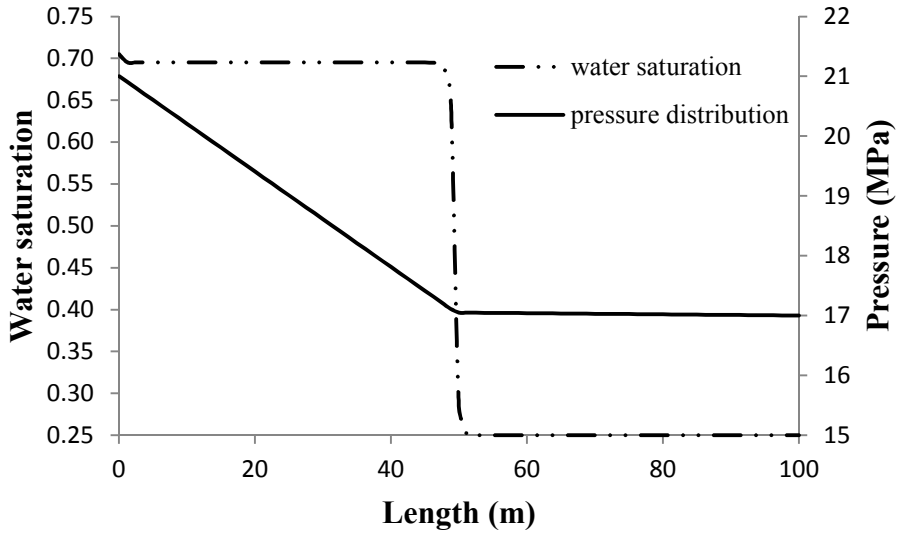

Figure 3.7 Pressure Distribution vs. Water Saturation at 0.25 Breakthrough Time in Case 2 ($\mu_o < \mu_w$)

Comparison of saturation profiles

As shown in the figures above the saturation profiles in the two cases show the same trend. The shock front is moving from the injector to the producer and eventually water breaks through. The average reservoir pressure keeps increasing with time. The break point is observed in pressure profile at the location where the water front is passing through.

The differences are shown by Figure 3.8. As shown, the front saturation is different in case 1($\mu_o / \mu_w = 20$) and case 2 ($\mu_o / \mu_w = 0.05$). The front saturation keeps constant around 1-S_{or} in case 2 ($\mu_o / \mu_w = 0.05$) while in case 1 ($\mu_o / \mu_w = 20$) it is only around 0.43 resulting continuously increasing water saturation after water breakthrough. Due to the different mobility ratio water breaks through at different times. When the water is less dense compared with oil, water travels faster than oil leading to an early breakthrough

time. This can be proved by the comparison between these two cases. In case 1, the water viscosity is 20 times less than the oil viscosity, however, in the second case water viscosity is 20 times larger than oil viscosity. The corresponding breakthrough time of case 1 and case 2 is 27 days, and 120 days, respectively.

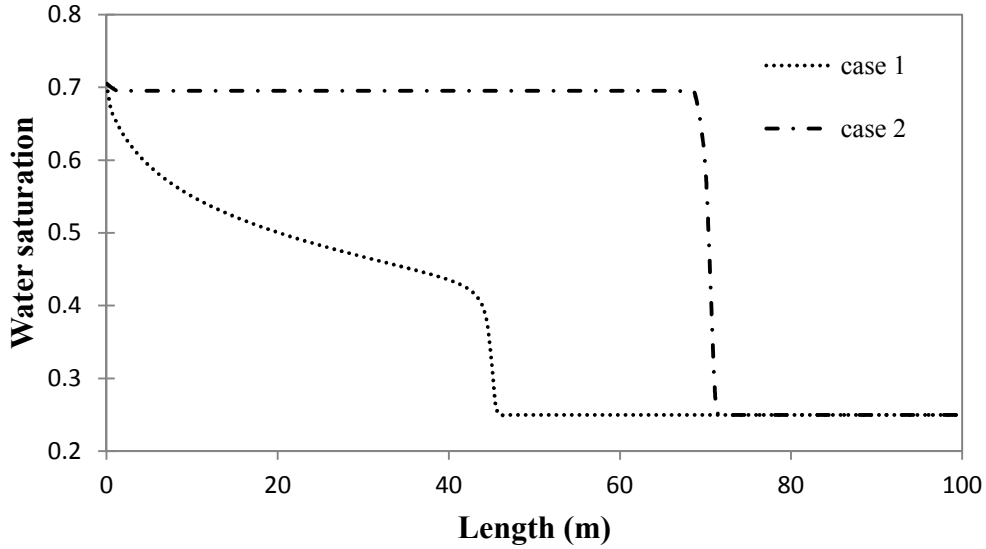

Figure 3.8 Water Saturation Profile at 0.5 Breakthrough Time of Each Case

3.4.3.2 Total Fluid Velocity

Recall the equation (2.4)

$$\frac{\partial}{\partial x}(u_x + u_o) = \frac{\partial u_t}{\partial x} = 0 . \qquad (2.4)$$

Equation (2.4) indicates a constant total flow rate along the length. Although the flow rate remains constant along the distance it will change with time.

Comparison of velocity distribution

The velocity distribution varies with time. The results of the simulation show that the total fluid velocity increases during the injection when the water viscosity is less than oil viscosity ($\mu_o > \mu_w$), i.e. case 1. The front saturation of case 1 is less than the maximum water saturation of 70%; hence after breakthrough the water saturation continues to increase as does the total velocity. In the case when oil is less viscous than water (i.e. case 2, $\mu_o < \mu_w$), the total fluid velocity deceased then remained almost constant. The front saturation of this case is around 70% therefore after breakthrough the total velocity remains constant. Figure 3.9 shows that the total fluid velocity in case 1 ($\mu_o / \mu_w = 20$) gradually increases from 1.6×10^{-6} m/s to 3.5×10^{-6} m/s with time, in the meanwhile in case 2 ($\mu_o / \mu_w = 0.05$) the total fluid velocity starts with 17×10^{-6} m/s then drops to 1.7×10^{-6} m/s and after that stays almost constant during water flooding.

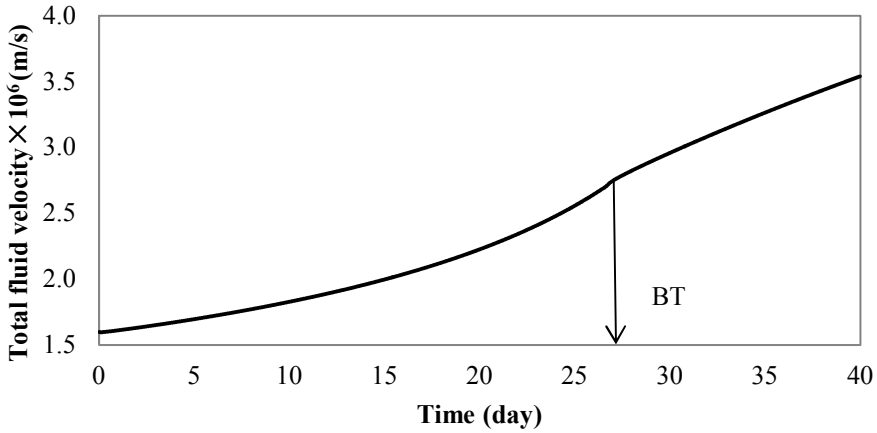

3.8a (case 1 $\mu_o > \mu_w$)

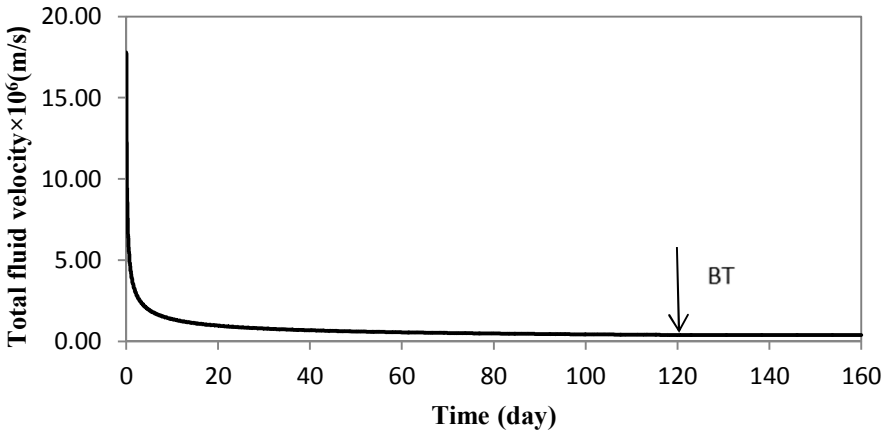

3.8b (case 2 $\mu_o < \mu_w$)

Figure 3.9 Total Fluid Velocity

The time dependent total velocity can be also observed by defining F_w as:

$$F_w = u_t \cdot f_w, \tag{3.51}$$

the change of F_w with water saturation in case 1 ($\mu_o > \mu_w$) at different times (0.25BT, 0.5BT, 0.75BT and BT) are shown in Figure 3.10. In this figure the graph of F_w shifts at different time steps. Since the fractional flow function f_w is a function only of water saturation, F_w changes with the varying total fluid velocity at different times.

The total fluid velocity is not constant during water flooding when the pressure boundary conditions are kept constant. In fact, it is a function of time only.

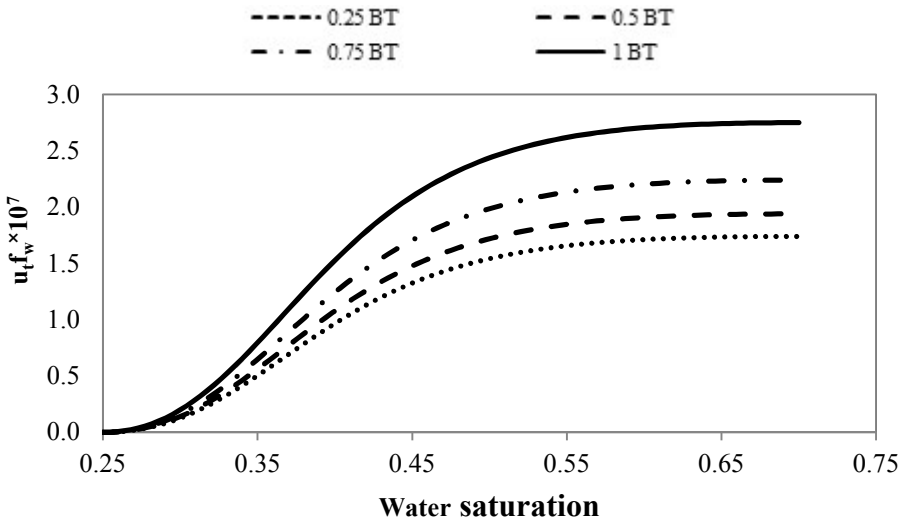

Figure 3.10 F_w vs. Water Saturation

Since the velocity does not remain constant, the shock front velocity is varying with time. The breakthrough time cannot be calculated by simply using length divided by front velocity. The Buckley-Leverett theory for a constant flow rate therefore fails to determine water breakthrough time under fixed constant pressure boundaries.

3.5 Comparison between Numerical and Analytical Solutions

In Section 2.1.2, the analytical solution (Johansen and James, 2012) was introduced as an extension of the Buckley-Leverett theory to constant pressure boundary conditions. This method is applicable for varying total fluid velocity before and after water breakthrough. Important information, such as the total velocity, the pressure distribution and water breakthrough time, can be calculated from the equations provided by this analytical method. The results of both the numerical solution and the analytical solution will be

compared in this section.

The numerical solution was completed using two different cases in Section 3.4. It is necessary to test the validity of the numerical solution by applying the analytical method under the same conditions. In this section, the comparison between the numerical and the analytical solutions is illustrated and discussed.

3.5.1 Numerical and Analytical Comparison

For the purpose of convenience, the total fluid velocity values calculated by both the numerical and the analytical methods are presented in the same figure. The two case comparisons are shown and the results show a good agreement between the numerical and analytical solutions. As shown in Figure 3.11, the numerical solution agrees well with the analytical solution before and after water breakthrough for both cases. The numerical and analytical solutions in case 2 are almost identical (Figure 3.11b). The water breakthrough time in each case, generated by numerical simulation is slightly earlier compared to the analytical solution. The breakthrough time for the first case ($\mu_o > \mu_w$) is calculated as 28.5 days by analytical solution compared to 27 days generated from the numerical solution. In the second case ($\mu_o < \mu_w$) the analytical breakthrough time is 122.7 days, approximately 3 days later compared with 120 days calculated by the numerical method. This is primarily due to the numerical smearing effect on the water displacement front which makes a unique definition of breakthrough time impossible. The comparison of the numerical and analytical work validates the finite-difference method presented in previous sections. Figure 3.11a shows a break point in the analytical solution when the water front approaches the outlet (time is close to the breakthrough time) due to round-off error. By substituting equation (2.10) into equation (2.9), the total

fluid velocity before breakthrough time can be rewritten as:

$$u_t = \frac{\Delta p}{\frac{\zeta x_f}{f'(S_{wf})} - \frac{x_f}{\lambda_o} + \frac{L}{\lambda_o}}. \tag{3.52}$$

Equation (3.52) indicates that when the water front approaches the outlet the front position x_f is infinitely close to the total length L causing the round-off numerical error during the calculation.

The error can be minimized by using total length (L) instead of actual front position (x_f) when the distance between water front and total length is less than one meter. The result after minimizing round-off error is shown in Figure 3.12. As shown, the substitution of the total length reduces the round-off error.

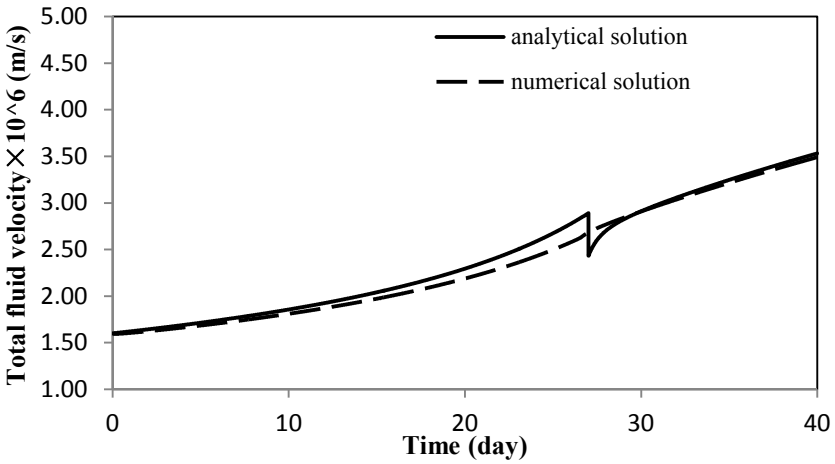

3.10a (case 1 $\mu_o > \mu_w$)

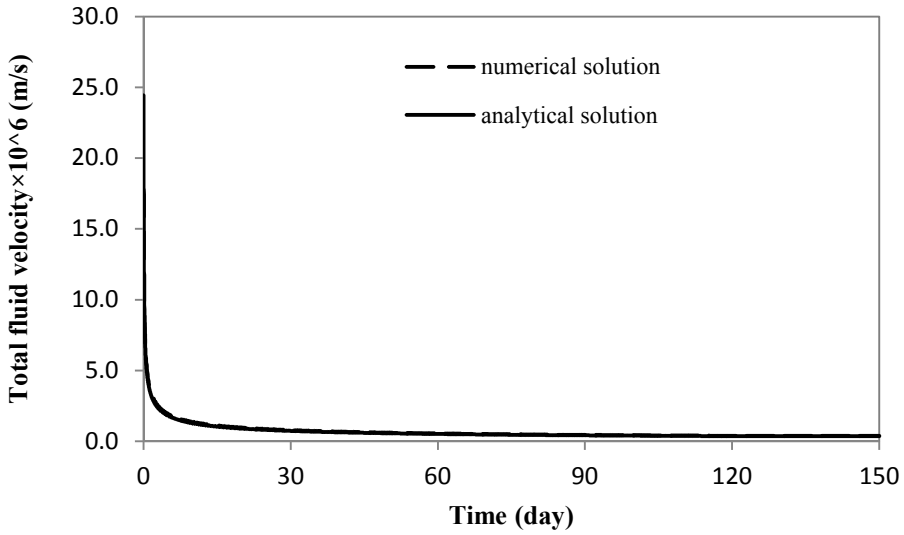

3.10b (case 2 $\mu_o<\mu_w$)

Figure 3.11 Comparison between Numerical and Analytical Solutions

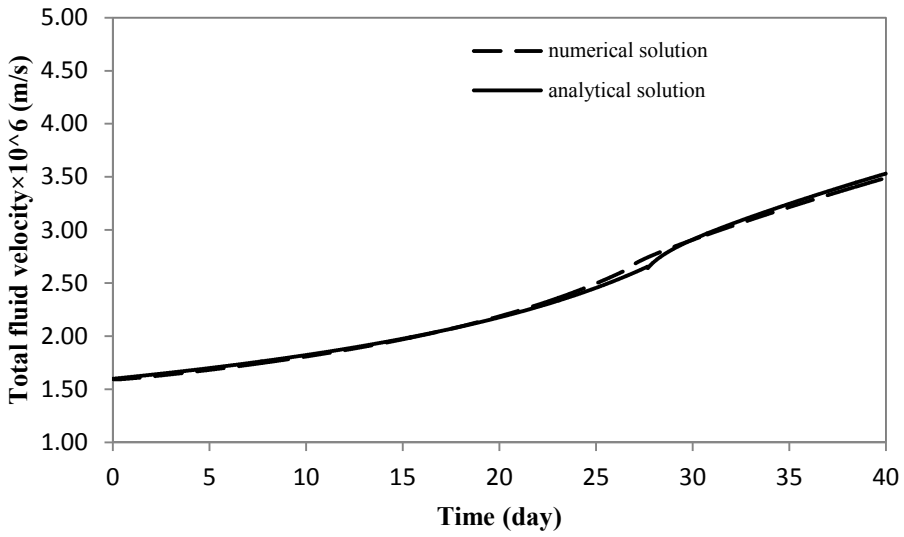

Figure 3.12 Comparison between Numerical and Analytical Solutions of Case 1 after Minimizing Round-off Error

3.5.2 Discussion of Numerical Errors

The stability of the numerical method is important as it directly affects the accuracy of

the numerical solutions. If computational errors are introduced in any step, they may be amplified during the computing process and obtaining reasonable information from the simulation becomes impossible.

Therefore, the selection of an appropriate formulation for the reservoir simulation becomes a key factor.

In the current study, a single point upstream weighting method has been applied to obtain the mobility between two blocks. It is well known that single point upstream approach is a first order approximation in which mobility between two blocks is assumed to be equal to the upstream block's mobility, and also that the appropriate stability criterion for this scheme is the CFL condition discussed in Section 3.2.3.1 equation (3.25). In the numerical simulation, the solutions are obtained by applying the upstream method in which the average fluid mobility is calculated from the water saturation from the previous grid block. However, if the downstream water saturation is applied, the water will not be able to flow. The upstream method is conditionally stable while the downstream is unconditionally unstable.

The accuracy of simulation results also depends on the number of grid blocks. A better agreement between the numerical and analytical solutions can be achieved by refining the number of grid blocks during simulation. Figure 3.13 shows the water saturation profiles at different numbers of grid blocks compared to analytical solution which is calculated by using equation (2.10). As indicated by this figure, by refining grids from 100 to 1000 the numerical dispersion is alleviated by reducing the truncation error (first order in both time and space).

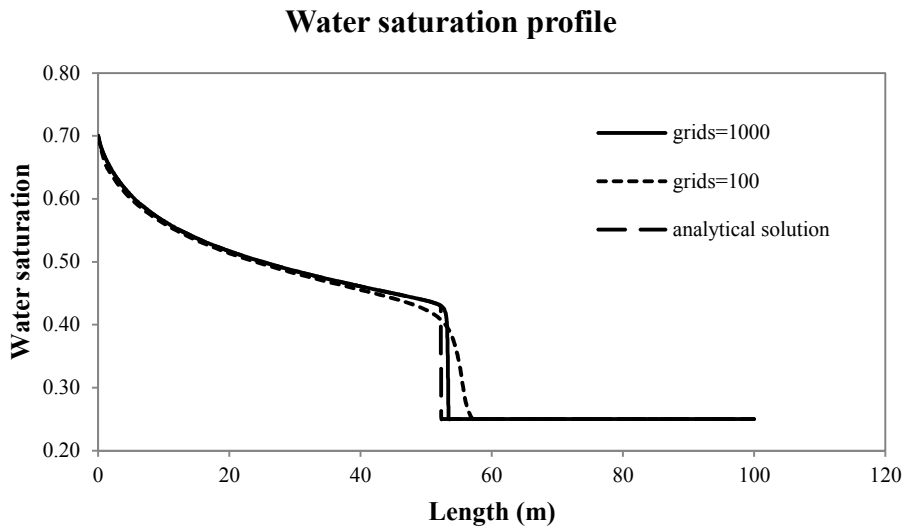

Figure 3.13 Water Saturation Profile for Case 1 ($\mu_o > \mu_w$) under Different Numbers of Grid Blocks

3.6 Summary

In this chapter the simple water injection with constant pressure boundary conditions has been studied numerically using IMEPS method. The numerical solution has been validated by the great agreement between numerical and analytical solutions. Therefore, the numerical IMPES scheme is adopted for study of carbonated water injection (CWI) which is discussed in Chapter 4.

Chapter 4 Carbonated Water Injection

4.1 Introduction

The simple water injection, discussed in chapter 3, is a secondary oil recovery strategy focused on oil displacement and the pressure maintenance. After water injection, tertiary oil recovery (EOR) can be applied to increase incremental oil recovery. Following on chapter 3, here we will develop the mathematical model for injecting CO_2 in carbonated water injection (CWI) under constant pressure boundaries to predict oil recovery, saturation distribution and the pressure distribution from injector to producer.

Although much theoretical work has been done regarding CO_2 injection, there is limited work focusing on CWI. In this chapter a mathematical model is developed based on mass conservation to study the performance of CWI. The effects of viscosity and interfacial tension are considered in this model, as important factors in enhanced oil recovery (EOR). However, the oil swelling effect is not included in the model.

Since the WI model has been validated by comparing the analytical and numerical solutions, a modest extension from water injection to carbonated water injection is deemed valid. The numerical approach used in Chapter 3, therefore, also is used here.

4.2 Mathematical Model

The mathematical model is based upon the mass conservation equations that describe water-oil two-phase simultaneous flow. The free CO_2 gas phase is not present, and the solubility of CO_2 under high reservoir pressure is ignored, meaning that physically the

CO_2 only exists as a component of the liquid water or liquid oil phases. Differing from the water injection that is considered as a two-component two-phase fluid system, the CWI process is a three-component, two-phase problem. The black oil model is not applicable in this case since the mass of each phase (water or oil) is not conserved due to the transfer of CO_2 between the water and oil phases. In this section, a one-dimensional compositional model is developed to study the reservoir behavior and the performance of CWI.

The following assumptions are made in this numerical simulation:

1. Flow is one dimensional horizontal, i.e., the effect of gravity is neglected.
2. There is no source or sink term between injector and producer.
3. The capillary pressure effect is negligible.
4. The reservoir pressure is sufficiently high that no free CO_2 or hydrocarbon gases exist in the reservoir.
5. Water and oil flow simultaneously and CO_2 is present in solution in these two phases.
6. CO_2 transfers from the water to the oil phase but there is no mass transfer of oil and water components between phases.
7. The diffusion of CO_2 is ignored. The advance of CO_2 is only due to the movement of oil and water.
8. In an oil-CO_2-water fluid system, the equilibrium between oil and water saturated with CO_2 is reached instantaneously. The maximum solution of CO_2 in both oil and water phases is obtained at any point in time.
9. The formation properties such as porosity and permeability are constant during

the CWI process.

The compositional model is based on the mass conversation for each component—water, oil and CO_2, respectively:

$$\begin{aligned}
&\frac{\partial}{\partial t}\left[\rho_w^{RC}\phi S_w\left(1-c_{co_2}^w\right)\right]=\frac{\partial}{\partial x}\left[\rho_w^{RC}u_w\left(1-c_{co_2}^w\right)\right],\\
&\frac{\partial}{\partial t}\left[\rho_o^{RC}\phi S_o\left(1-c_{co_2}^o\right)\right]=\frac{\partial}{\partial x}\left[\rho_o^{RC}u_o\left(1-c_{co_2}^o\right)\right], \qquad (3.53)\\
&\frac{\partial}{\partial t}\left(\rho_o^{RC}\phi S_o c_{co_2}^o+\rho_w^{RC}\phi S_w c_{co_2}^w\right)=\frac{\partial}{\partial x}\left(\rho_o^{RC}u_o c_{co_2}^o+\rho_w^{RC}u_w c_{co_2}^w\right).
\end{aligned}$$

Since the densities of the water and oil phases vary with pressure and CO_2 solubility at different locations and times, for simplicity, the stock tank condition is chosen to be the reference state in which the densities of the water and oil phases are constant. Therefore, the above system of equations (3.53) can be rewritten as:

$$\begin{aligned}
&\frac{\partial}{\partial t}\left[\frac{\phi}{\rho^*_w}S_w\left(1-c_{co_2}^w\right)\right]=\frac{\partial}{\partial x}\left[\frac{u_w}{\rho^*_w}\left(1-c_{co_2}^w\right)\right],\\
&\frac{\partial}{\partial t}\left[\frac{\phi}{\rho^*_o}S_o\left(1-c_{co_2}^o\right)\right]=\frac{\partial}{\partial x}\left[\frac{u_o}{\rho^*_o}\left(1-c_{co_2}^o\right)\right], \qquad (3.54)\\
&\frac{\partial}{\partial t}\left[\frac{\phi}{\rho^*_w}S_w c_{co_2}^w\rho_w^{ST}+\frac{\phi}{\rho^*_o}S_o c_{co_2}^o\rho_o^{ST}\right]=\frac{\partial}{\partial x}\left[\frac{u_w}{\rho^*_w}c_{co_2}^w\rho_w^{ST}+\frac{u_o}{\rho^*_o}c_{co_2}^o\rho_o^{ST}\right].
\end{aligned}$$

where, ρ^*_w and ρ^*_o is the density ratio between stock tank conditions and reservoir conditions for the water and oil, respectively.

The saturation and CO_2 mass concentration equations are incorporated to solve the numerical model:

$$S_w+S_o=1, \qquad (3.55)$$

$$c_{co_2}^o=\gamma c_{co_2}^w, \qquad (3.56)$$

where, γ is the partition coefficient of CO_2 between the water and oil phases.

Equations (3.54), (3.55) and (3.56) describe the three-component two-phase flow, which contains five equations with five unknowns. The five unknowns are the saturation of oil and water (S_o , S_w), CO_2 mass concentrations in oil and water ($c^o_{co_2}$, $c^w_{co_2}$) and pressure (p).

4.3 Partitioning of CO_2 in a Three-component Two-phase System

The solubility of CO_2 in oil is two to ten times greater than its solubility in water in most cases. During carbonated water flooding, CO_2 transfers from the water to the oil resulting in a change in the oil's properties. An oil viscosity reduction with increasing CO_2 solubility in oil phase was observed by many experimental researchers (Enick and Klara, 1990). According to the results of the experiments, the oil swelling factor caused by dissolved CO_2 contributes to the additional oil recovery, especially in non-heavy oil reservoirs. Moreover, the residual oil saturation decreases with sufficiently low IFT due to the high CO_2 concentration in the oil phase. Therefore, determining the amount of CO_2 in the oil phase becomes a key step for carbonated water flooding simulation. However, due to the lack of information regarding the CO_2 distribution between oil and water after injection, a simple scheme is applied. In this calculation water and oil are assumed to be saturated by CO_2 simultaneously.

In three-phase flow, when the system reaches equilibrium, the CO_2 mole fractions in gas, water and oil satisfy the relation:

$$k^w_{co_2} x^w_{co_2} = k^o_{co_2} x^o_{co_2} = y_{co_2}, \tag{3.57}$$

where $k_{co_2}^{w}$ and $k_{co_2}^{o}$ are equilibrium coefficients regarding CO_2 mole fraction; $x_{co_2}^{w}$ and $x_{co_2}^{o}$ are CO_2 mole fraction in water and oil phases and y_{co_2} is the CO_2 mole fraction in the gas phase.

In this study two-phase flow (water and oil) is assumed. Therefore, the gas phase is no longer present in the system. The new relationship of CO_2 mole fractions in liquid phase is:

$$k_{co_2}^{w} x_{co_2}^{w} = k_{co_2}^{o} x_{co_2}^{o} . \tag{3.58}$$

The compositional model is based on the mass conservation; hence the mole fraction needs to be converted to mass concentration during the numerical calculation.

By converting to mass concentration the relationship of CO_2 mass concentration in liquid phase becomes:

$$\overline{k}_{co_2}^{w} c_{co_2}^{w} = \overline{k}_{co_2}^{o} c_{co_2}^{o} , \tag{3.59}$$

where, $\overline{k}_{co_2}^{w}$ and $\overline{k}_{co_2}^{o}$ are equilibrium coefficients regarding CO_2 mass concentration in separated systems (water-CO_2 and oil-CO_2).

Equation (3.59) can be also written as:

$$c_{co_2}^{o} = \frac{\overline{k}_{co_2}^{w}}{\overline{k}_{co_2}^{o}} c_{co_2}^{w} = \gamma c_{co_2}^{w} . \tag{3.60}$$

The partition coefficient (γ) of CO_2 in three-component two-phase fluid system is defined as the ratio between mass equilibrium coefficients:

$$\gamma = \frac{\overline{k}_{co_2}^{w}}{\overline{k}_{co_2}^{o}} . \tag{3.61}$$

In the lack of information as how CO_2 partitions between water and oil when CO_2 is insufficient to saturate both phases, a simple scheme is adopted. Since in this study we assume (1) the equilibrium between oil and water saturated with CO_2 is reached instantaneously, and (2) there is no interacting between water and oil components, the CO_2 solubility in water and oil as the function of pressure can be calculated from separate systems of water-CO_2 and oil-CO_2 (Ramesh and Dixon, 1972).

4.3.1 CO_2 Solubility

As discussed in previous section the partition coefficient γ is calculated from the mass equilibrium coefficients of CO_2 in water phase ($\overline{k}^{w}_{co_2}$) and CO_2 in oil phase ($\overline{k}^{o}_{co_2}$). To determine these two coefficients two fluid systems, water-CO_2 and oil-CO_2, are applied. In each system the CO_2 is present as both solvent in liquid phase and gas in vapour phase. The mass concentration of CO_2 in gas phase is assumed to be one.

4.3.1.1 CO_2 Solubility in Water

The compositional models used to simulate the enhanced oil recovery processes usually neglect the solubility of hydrocarbon in water. However, as an exception, CO_2 has much higher solubility in water compared to hydrocarbon components. Due to the solubility in water, CO_2-assisted water flooding is now applied for mobility control in oil recovery processes. In general, to increase the CO_2 solubility in the aqueous phase higher pressure and lower temperature conditions are required. The solubility of CO_2 in water has been studied by many researchers. Based on Henry's Law (Li and Nghiem, 1986) a model was

developed to predict the CO_2 solubility in liquid phase under the equilibrium fluid system. Using the same theory, Enick and Klara (1990) estimated the CO_2 solubility in distilled water. A compositional model was presented by Chang *et al*. (1998) to describe CO_2 flooding including the CO_2 solubility in water.

In this study, the models developed by Duan and Sun (2003) were selected. The model predicts the CO_2 solubility in both pure and salt water under a wide range of pressures and temperatures. The solubility model in their work is based on the balance of CO_2 chemical potential between the liquid and gas phases at equilibrium, i.e.

$$\ln\left(\frac{y_{co_2} p}{m_{co_2}}\right) = \frac{\mu_{co_2}^{l(0)} - \mu_{co_2}^{v(0)}}{RT} - \ln\varphi_{co_2} + \ln\alpha_{co_2}, \tag{3.62}$$

where $\mu_{co_2}^{l(0)}$ and $\mu_{co_2}^{v(0)}$ are the standard liquid and gas chemical potential at ideal conditions, y_{co_2} is the mole faction of CO_2 in the gas phase (which is assumed to be one during the simulation), φ_{co_2} is CO_2 fugacity coefficient, α_{co_2} is activity coefficient, respectively, and m_{co_2} is molality of CO_2 (mol/kg) in the liquid phase.

Since CO_2 is assumed to occupy the whole gas phase and $\mu_{co_2}^{v(0)}$ is set to zero, equation (4.9), regarding molality of CO_2 in the water phase, can be rewritten as

$$\ln m_{co_2} = \ln\left(\varphi_{co_2} p\right) - \frac{\mu_{co_2}^{l(0)}}{RT}, \tag{3.63}$$

where, the term $\frac{\mu_{co_2}^{l(0)}}{RT}$ and φ_{co_2} can be calculated from the correlations provided.

The CO_2 mass concentration in the water-CO_2 fluid system can be written as:

$$c_{co_2}^{w,w-co_2} = \frac{\mathrm{MW}_{co_2} \cdot m_{co_2}}{1000}. \quad (3.64)$$

Since CO_2 is assumed to take over the whole gas phase, the mass equilibrium coefficient ($\bar{k}_{co_2}^{w}$) can be calculated from following equation:

$$\bar{k}_{co_2}^{w} = \frac{1}{c_{co_2}^{w,w-co_2}}. \quad (3.65)$$

4.3.1.2 CO_2 Solubility in Oil

The major parameter that affects the results of CO_2 flooding in an oil reservoir is the CO_2 solubility in the oil phase. A higher solubility results in a less viscous oil, thus increasing the oil mobility. Moreover, with dissolved CO_2, oil swelling occurs during CO_2 flooding. Oil swelling helps to increase oil recovery under unchanged residual oil saturation. Mungan (1964) experimentally showed that the reduction of oil water IFT enhances the efficiency of water injection. In CWI, the IFT can be further decreased due to the dissolved CO_2 in the water and oil phases, resulting in an improved overall performance. Due to these important effects on the oil recovery process, CO_2 solubility in oil has been studied by many researches. A graphical correlation (Welker, 1963) of CO_2 solubility was developed as a function of pressure and oil API gravity at a constant temperature. Simon and Graue (1965) presented solubility data for dead oils at a temperatures range of 43.33 ^{o}C to 121.1 ^{o}C and pressures up to 15.86 MPa. Later on, Mehrotra and Svrcek (1986) calculated the CO_2 solubility at pressures up to 6.38 MPa and temperatures from 23.89 ℃ to 97.22 ℃. Emera and Sarma (2006) developed a genetic algorithm based on experimental data to predict the CO_2 solubility and oil phase properties as a function of

dissolved CO_2. The results of these correlations have been validated by published experimental data with a lower error compared to other correlations.

In this study the approach of Emera and Sarma (2006) using GA-based correlations are adopted to calculate CO_2 solubility as well as other oil properties.

In a CO_2-oil fluid system two phases (CO_2 and oil) are assumed to present. Since CO_2 is in the gaseous state the following correlations are applied to calculate the mole fraction of CO_2 in oil phase ($x_{co_2}^{o,o-co_2}$):

$$x_{co_2}^{o,o-co_2} = 1.748 - 0.5632Y + 3.273Y^{0.704} - 4.3Y^{0.4425}, \tag{3.66}$$

where,

$$Y = \gamma_o \left[0.006897 \frac{(1.8T + 32)^{1.125}}{p - p_b} \right]^{\exp\left(\frac{1}{MW_o}\right)}.$$

The above equations show that the CO_2 solubility in this GA-based models depends on the oil specific gravity (γ_o), the oil bubble point pressure (p_b), temperature (T) and the oil molecular weight (MW_o).

The CO_2 mass concentration can be then calculated by converting from the mole fraction:

$$\begin{aligned} c_{co_2}^{o,o-co_2} &= \frac{M_{co_2}}{M_{co_2} + M_o} = \frac{MW_{CO_2} \cdot x_{co_2}^{o,o-co_2}}{MW_{CO_2} \cdot x_{co_2}^{o,o-co_2} + (1 - x_{co_2}^{o,o-co_2}) MW_o} \\ &= \frac{MW_{CO_2} \cdot x_{co_2}^{o,o-co_2}}{MW_o - x_{co_2}^{o,o-co_2} \left(MW_o - MW_{CO_2} \right)}, \end{aligned} \tag{3.67}$$

where M_o and M_{co_2} are mass of oil and CO_2, respectively.

According to the assumption made previously (CO_2 occupies the entire gas phase) the mass equilibrium coefficient ($\overline{k}_{co_2}^{w}$) is expressed as:

$$\bar{k}^{o}_{co_2} = \frac{1}{c^{o,o-co_2}_{co_2}}. \tag{3.68}$$

All the information used to determine the partition coefficient (γ) of CO_2 in a CWI fluid system are known from the above correlations under reservoir condition for a specific oil composition, hence, γ now can be calculated using equation (3.61).

4.4 Fluid Characterization

Due to the presence of CO_2 in the liquid phase, the properties of oil and water vary during carbonated water flooding. Oil swelling and the reduction of oil viscosity are major mechanisms that affect the oil recovery in CWI; hence, these need to be evaluated during the calculation with the change of total pressure and CO_2 mass concentration in each phase. The dissolved CO_2 in the water phase also results in a variation of water properties.

4.4.1 Oil Phase Properties

4.4.1.1 CO_2-Oil Viscosity

Oil viscosity decreases significantly with increasing of CO_2 solubility. In the isothermal reservoir condition, oil viscosity varies mainly due to the change of CO_2 mass concentration and total pressure.

The correlation for oil viscosity used here is the GA-based model (Emera and Sarma, 2006) shown in Section 2.4.1:

$$\mu_o = y\mu_{oi} + A\left(\frac{x^{o}_{co_2}}{\mu_{oi}}\right), \tag{2.16}$$

where

$$y = X^B,$$

$$X = \left[C\mu_{oi} \left(\frac{p}{1.8T + 32} \right)^D \right]^{\left(\gamma_o x^o_{co_2}\right)},$$

where A, B, C and D are constants provided in Table 2.1.

4.4.4.2 Change of CO_2-Oil Density

The volume of reservoir oil expands with increasing amounts of dissolved CO_2, but is reduced under higher pressures. Therefore, the reservoir oil density is changed by the effect of both total pressure and CO_2 mass concentration. The oil density increased with an increase of CO_2 solubility which results from the higher pressure (DeRuiter *et al*., 1994). As mentioned in Section 2.4.2 the density correlation (equation (2.17)) in GA-based model (Emera and Sarma, 2006) is adopted in this study.

$$\rho_o = \rho_{oi} - 0.10276 y^{0.608} + 0.1407 y^{0.6133}, \qquad (2.17)$$

where

$$y = \frac{\gamma_o \rho_{oi} \left(p - p_b \right)^{1.25}}{1.8T + 32}.$$

4.4.2 Carbonated Water Properties

4.2.2.1 Carbonated Water Viscosity

A correlation has been proposed (Kestin *et al*., 1978) to calculate the water viscosity where the water viscosity is a function of temperature, pressure and salt concentration but not CO_2 concentration. Since water viscosity is minimally affected by the dissolved CO_2,

we assume that the carbonated water viscosity remains constant irrespective of CO_2 concentration.

4.2.2.2 The Change of Carbonated Water Density

The density of carbonated water varies as a function of pressure. Compared to pressure the effect of dissolved CO_2 on water density is very small which is assumed to be negligible this study. The model of water density under a certain pressure range (34 MPa to 30 MPa) and given reservoir temperature (80 ℃ to 250 ℃) is generated by **PVTsim™** Calcep simulator. By regression, the expression of water density in SI unit is:

$$\rho_w^{RC} = \frac{\rho_w^{ST}}{\left(-2 \cdot 10^{-4} p + 1.0556\right)} \tag{3.69}.$$

4.4.3 IFT of Water-oil

Carbon dioxide (CO_2) is miscible in both the oil and water phases and it is assumed that the interfacial tension between these two liquids decreased with increasing CO_2 concentration. A significant removal of residual oil after simple water flooding has been observed with decreasing IFT (Abrams, 1975). According to the experiment (Shen *et al*., 2006), the residual oil saturation only decreases by reducing IFT to a certain range. In the low interfacial tension region (0.00015 N/m < σ < 0.002 N/m), the residual oil is reduced, thus increasing the oil relative permeability (Kumar *et al*., 1985). However, the interfacial tension between the two liquid phases cannot be measured in this numerical study. Due to limited available literature, the interfacial tension is assumed to be a simple

linear correlation based on the IFT data of water-octane provided by the book (Danesh, 1998). The water-oil IFT (N/m) changes with reservoir temperature (℃) and CO_2 mass concentration:

$$\sigma_{ow} = -0.025c^{o}_{co_2} + 0.02 - 3.235 \cdot 10^{-5}(T - 80)\,. \tag{3.70}$$

To simplify, we assume that the residual oil saturation in this study changes linearly as a function of IFT, with IFT under a low interfacial tension region (0.00015 N/m < σ < 0.002 N/m):

$$S_{or} = S_{or}{}^{0} - 0.039677867\sigma_{ow}{}^{-1}, \tag{3.71}$$

where $S_{or}{}^{0}$ is the reference residual oil saturation (the residual oil saturation before CWI).

4.5 Numerical Simulations

The problem to be solved is a three-component two-phase horizontal one-dimensional fluid system. Carbonated water is injected on one side and oil is produced from the other side of reservoir under constant pressure boundary conditions. The procedures of solution are similar to water flooding simulation which has been discussed in Chapter 3. The IMPES method was used for numerical calculation in order to evaluate the performance of CWI. By substituting equations (3.55) and (3.56) into equation (3.54), the pressure distribution is first solved by applying the known boundary conditions. Water saturation and CO_2 solubility in the water phase are then updated by pressure which was solved previously. The solution from the IMPES method is conditionally stable depending on

the size of time step (Δt), therefore, the appropriate time step need to be selected. As discussed in Section 3.2.3.1, the time step selection here follows the same constraint as the one we adopted in water flooding called CFL (Courant *et al*., 1928).

As mentioned previously, the carbonated water injection model here is an extension of water injection model. The same numerical scheme has been applied in both plain water flooding and carbonated water flooding. Since the numerical solutions of WI have been validated in Chapter 3 the numerical model of CWI is also validated.

4.6 Case Study

Several cases have been studied to validate the simulation results. In order to investigate the factors that affect oil recovery, different scenarios (such as different injection pressures and reservoir temperatures) are included. Since an expected IFT reduction occurs while increasing reservoir temperature, the effect of IFT is also evaluated in this study. Cases are developed under the constant pressure boundary conditions and compared with water injection. The summary conditions applied in different cases studies are shown in Table 4.3. The information used to processed the numerical simulation is from textbook (Danesh, 1998).

4.6.1 Initial Conditions

4.6.1.1 Oil Initial Composition

The initial oil composition is required in order to calculate and update the CO_2-oil properties.

Table 4.1 provides the information of initial oil composition in mole fraction:

Table 4.1 Initial Oil Composition

Component	Mol %
N2	0.02
CO2	1
C1	13.765
C2	4.011
C3	0.986
iC4	0.742
nC4	0.478
iC5	0.42
nC5	0.303
C6	1.571
C7	76.704

4.6.1.2 Initial Reservoir and Fluid Properties

The initial reservoir and fluid properties are required before proceeding to the computing process. The initial information to solve the problem is listed in

Table 4.2:

Table 4.2 Initial Information regarding Reservoir and Fluid Properties

Data	Units (SI)	CWI	WI
p_{res}	MPa	31	
p_{out}	MPa	30	
μ_{oi}	Pa·s	0.009	
μ_w	Pa·s	0.001	
$c_{co_2}^{w\ in}$	--	0.0386	_
$c_{co_2}^{o\ in}$	--	0.56	_
$c_{co_2}^{w\ res}$	--	0.0018718	_
$c_{co_2}^{w\ res}$	--	1.29×10-4	_
ρ_o^{ST}	kg/m^3	874.2	
ρ_w^{ST}	kg/m^3	999	
S_{or}^{0}	--	0.3	
S_{wc}	--	0.25	
L	m	100	
ϕ	--	0.18	
K	m^2	1×10^{-12}	
k_{ro}	--	$k_{ro}=0.8(\frac{1-S_w-S_{or}}{1-S_{wc}-S_{or}})^2$	
k_{rw}	--	$k_{rw}=0.2(\frac{S_w-S_{or}}{1-S_{wc}-S_{or}})^2$	

Table 4.3 Summary of CWI Case Studies

Case	Condition
1 (different injection pressures)	Injection pressure: 1) 33MPa 2) 32MPa
2a (high IFT, 0.0043 N/m)	80℃
2b (low IFT, 0.000174 N/m)	250℃

4.6.2 Case 1: Different Injecting Pressures

In the first case CWI is conducted under the same injection pressure as the water injection (33 MPa) initially. A slightly lower injection pressure, 32 MPa, is then used in subsequent cases in order to obtain the same water breakthrough time as the pure water injection. The reservoir temperature is kept constant, at 80 ℃ for both injection conditions.

4.6.2.1 Discussion

The saturation profile shown in Figure 4.1 shows that after 25 days the water front of CWI breaks through, however, the water front of WI is only three quarters of the way from injector to producer, i.e. 72 m. Compared to CWI, the water front in pure water injection moves more slowly indicating a later water breakthrough in the WI process. Due to oil viscosity reduction (from 9 cP to 1 cP) the displacement front moves faster leading to an earlier water breakthrough in the case of CWI.

The average water saturation behind the front ($\overline{S_w}$) (Welge, 1952) in CWI and WI can be calculated using the integration of water saturation divided by the total length which equals to 0.53 and 0.5 in CWI and WI, respectively. The oil recovery factor (RF) then can be calculated by:

$$RF=\frac{\left(1-S_{wc}\right)\phi V_b-\left(1-\overline{S_w}\right)\phi V_b}{\left(1-S_{wc}\right)\phi V_b}=\frac{\overline{S_w}-S_{wc}}{1-S_{wc}}. \tag{3.72}$$

In CWI, the recovery factor is 0.373 which is greater than 0.333 in WI indicating better oil recovery using CWI even though the breakthrough time is less.

Since the average water saturation of both CWI and WI are known, the oil production per pore volume injected (J) can be calculated by:

$$J = \frac{\text{Total oil production}}{\text{Total pore volume injected}} = \frac{\left(1 - S_{wc}\right)\phi L - \left(1 - \overline{S_w}\right)\phi L}{\overline{S_w} L_f}, \qquad (3.73)$$

where L_f is front location.

According to equation (3.73) the oil production per pore volume injected in CWI is 0.095. Although a better oil recovery is achieved using CWI, WI has higher oil production with one pore volume injection, which is 0.125 compared to 0.095 in CWI.

The other factor to evaluate the performance of an EOR is known as total or overall sweep efficiency. This factor can be divided into three different sweep efficiencies. In the 2-D area the swept region by the displacing fluid would never equal the entire reservoir area because of economic constraints. The ratio of the swept area over the reservoir area is the areal sweep efficiency (E_a). The areal sweep efficiency is primarily a function of the mobility ratio, reservoir heterogeneity, cumulative volume of water injected and waterflood pattern configuration.

Due to the vertical heterogeneities within the reservoir, some parts of the reservoir will not be reached by the displacing fluid. A vertical sweep efficiency (E_v) is introduced to account for the vertical heterogeneity. In addition to these two factors, microscopic displacement efficiency (E_m) describes the displacement efficiency at the pore scale. Microscopic displacement efficiency is controlled by the balance of gravity, capillary and viscous forces and also pore size distribution. Based on these three sweep efficiencies, the total sweep efficiency (E_t) can be estimated as:

$$E_t = E_a \cdot E_v \cdot E_m . \tag{3.74}$$

However, in this numerical study CWI is performed horizontally with constant boundary pressure conditions. Therefore, the results fail to evaluate the total sweep efficiency which requires the information from the 3-D mathematical model.

A later water breakthrough can be reached by lowering the injection pressure. Figure 4.2 shows the water saturation profile after 38 days with a change of injection pressure to 32 MPa for the CWI case. After 38 days, the water fronts of both CWI and WI break through at the same time (as designed).

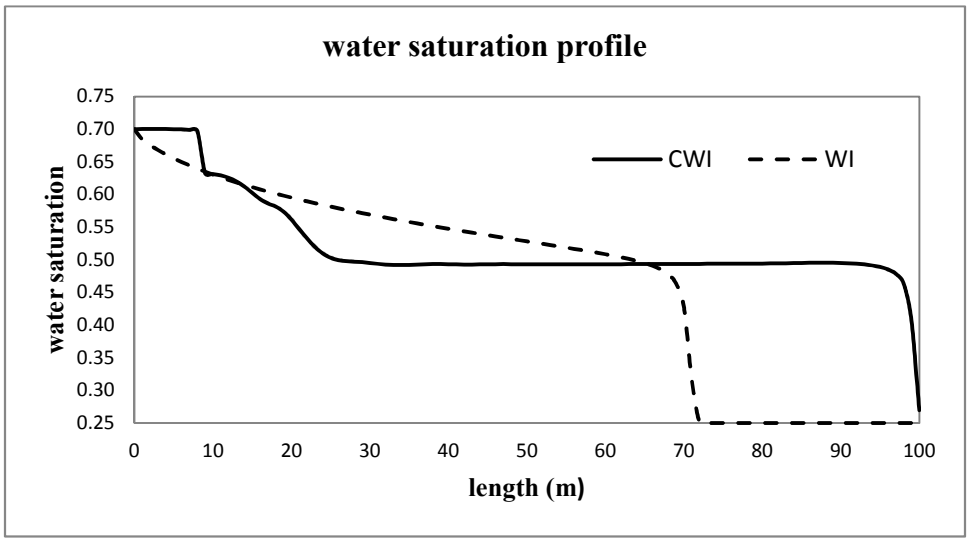

Figure 4.1 Water Saturation Profiles of CWI and WI under 33 MPa Injecting Pressure after 25 Days

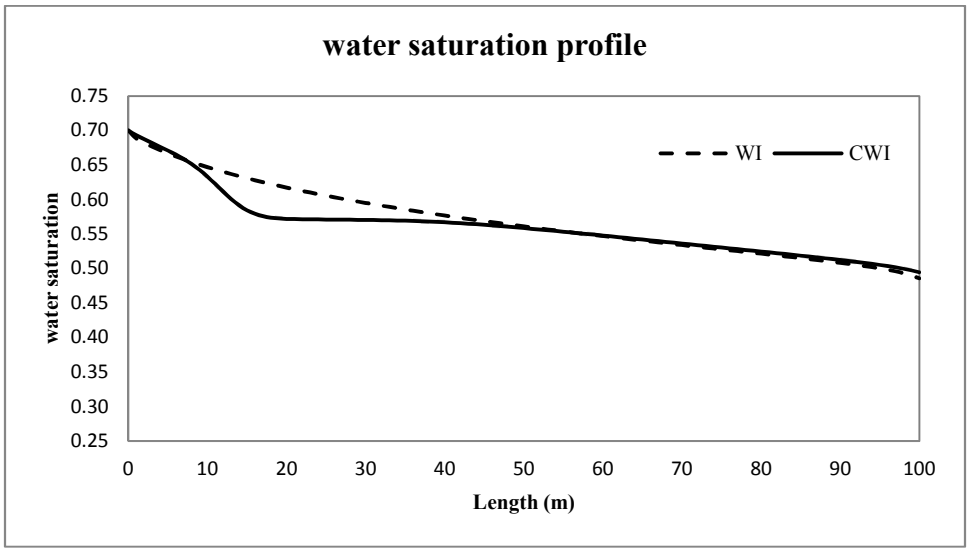

Figure 4.2 Water Saturation Profiles of CWI and WI under 32 MPa Injecting Pressure after 38 Days

4.6.3 Case 2: Different Reservoir Temperatures

In the second case two scenarios are applied to study the effect of IFT on additional oil recovery. As shown by (Okoye *et al*., 1988) IFT decreases with increasing temperature. Two scenarios are presented in this section based upon two different reservoir temperature conditions. The constant pressure boundary conditions are still applicable in this section. A comparison between CWI and WI is also provided by simulation solutions. In order to reach the same breakthrough time carbonated water is injected under a pressure of 32 MPa for both scenarios while the water is injected at a pressure of 33 MPa. Since carbonated water is injected under the sufficiently high pressure (32 MPa), the initial CO_2 concentration and CO_2 solubility in water and oil phases are not affected by the change of temperature between two scenarios.

4.6.3.1 Case 2a: Higher IFT (lower reservoir temperature)

In the lower reservoir temperature carbonated water is injected at 80℃. The IFT varies based on equation (3.70). The decrease in IFT occurs due to the increasing solubility of CO_2 in the oil phase. However, with a maximum CO_2 solubility in the oil phase the IFT still does not reach to low IFT region (0.00015 N/m< σ <0.002 N/m) allowing for effective reduction in residual oil saturation (Torabzadey, 1984). The residual oil saturation, therefore, remains constant, at 0.25, during the flooding.

4.6.3.2 Case 2b: Lower IFT (higher reservoir temperature)

In order to investigate the impact of low IFT on oil recovery process a higher reservoir temperature, 250℃, is examined to reduce the IFT, thus decrease the residual oil saturation.

4.6.3.3 Discussion

The saturation profiles at a breakthrough time of 38 days are shown in Figure 4.3 for both the low IFT (IFT = 0.000174 N/m), and high IFT (IFT=0.0043 N/m) and the pure WI. Because the amount of residual oil is not affected in the high IFT range, (larger than 0.002 N/m in this case), the maximum water saturation (1-S_{or}) is the same as the one in WI. In the high temperature system (low IFT), the IFT decreases with increasing CO_2 concentration; hence, more oil is recovered under lower IFT conditions. This can be verified by examining the water saturation profile for the low IFT (high temperature) case. The water saturation in this case is much higher close to the injection point. However, due to insufficient CO_2 solubility, after a sharp reduction the curve follows the same saturation profile as it does in case 2a (high IFT). The overlapping water saturation

profile of the three processes are shown in Figure 4.3 implies the same fluid behavior. This confirms the calculation results from previous work (Noel, 1964) which stated that due to the contact with oil the initial carbonated water injected loses its CO_2 and then proceeds as plain water. Thus, the CO_2 moves behind the pure water in CWI.

Since the temperature in case 2b (low IFT) is much higher than in case 2a (high IFT), the IFT is decreased to within the range whereby the residual oil saturation is decreased (equation (3.71)) and recovery factor is increased. Figure 4.4 shows the change in residual oil saturation and CO_2 concentration in the oil phase along the length of the core. Once the CO_2 mass concentration is larger than 56%, a sufficiently low IFT is reached leading to lower residual oil saturation.

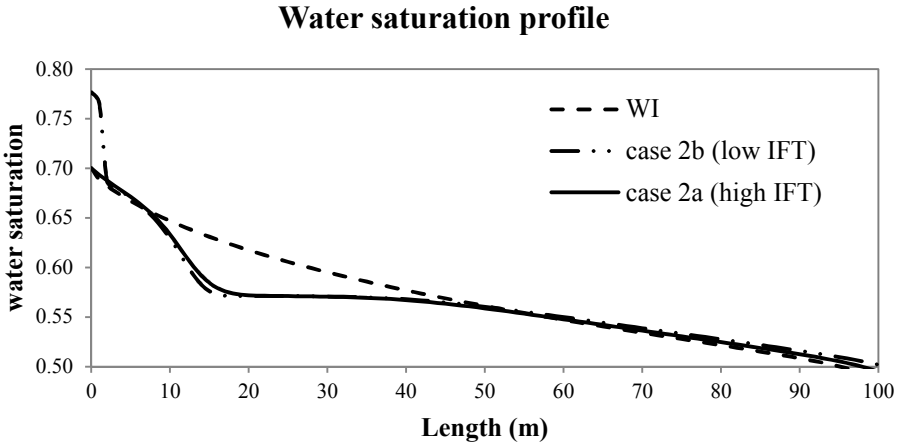

Figure 4.3 Water Saturation Profile after 38 Days

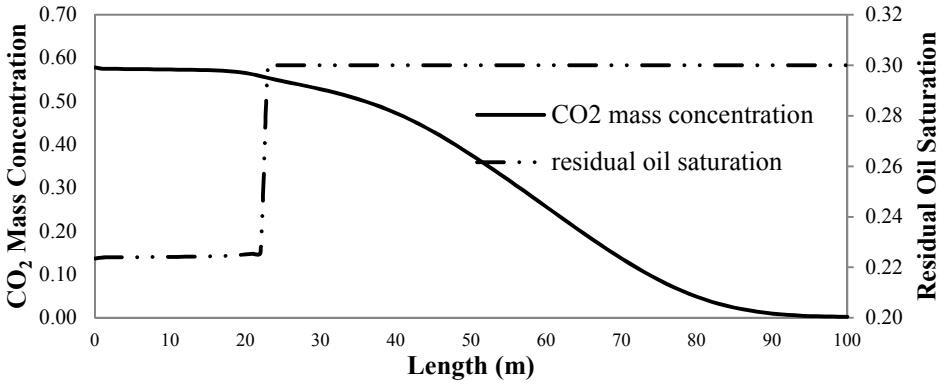

Figure 4.4 CO_2 Mass Concentration vs. Residual Oil Saturation over 200 Days

4.6.4 Viscosity Effect

Although the residual oil saturation stays constant with both CWI at high IFT (case 2a) and WI increased oil recovery is observed with CWI. Figure 4.5 shows a comparison between water saturation profiles of case 2a (high IFT) and simple water injection after 200 days of injection. The water saturation (lower oil saturation) when injected with carbonated water compared to pure water injection. In other words, more oil will be produced during the CWI process. This is mainly because of the deceasing oil viscosity with increasing CO_2 concentration. This is illustrated in Figure 4.6.

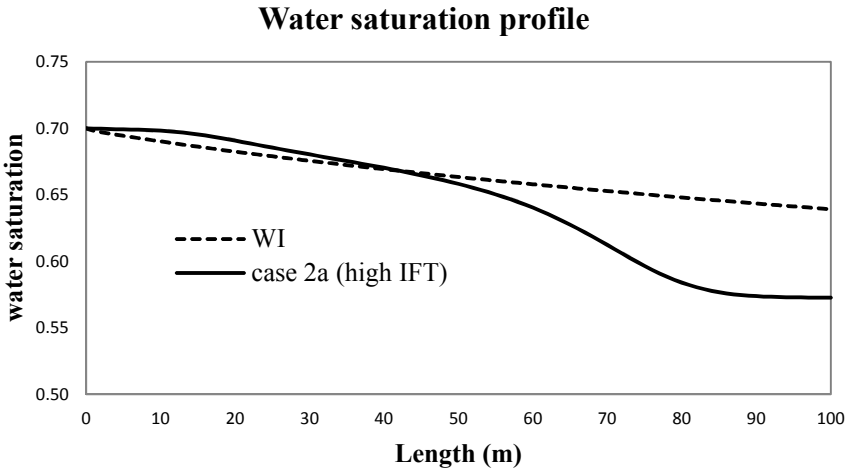

Figure 4.5 Water Saturation Profile after 200 Days

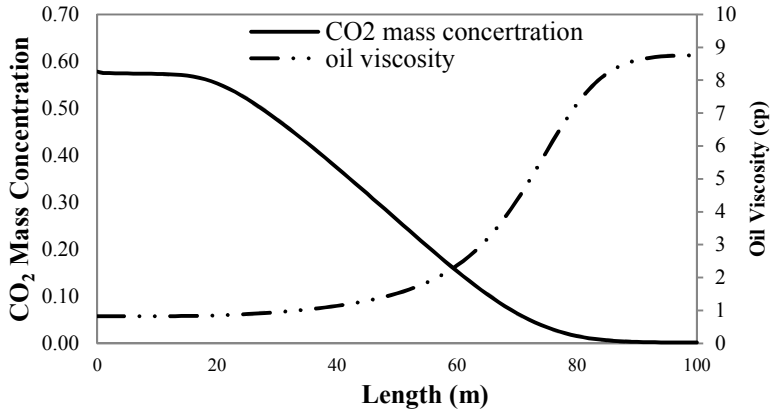

Figure 4.6 CO_2 Mass Concentration vs. Oil Viscosity over 200 Days of Case 2a

4.6.5 Cumulative Oil Production and Recovery Factor of CWI and WI

The cumulative amount of oil produced in case 2a (IFT = 0.0043 N/m), case 2b (IFT = 0.000174 N/m) and water flooding are plotted in Figure 4.7. The CWI, with a low IFT, has the best result followed by CWI at a high IFT condition. Compared to CWI, less oil can be recovered by pure water flooding.

After 200 days, the recovery factor (*RF)* for low IFT CWI is 0.68, 6% higher than the recovery factor for a high IFT in CWI which is 0.62. The WI has the lowest recovery factor at 0.55 in this case.

Based on the numbers shown above the most desirable oil recovery performance is achieved by lowering interfacial tension (case 2b). Due to the sufficiently low interfacial tension between water and oil (0.000174 N/m), the residual oil saturation has been reduced during CWI process. Moreover, the oil viscosity is also reduced in this low interfacial tension fluid system by the solution of CO_2 in the oil phase. The combination of effects in reduction of oil viscosity and residual oil saturation results in the most desirable scenario in case 2b shown by Figure 4.7. With the high interfacial tension (0.0043 N/m) in case 2a, the residual oil saturation stays constant during the CWI process. However, the oil viscosity is decreasing with increasing CO_2 concentration in oil phase. As indicated by Figure 4.7 more oil is recovered in case 2a due to the oil viscosity reduction compared with plain water injection (WI).

In conclusion, additional oil recovery using carbonated water injection is due to the oil viscosity reduction by dissolved CO_2. In addition, if the fluid system is close to miscibility and low IFT can be obtained, the significant increase in oil recovery will be observed due to reduction in residual oil saturation. However, in the case when the fluid system is far from miscibility the oil viscosity reduction plays the main role in oil recovery enhancement.

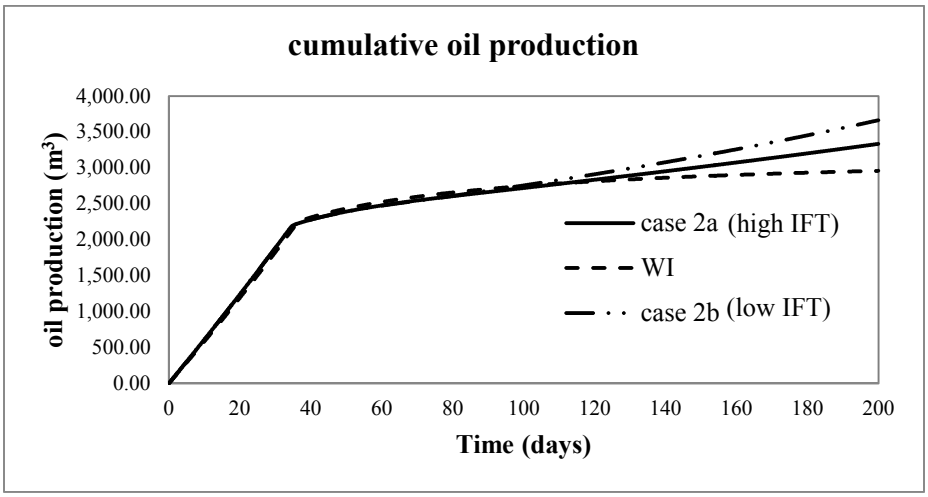

Figure 4.7 Cumulative Oil Production after 200 Days

Chapter 5 Conclusions and Recommendations

5.1 Conclusions

The thesis mainly focuses on the oil recovery processes in both water injection (WI) and carbonated water injection (CWI). These oil recovery processes are considered under constant pressure boundary conditions. Numerical solutions are calculated by an IMPES block-centered finite-difference method using upstream evaluation of mobilities. In WI, due to varying total fluid velocity under fixed pressure boundaries, the classical Buckley–Leverett theory for a constant total fluid velocity is not applicable. Based on mass conservation, the numerical simulation is performed in Matlab®. The numerical solution is then compared to an existing analytical extension of the classical Buckley–Leverett theory for a constant pressure boundary and the WI simulation model is validated. As an extension of WI model the model of CWI, therefore, is validated. Results for different case studies are shown. The comparison is also used to illustrate the impact of numerical errors by showing how the numerical solution approaches the analytical solution when the number of grid blocks is refined.

In carbonated water injection, CO_2 is dissolved in the water phase prior to injection. After injection, CO_2 will partition in both the water and oil phases. The fractions of CO_2 in each phase are the main variables that affect the recovery factor. This work presents the results of CWI by combining both thermodynamics and reservoir simulation models. The effects of oil recovery in CWI are also discussed in this work.

The findings are presented next.

The conclusions of WI can be summarized as:

1. The total fluid velocity changes with time for constant pressure boundary conditions.
2. We successful applied the constant pressure boundary conditions of the Buckley-Leverett theory extension.
3. A numerical solution was compared to the analytical extension with good agreement for different fluid systems.

Carbonated water injection was studied under different scenarios: 1) different injection pressures (33 MPa and 32 MPa), and 2) different reservoir temperatures: 80℃ (high IFT) and 250℃ (low IFT) resulting in the following conclusions:

1. An early breakthrough has been found with a higher injection pressure. The postponed breakthrough time can be realized by decreasing injection pressure.
2. IFT is decreasing with increasing temperature. With maximum CO_2 solubility low IFT can be reached. Contrary to the high temperature, in a low temperature reservoir (80 ℃) high IFT fluid system is present.
3. A reduction of residual oil saturation in low IFT under the higher temperature (250℃ in this case) is observed resulting in a higher cumulative oil production.

As EOR, CWI have been also compared with WI (secondary oil recovery) under the same breakthrough time. The main conclusions are summarized as follows:

1. In low temperature fluid system the viscosity is the main mechanism of

enhancing oil recovery.

2. In high temperature fluid system both reduction of viscosity and IFT contribute to the additional oil recovery.
3. The CWI, with a low IFT, has the best result followed by CWI in a high IFT condition. Compared to CWI, less oil can be recovered by water flooding.

Table 5.1 Summary of CWI with Different Conditions

Case	Condition	Result
1 (different injection pressures)	Variable injection pressure	1. High pressure led an early breakthrough 2. Decreasing the injection pressure prolonged breakthrough
2a (high IFT, 0.0043 N/m)	80 ℃	1. High IFT fluid system existed 2. No change of residual oil was observed
2b (low IFT, 0.00017375 N/m)	250 ℃	1. Low IFT fluid system was present 2. A reduction of residual was observed 3. High cumulative oil production was shown

5.2 Recommendations

During this study, some aspects of CWI for oil recovery were theoretically investigated. Due to the limitation of this theoretical research the important information, such as IFT, cannot be measured experimentally. The numerical solutions have not been compared with or validated against experimental data. Therefore, a further experimental investigation is recommended for a deeper understanding of CWI in EOR. The effects of

CO_2 diffusion in the fluid system was neglected in this work. Further research can be carried on by accounting for the diffusion of CO_2 in both water and oil phases. This research is conducted for a 1-D model. To have full evaluation of CWI a 3-D mathematical study is recommended to the deeper comprehension.

Bibliography

Abrams, A. (1975). The influence of fluid viscosity, interfacial tension, and flow velocity on residual oil saturation left by waterflood. *Old SPE Journal, 15*(5), 437-447.

Chang, Y.-B., Coats, B., and Nolen, J. (1998). A compositional model for CO2 floods including CO2 solubility in water. *SPE Reservoir Evaluation & Engineering, 1*(2), 155-160.

Courant, R., Friedrichs, K., and Lewy, H. (1928). Über die partiellen Differenzengleichungen der mathematischen Physik. *Mathematische Annalen, 100*(1), 32-74.

Danesh, A. (1998). *PVT and phase behaviour of petroleum reservoir fluids* (Vol. 47): Elsevier Science.

Davies, P. n. (1994). *[16] 1 Oil Supply and Demand in the 1990s.* Paper presented at the 14th World Petroleum Congress.

DeRuiter, R., Nash, L., and Singletary, M. (1994). Solubility and displacement behavior of a viscous crude with CO2 and hydrocarbon gases. *SPE Reservoir Engineering, 9*(2), 101-106.

Dong, Y., Dindoruk, B., Ishizawa, C., Lewis, E., and kubicek, t. (2011). *An Experimental Investigation of Carbonated Water Flooding.* Paper presented at the SPE Annual Technical Conference and Exhibition.

Dooley, J. J., Davidson, C. L., and Dahowski, R. T. (2009). *An assessment of the commercial availability of carbon dioxide capture and storage technologies as of June 2009*: Pacific Northwest National Laboratory.

Duan, Z., and Sun, R. (2003). An improved model calculating CO< sub> 2</sub> solubility in pure water and aqueous NaCl solutions from 273 to 533 K and from 0 to 2000 bar. *Chemical Geology, 193*(3), 257-271.

Dullien, F. A. (1991). *Porous media: fluid transport and pore structure*: Access Online via Elsevier.

Emera, M., and Sarma, H. (2006). *A Genetic Algorithm-Based Model to Predict CO-oil Physical Properties for Dead and Live Oil.* Paper presented at the Canadian International Petroleum Conference.

Enick, R. M., and Klara, S. M. (1990). CO2 solubility in water and brine under reservoir conditions. *Chemical Engineering Communications, 90*(1), 23-33.

Ghomian, Y., Pope, G., and Sepehrnoori, K. (2008). *Hysteresis and field-scale optimization of WAG injection for coupled CO2-EOR and sequestration.* Paper presented at the SPE Symposium on Improved Oil Recovery.

Holm, L. (1961). A comparison of propane and carbon dioxide solvent flooding processes. *AIChE Journal, 7*(2), 179-184.

Höök, M., Hirsch, R., and Aleklett, K. (2009). Giant oil field decline rates and their influence on world oil production. *Energy Policy, 37*(6), 2262-2272.

Jarba, M., and Anazi, B. D. (2009). A Comparison Study of the of the CO 2-Oil Physical Properties-Literature Correlations Accuracy Using Visual Basic Modeling Technique. *Oil and Gas Business*.

Jiang, H., Nuryaningsih, L., and Adidharma, H. (2012). *The Study of Timing of Cyclic Injections in Miscible CO2 WAG.* Paper presented at the SPE Western Regional Meeting.

Jordan, R. (1998). *Factors Influencing Oil Demand and the Range of Call on Middle Eastern Crude Production in 2010.* Paper presented at the Abu Dhabi International Petroleum Exhibition and Conference.

Kechut, N. I., Sohrabi, M., and Jamiolahmady, M. (2011). *Experimental and Numerical Evaluation of Carbonated Water Injection (CWI) for Improved Oil Recovery and CO2 Storage.* Paper presented at the SPE EUROPEC/EAGE Annual Conference and Exhibition.

Kestin, J., Khalifa, H. E., Abe, Y., Grimes, C. E., Sookiazian, H., and Wakeham, W. A. (1978). Effect of pressure on the viscosity of aqueous sodium chloride solutions in the temperature range 20-150. degree. C. *Journal of Chemical and Engineering Data, 23*(4), 328-336.

Kumar, S., Torabzadeh, S., and Handy, L. (1985). *Relative permeability functions for high-and low-tension systems at elevated temperatures.* Paper presented at the SPE California Regional Meeting.

Lake, L. W. (1989). Enhanced oil recovery.

Li, Y. K., and Nghiem, L. X. (1986). Phase equilibria of oil, gas and water/brine mixtures from a cubic equation of state and Henry's law. *The Canadian Journal of Chemical Engineering, 64*(3), 486-496.

Lin, E., and Huang, E. (1990). The effect of rock wettability on water blocking during miscible displacement. *SPE Reservoir Engineering, 5*(2), 205-212.

Lohrenz, J., Bray, B., and Clark, C. (1964). Calculating viscosities of reservoir fluids from their compositions. *Journal of Petroleum Technology, 16*(10), 1171-1176.

Mahinpey, N., Ambalae, A., and Asghari, K. (2007). In situ combustion in enhanced oil recovery (EOR): A review. *Chemical Engineering Communications, 194*(8), 995-1021.

Mehrotra, A. K., and Svrcek, W. Y. (1986). Viscosity of compressed Athabasca bitumen. *The Canadian Journal of Chemical Engineering, 64*(5), 844-847.

Melzer, L. S., and Midland, T. (2012). Carbon Dioxide Enhanced Oil Recovery (CO2 EOR): Factors Involved in Adding Carbon Capture, Utilization and Storage (CCUS) to Enhanced Oil Recovery.

Mungan, N. (1964). Role of Wettability and Interfacial Tension in Water Flooding. *Old SPE Journal, 4*(2), 115-123.

Mungan, N. (1981). Carbon dioxide flooding-fundamentals. *Journal of Canadian Petroleum Technology, 20*(01).

Needham, R. B., and Doe, P. H. (1987). Polymer flooding review. *Journal of Petroleum Technology, 39*(12), 1,503-501,507.

Noel, D. (1964). A calculation method for carbonated water flooding. *Old SPE Journal, 4*(1), 9-20.

Nuryaningsih, L., Jiang, H., and Adidharma, H. (2010). *Experimental Study on Optimum Half-Cycle Slug Size of Water Alternating Gas Under Tertiary Miscible Carbon Dioxide Flooding.* Paper presented at the SPE International Conference on CO2 Capture, Storage, and Utilization.

Okoye, C., Oungpasuk, P., and Wang, P. (1988). *Elevated temperature multiphase rock-fluid properties for high and low tension systems.* Paper presented at the International Meeting on Petroleum Engineering.

Patel, P., Christman, P., and Gardner, J. (1987). Investigation of Unexpectedly Low Field-Observed Fluid Mobilities During Some CO2 Tertiary Floods. *SPE Reservoir Engineering, 2*(4), 507-513.

Ramesh, A., and Dixon, T. (1972). *Numerical simulation of carbonated waterflooding in a heterogeneous reservoir.* Paper presented at the Fall Meeting of the Society of Petroleum Engineers of AIME.

Rao, D. N., and Lee, J. I. (2003). Determination of gas–oil miscibility conditions by interfacial tension measurements. *Journal of colloid and interface science, 262*(2), 474-482.

Riazi, M. (2011). *Pore scale mechanisms of carbonated water injection in oil reservoirs.* Heriot-Watt University.

Riazi, M., Sohrabi, M., Jamiolahmady, M., Ireland, S., and brown, c. (2009). *Oil recovery improvement using CO2-enriched water injection.* Paper presented at the EUROPEC/EAGE Conference and Exhibition.

Rogers, J., and Grigg, R. (2000). *A literature analysis of the WAG injectivity abnormalities in the CO2 process.* Paper presented at the SPE/DOE Improved Oil Recovery Symposium.

Roorda, J. n. (1979). *RTD 1 (2) Petroleum in World Energy Balances to the Year 2000.* Paper presented at the 10th World Petroleum Congress.

Rowe Jr, A. M., and Chou, J. C. (1970). Pressure-volume-temperature-concentration relation of aqueous sodium chloride solutions. *Journal of Chemical and Engineering Data, 15*(1), 61-66.

Sheldon, J., Zondek, B., and Cardwell, W. (1959). One-dimensional, incompressible, noncapillary, two-phase fluid flow in a porous medium. *Trans. SPE AIME, 216*, 290-296.

Shen, P., Zhu, B., Li, X.-B., and Wu, Y.-S. (2006). *The influence of interfacial tension on water-oil two-phase relative permeability.* Paper presented at the SPE/DOE Symposium on Improved Oil Recovery.

Simon, R., and Graue, D. (1965). Generalized correlations for predicting solubility, swelling and viscosity behavior of CO2-crude oil systems. *Journal of Petroleum Technology, 17*(1), 102-106.

Siregar, S., Mardisewojo, P., Kristanto, D., and Tjahyadi, R. (1999). *Dynamic Interaction Between CO2 Gas and Crude Oil in Porous Medium.* Paper presented at the SPE Asia Pacific Improved Oil Recovery Conference.

Sohrabi, M., Riazi, M., Jamiolahmady, M., Ireland, S., and Brown, C. (2009a). *Enhanced Oil Recovery and CO2 Storage by Carbonated Water Injection.* Paper presented at the International Petroleum Technology Conference.

Sohrabi, M., Riazi, M., Jamiolahmady, M., Ireland, S., and Brown, C. (2009b). *Mechanisms of Oil Recovery by Carbonated Water Injection.* Paper presented at the International Symposium of the Society of Core Analysts held in Noordwijk aan Zee, The Netherlands.

Stahl, C. R., Gibson, M. A., and Knudsen, C. W. (1987). Thermally-enhanced oil recovery method and apparatus: Google Patents.

Stone, H., and Garder Jr, A. (1961). 1518-G-Analysis of Gas-Cap or Dissolved-Gas Drive Reservoirs. *Old SPE Journal, 1*(2), 92-104.

Torabzadey, S. (1984). *The effect of temperature and interfacial tension on water/oil relative permeabilities of consolidated sands.* Paper presented at the SPE Enhanced Oil Recovery Symposium.

Tunio, S. Q., Tunio, A. H., Ghirano, N. A., and El Adawy, Z. M. (2011). Comparison of different enhanced oil recovery techniques for better oil productivity. *International Journal of Applied Science and Technology, 1*.

Tzimas, E., Georgakaki, A., Garcia Cortes, C., and Peteves, S. (2005). Enhanced oil recovery using carbon dioxide in the European energy system. *European Commission Joint Research Centre, Report EUR, 21895*.

Welge, H. (1952). A simplified method for computing oil recovery by gas or water drive. *Journal of Petroleum Technology, 4*(4), 91-98.

Welker, J. (1963). Physical properties of carbonated oils. *Journal of Petroleum Technology, 15*(8), 873-876.

Zain, Z., Kechut, N., Ganesan, N., Noraini, A., and Raja, D. (2001). *Evaluation of CO2 Gas Injection for Major Oil Production Fields in Malaysia-Experimental Approach Case Study: Dulang Field.* Paper presented at the SPE Asia Pacific Improved Oil Recovery Conference.

Zekri, A., Shedid, S., and Almehaideb, R. (2007). *Possible Alteration of Tight Limestone Rocks Properties and the Effect of Watershelding on the Performance of SC CO2 Flooding for Carbonate Formation.* Paper presented at the SPE Middle East Oil and Gas Show and Conference.

Appendix A Unit conversion factors

Covert from	To	Multiply by	Inverse
Area			
acre	m^2	4.047 E+3	2.471 E-4
ft^2	m^2	9.290 E-2	1.176 E+1
Density			
pound/ft^3	kg/m^3	1.602 E+1	6.243 E-2
Mass			
pound	kg	4.536 E-1	2.205 E+0
Pressure			
psi	Pa	6.895E+3	1.450 E-4
atm	Pa	1.013E+3	9.869 E-6
bar	Pa	1.000 E+5	1.000 E-5
Permeability			
mD	m^2	9.869 E-16	1.013E+15
Time			
day	s	8.64 E+4	1.157 E-5
hour	s	3.600 E+3	2.778 E-4
Viscosity			
cp	Pas	1.000 E-3	1.000 E+3
Volume			
ft^3	m^3	2.832 E-2	3.531 E+1
barrel	m^3	1.590 E-1	6.290 E+0
Length			
ft	m	3.048 E-1	3.218 E+0
inch	m	2.540 E-2	3.937 E+1
Interfacial tension			
dyn/cm	N/cm	1.000 E-3	1.000 E+3

Appendix B Pre-print: Solutions of Multi-Component, Two-Phase Riemann Problems with Constant Pressure Boundaries

Transport in Porous Media

Fractional Flow Analysis for Multi-Component Problems with Constant Pressure Boundaries

--Manuscript Draft--

Manuscript Number:	
Full Title:	Fractional Flow Analysis for Multi-Component Problems with Constant Pressure Boundaries
Article Type:	Original Research Paper
Keywords:	Buckley-Leverett; fractional flow theory; constant pressure boundaries; Reimann problems
Corresponding Author:	Thormod E Johansen, PhD Memorial University of Newfoundland St. John's, Newfoundland CANADA
Corresponding Author Secondary Information:	
Corresponding Author's Institution:	Memorial University of Newfoundland
Corresponding Author's Secondary Institution:	
First Author:	Thormod E. Johansen, Ph.D.
First Author Secondary Information:	
Order of Authors:	Thormod E. Johansen, Ph.D.
	Lesley James, Ph.D.
Order of Authors Secondary Information:	
Abstract:	Fractional flow theory has been used to describe the linear, incompressible, fluid displacement in a porous medium under constant flux conditions without dispersion. The hyperbolic problem is usually associated with moving shock fronts mathematically describing the changing location of the abrupt change in fluid composition. Realistically, reservoirs are often produced under constant pressure boundaries with a constant injection pressure and a constant well flowing pressure. Here, we extend the Buckley-Leverett's classic fractional flow theory to multicomponent problems with constant pressure boundaries. We review Riemann problems and derive expressions for the volumetric flux, both before and after breakthrough of multiple component waves. Expressions for predicting the breakthrough time and calculating the pressure profile from outlet to inlet as well as generalised formulas are presented. Finally, two waterflooding cases and a polymer case are developed for time dependent pressure boundaries to demonstrate and exemplify the constant pressure boundary solution to fractional flow theory.

Fractional Flow Analysis for Multi-Component Problems with Constant Pressure Boundaries

Thormod E. Johansen[1] and Lesley A. James[2]

Faculty of Engineering & Applied Science

Memorial University of Newfoundland

St. John's, Newfoundland A1B 3X5

Canada

001-709-864-3431[1]; 001-709-864-2485[2]

001-709-864-4042

thormodj@mun.ca[1]; ljames@mun.ca[2]

Fractional flow theory has been used to describe the linear, incompressible, fluid displacement in a porous medium under constant flux conditions without dispersion. The hyperbolic problem is usually associated with moving shock fronts mathematically describing the changing location of the abrupt change in fluid composition. Realistically, reservoirs are often produced under constant pressure boundaries with a constant injection pressure and a constant well flowing pressure. Here, we extend the Buckley-Leverett's classic fractional flow theory to multicomponent problems with constant pressure boundaries. We review Riemann problems and derive expressions for the volumetric flux, both before and after breakthrough of multiple component waves. Expressions for predicting the breakthrough time and calculating the pressure profile from outlet to inlet as well as generalised formulas are presented. Finally, two waterflooding cases and a polymer case are developed for time dependent pressure boundaries to demonstrate and exemplify the constant pressure boundary solution to fractional flow theory.

Key words: Buckley-Leverett; fractional flow theory; constant pressure boundaries; Reimann problems;

EOR: Enhanced Oil Recovery

1. Introduction

The Buckley-Leverett solution (1941) is synonymous with fractional flow theory where an immiscible fluid displaces another in one-dimensional flow in a porous medium. Physically, fractional flow theory describes the linear displacement of one phase by another immiscible phase where there is a front described by a shock or sudden change in concentration. In its simplest form it describes one component displacing another immiscible component in one dimension in the absence of diffusive and compressible flow, i.e. water displacing oil (Buckley and Leverett 1941, Welge 1952). Mathematically, the Buckley-Leverett equation is a first order hyperbolic partial differential conservation equation in time and space.

This concentration shock (oil-water interface) travels from the start (injection) to the end (production) as depicted in Figures 1 and 2.

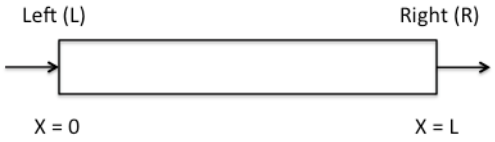

Fig. 1 One-dimensional Riemann problem

Instead of a shock, the interface between the two phases may exhibit a gradual change in concentration indicated as a rarefaction wave, ν_i or ν_{i-1} in Fig. 2.

Fractional flow problems are mathematically known as Riemann problems that can be solved using the method of characteristics. Riemann problems are hyperbolic first order partial differential equations with a constant initial value and a constant injected value. The method of characteristics finds a characteristic curve of the Riemann problem where the partial differential equation becomes an ordinary differential equation and where an analytical solution can be found.

The objective of this work is to extend the Buckley-Leverett theory from the constant flux condition to constant pressure boundaries for multicomponent systems. The mathematical formulation is derived for time before the first wave breaks through, time after the first wave breaks through but before the next wave,

time after the subsequent wave and then generally. Three cases are used to demonstrate the constant pressure boundary multicomponent extension to the Buckley-Leverett solution; case 1a) waterflooding with $\mu_o/\mu_w = 0.2$, case 1b) waterflooding with $\mu_o/\mu_w = 20$ and case 2) polymer flooding with a single polymer component residing in the aqueous phase (Johansen and Winther, 1988). This constant pressure multicomponent extension to the Buckley-Leverett equation is particularly important as many actual fields are operated under constant pressure boundaries and being a generalised analytical solution it can be readily adapted and used for better predicting production rates.

2. Riemann Problems

Given a hyperbolic system of conservation laws such as an *n*-component two phase model for one dimensional flow in porous media subject to standard fractional flow assumptions (1D constant volume flow with negligible dispersion). If $F_i = F_i(u_1,...,u_{n-1})$ is the fractional flux function for component i, and $\boldsymbol{u} = [u_1,....,u_{n-1}]$ represents the overall volume fraction of the fluid component(s) where the sum of the individual components must be one ($\sum_{i=1}^{n} u_i = 1$), the conservation of mass model under consideration may be written as

$$\phi \frac{\partial}{\partial t}[u_i + a_i(\boldsymbol{u})] + u_T \frac{\partial F_i}{\partial x} = 0 \,;\, i = 1,...,n-1 \tag{2.1}$$

where $a(\boldsymbol{u})$ is volume fraction of the stagnant part of component i, e.g. caused by adsorption. Furthermore, ϕ is porosity and u_T is the constant volumetric flux. If we have two phases, $F_i = fu_{i1} + (1-f)u_{i2}$; $u_i = Su_{i1} + (1-S)u_{i2}$ where u_{ij} is volume fraction of component i in phase j, S is saturation of phase 1 and f is the fractional flow function of phase 1, we assume the model can be reformulated as

$$\frac{\partial \boldsymbol{u}}{\partial t} + \frac{u_T}{\phi} \boldsymbol{A}(\boldsymbol{u}) \frac{\partial \boldsymbol{u}}{\partial x} = 0 \tag{2.2}$$

where $\boldsymbol{A}(\boldsymbol{u})$ is an $(n-1)\times(n-1)$ matrix with *real* eigenvalues $\lambda_1,....,\lambda_{n-1}$ (since we assume the system in equation (2.2) is hyperbolic).

We assume the solution for the multi component *Riemann problem* described by equation (2.2) is known for the case when the volumetric flux u_T is constant both in x and t. A *Riemann problem* is an initial/boundary value problem with constant states

$$\begin{aligned} \boldsymbol{u}(0,t) &= \boldsymbol{u}^L \;\; ; t \geq 0 \\ \boldsymbol{u}(x,0) &= \boldsymbol{u}^R \; ; 0 \leq x \leq L \end{aligned} \tag{2.3}$$

where L is the length of the 1D medium. As explained in the introduction, in this paper the constant flux solution is used to determine the solution of the associated problem with constant pressure boundaries, $p_{in} = p(0,t)$; $p_{out} = p(L,t)$. For such constant pressure boundaries, the volumetric flux will be constant as a function of x because of the incompressibility assumption, however $u_T = u_T(t)$ will be time dependent. The constant volumetric flux solution consists of a sequence of self - similar waves (i.e. waves that can be described as a function of $\xi = x/t$) connecting the two states $\boldsymbol{u}^L, \boldsymbol{u}^R$, in such a way that the overall wave velocity increases from $\boldsymbol{u}^L$ to $\boldsymbol{u}^R$. Each of these elementary waves belongs to one of the eigenvalues $\lambda_1,...,\lambda_{n-1} = x/t$ either as a Rarefaction wave (smooth) or a Shock wave (including contact discontinuity). Any two adjacent waves are separated by a constant state. The solution of the associated problem with constant pressure boundaries and the constant flow rate solution are congruent in the sense that either solution at a given time can be obtained from the other by stretching the x-axis. The sequence of elementary waves is illustrated in Fig. 2, where also the nomenclature used in this paper is defined.

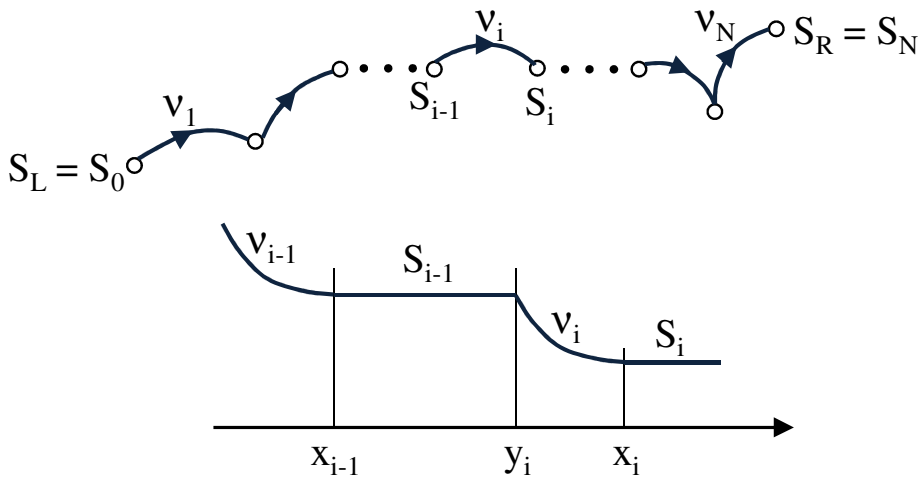

Fig. 2 Elementary Waves

We assume that each wave can be defined by the parameter S (e.g. phase saturation). The leading edge of the wave ν_i is x_i and the trailing edge is y_i for shocks $x_i = y_i$. Also, it is possible to have $x_{i-1} = y_i$, such as in the classic Buckley Leverett solution, where a shock has the same velocity as the leading edge of the trailing rarefaction wave. Any two waves ν_{i-1}, ν_i are separated by a constant state S_{i-1}.

Consider the case where ν_i is a rarefaction wave, parameterized by S. We do not assume that the system is strictly hyperbolic, so $\lambda_i - \lambda_k$ may change sign for any pair of eigenvalues. Hence, we cannot assume that the elementary waves correspond one by one to a sequence of increasing eigenvalues. Instead, $\nu_i(S) = \lambda_k(S)$ for some k. If ν_i is a shock, it must satisfy the Rankine-Hugoniot condition (shock mass conservation) for each component, which in particular means it will satisfy

$$\nu_i = \frac{[F_k]}{[u_k]}; k = 1,....,n-1 \tag{2.4}$$

where [-] represents a jump from one side of the shock to the other. This equation gives rise to $n-1$ elementary shock waves corresponding to each of the eigenvalues $\lambda_1, \lambda_2, ..., \lambda_{n-1}$.

In our notation, the propagation velocity of a wave ν_i is $V_i = \frac{u_T}{\phi}\nu_i$.

If $\frac{u_T}{\phi}\nu_i \; ; i = 1, ..., N$ represents the solution of the constant flux Riemann problem connecting $\boldsymbol{u}^L, \boldsymbol{u}^R$, the solution of the constant pressure boundary solution is represented by $\frac{u_T(t)}{\phi}\nu_i \; ; i = 1, ..., N$.

In brief, this paper assumes we know the solution (unique or not) of a multi-component Riemann problem subject to the assumption of constant volumetric flux u_T. The main result of the paper is to determine the function $u_T(t)$ for the case of constant pressure boundaries for the same Riemann problem. In this derivation we also obtain closed expressions for the time when a given state is breaking through at the outlet end. Furthermore, we determine the pressure distribution at any time in $0 \le x \le L$.

3. Determination of the volumetric flux $u_T(t)$ for constant pressure boundaries

We will without ambiguity, since eigenvalues (λ) do not appear in this section, let $\lambda_T = K\sum_{j=1}^{2}(k_{rj} / \mu_j)$ denote total mobility, where K is permeability, k_{rj} phase relative permeability and μ_j phase viscosity. We assume, in this section, constant pressure boundaries; $p_{in} = p(0,t)$; $p_{out} = p(L,t)$, and u_T is constant as a function of x but not t. We obtain

$$u_T = -\lambda_T \frac{\partial p}{\partial x} \Rightarrow \Delta p = u_T \int_0^L \frac{dx}{\lambda_T} \quad ; \Delta p = p_{in} - p_{out} \tag{3.1}$$

Let $t_{BT,i}$ be the time when the leading edge of a wave ν_i is breaking through at the outlet end $x = L$.

3.1. The Case $t \le t_{BT,N}$

We first derive explicit expressions for the velocity, $u_T(t)$, before the fastest wave breaks through at the outlet end, and the time when this breakthrough occurs, $t_{BT,N}$. Assuming we know $u_T(\tau)$ at any time $\tau \le t_{BT,N}$ and letting $\Psi(t) = \int_0^t u_T(\tau)d\tau$, we first use integration by parts for a rarefaction wave ν_i as follows:

$$u_T \int_{y_i}^{x_i} \frac{dx}{\lambda_T} = u_T \left[\frac{x}{\lambda_T}\Big|_{y_i}^{x_i} + \int_{S_{i-1}}^{S_i} x(s)\frac{\lambda_T'}{\lambda_T^2}ds \right] = u_T \left[\frac{x_i}{\lambda_T(S_i)} - \frac{y_i}{\lambda_T(S_{i-1})} + \frac{\Psi(t)}{\phi}\int_{S_{i-1}}^{S_i} \frac{\nu_i \lambda'}{\lambda_T^2}ds \right]$$
$$= u_T \left[\frac{x_i}{\lambda_T(S_i)} - \frac{y_i}{\lambda_T(S_{i-1})} + \frac{\Psi(t)}{\phi}(-\frac{\nu_i}{\lambda_T}\Big|_{S_{i-1}}^{S_i} + \int_{S_{i-1}}^{S_i} \frac{\nu_i'}{\lambda_T}ds) \right] = u_T \frac{\Psi(t)}{\phi}\int_{S_{i-1}}^{S_i} \frac{\nu'}{\lambda_T}ds \quad (3.2)$$

Obviously, if the wave is a shock, this integral is zero. We, therefore, define

$$\mathrm{I}_i = \begin{cases} 0 & \textit{if wave } i \textit{ is a shock} \\ \int_{S_{i-1}}^{S_i} \frac{\nu_i'}{\lambda_T}ds & \textit{if wave } i \textit{ is a rarefaction} \end{cases} \quad (3.3)$$

We can now write equation (3.1) as

$$\Delta p = u_T \left[\sum_{i=1}^{N} [\frac{y_i - x_{i-1}}{\lambda_T(S_{i-1})} + \frac{\Psi(t)}{\phi}\mathrm{I}_i] + \frac{L - x_N}{\lambda_T(S_R)} \right], \quad (3.4)$$

and define the following where $V_i(S) = \frac{u_T}{\phi}\nu_i(S)$:

$$\nu_i(S) = \begin{cases} \nu_i(S) & \textit{if } i \textit{ is rarefaction} \\ \frac{[F_i(S)]}{[S]} & \textit{if } i \textit{ is shock} \end{cases} \quad (3.5)$$

Given the leading edge of the wave, x_i and the trailing edge, y_i, we can relate the velocity of the leading edge (dx/dt) and the velocity of the trailing edge of the shock (dy/dt) to the propagation velocity of the wave, $V(S)$.

$$\frac{dy_i}{dt} = V_i(S_{i-1}) \quad ; \frac{dx_{i-1}}{dt} = V_{i-1}(S_{i-1}) \quad ; i = 1,....N-1 \quad (3.6)$$

If we define constants, $\beta_i = \frac{\nu_i(S_{i-1})}{\nu_N(S_R)}$; $\alpha_i = \frac{\nu_i(S_i)}{\nu_N(S_R)}$ where subscript *R* is the saturation at the right hand side (the exit), equation (3.6) implies that

$$\frac{dy_i}{dx_N} = \beta_i \quad ; \frac{dx_{i-1}}{dx_N} = \alpha_{i-1} \quad ; i = 1, ..., N-1 \quad ; \quad \alpha_0 = 0 . \tag{3.7}$$

Since $x_N = y_i = x_i = 0$ at $t = 0$,

$$y_i = \beta_i x_N \quad ; \quad x_{i-1} = \alpha_{i-1} x_N . \tag{3.8}$$

Hence,

$$\frac{y_i - x_{i-1}}{\lambda_T(S_{i-1})} = r_i x_N \; ; \; r_i = \frac{\beta_i - \alpha_{i-1}}{\lambda_T(S_{i-1})} \tag{3.9}$$

Substituting this into equation (3.4), we obtain

$$\Delta p = u_T \left[\sum_{i=1}^{N} r_i \cdot x_N + \frac{\Psi(t)}{\phi} \sum_{i=1}^{N} \mathrm{I}_i + \frac{L - x_N}{\lambda_T(S_R)} \right] \tag{3.10}$$

The leading edge of the wave, at breakthrough, is $x_N = \frac{\Psi(t)}{\phi} \nu_N(S_R)$, the pressure difference is defined as

$$\Delta p = u_T \left[A x_N + B \right] \tag{3.11}$$

where

$$A = \sum_{i=1}^{N} r_i + \frac{1}{\nu_N(S_R)} \sum_{i=1}^{N} \mathrm{I}_i - \frac{1}{\lambda_T(S_R)} \quad ; \quad B = \frac{L}{\lambda_T(S_R)} \tag{3.12}$$

Using equation (3.11) and

$$\frac{dx_N}{dt} = \frac{u_T}{\phi} \nu_N(S_R) = \frac{\Delta p \nu_N(S_R)}{\phi(A x_N + B)} , \tag{3.13}$$

integration gives

$$A x_N^2 + 2 B x_N = C t \tag{3.14}$$

where

$$C = 2 \Delta p \nu_N(S_R) / \phi . \tag{3.15}$$

Accepting only the positive root in equation (3.14), the location of the leading edge of the fastest wave is given by

$$x_N(t) = \frac{-B + \sqrt{B^2 + 4ACt}}{A} \tag{3.16}$$

Furthermore, we can find an explicit expression for the break through time of wave ν_N by substituting $x_N = L$ in equation (3.14), i.e.

$$t_{BT,N} = \frac{AL^2 + 2BL}{C} \tag{3.17}$$

Finally, the pressure at the leading edge of the fastest wave, before this wave breaks through at time $t_{BT,N}$ is calculated as

$$p_N(t) = p_{out} + u_T \int_{S_{N-1}}^{S_R} \frac{dS}{\lambda_T(S)} = p_{out} + \frac{u_T}{\lambda_T(S_R)}(L - x_N(t)) . \tag{3.18}$$

The pressure at any location can then be calculated backwards (towards the inlet end) using equation (3.10).

The above applies to $t \le t_{BT,N}$. We next describe how $u_T(t)$ is calculated for $t_{BT,N} < t \le t_{BT,N-1}$, i.e. after the break through of the first wave.

3.2. The Case $t_{BT,N} < t \le t_{BT,N-1}$

If the fastest wave is a shock ν_N with a constant saturation state, S_{N-1}, separating ν_{N-1} from ν_N, the velocity, $u_T(t)$, for $t_{BT,N} < t \le t_{BT,N-1}$ is calculated exactly as above, simply by removing ν_N and putting $S_R = S_{N-1}$. This is because we already know $\Psi(t)$ for $t \le t_{BT,N}$. If the first wave is a rarefaction, the calculation of $u_T(t)$ is as described below.

Let S between $S_N = S_R$ and S_{N-1} be arbitrary but fixed. Let $x(S, t_{BT,N})$ be the location of S at time $t_{BT,N}$, i.e. the time when ν_N breaks through with its leading edge at $x = L$. Also, let t_S be the time when S arrives at $x = L$. This is illustrated in Fig. 3.

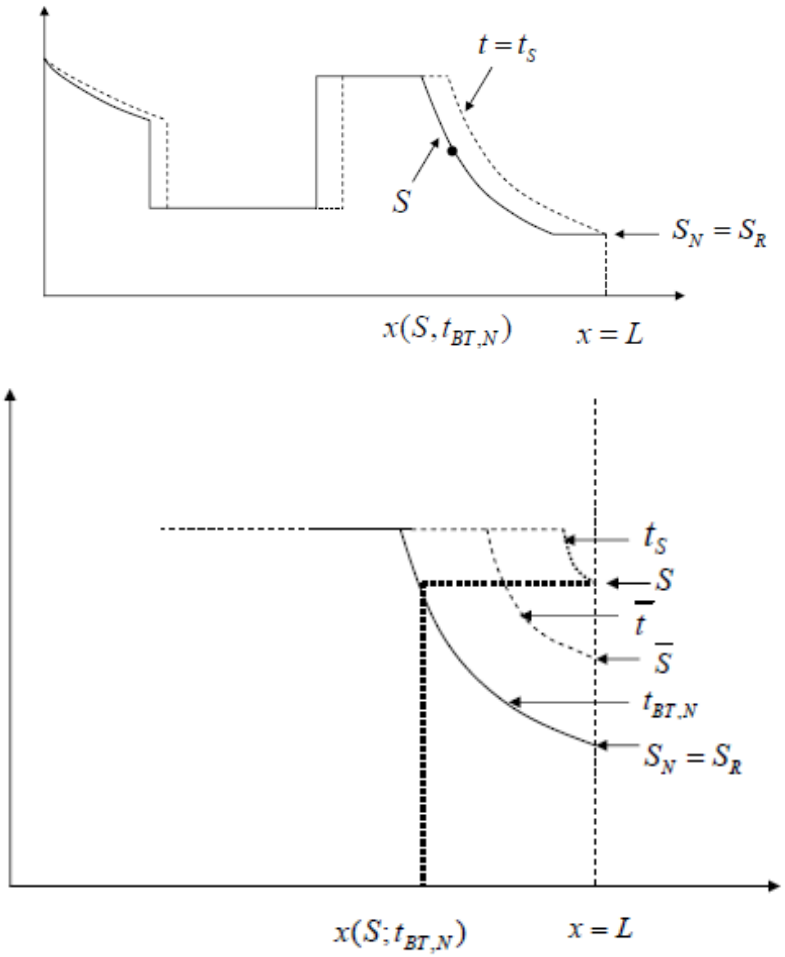

Fig. 3 Example of a Rarefaction Wave at Breakthrough

Let $\hat{t}$ be a time between $t_{BT,N}$ and t_S, and let $\hat{S}$ be the value of S at $x = L$ at $t = \hat{t}$. Assuming we know $u_T(t)\,; t \le \hat{t}$, then

$$x(S;\hat{t}) = \frac{v_N(S)}{\phi}\Psi(\hat{t}) \tag{3.19}$$

and

$$\Delta p = u_T(\hat{t})\left[\sum_{i=1}^{N}\frac{y_i - x_{i-1}}{\lambda_T(S_{i-1})} + \frac{\Psi(\hat{t})}{\phi}\sum_{i=1}^{N-1} I_i + \frac{\Psi(\hat{t})}{\phi}\int_{S_{N-1}}^{\hat{S}}\frac{v_N'(s)ds}{\lambda_T(s)}\right], \tag{3.20}$$

giving

$$u_T(\hat{t}) = \frac{\Delta p}{\sum_{i=1}^{N}\frac{y_i - x_{i-1}}{\lambda_T(S_{i-1})} + \frac{x(S,\hat{t})}{v_N(S)}\left[\sum_{i=1}^{N-1} I_i + \int_{S_{N-1}}^{\hat{S}}\frac{v_{N-1}'(s)ds}{\lambda_T(s)}\right]} \tag{3.21}$$

or

$$u_T(\hat{t}) = \frac{\Delta p}{x(S,\hat{t})\left\{\sum_{i=1}^{N} r_i + \frac{1}{\nu_N(S)}\left[\sum_{i=1}^{N-1} I_i + \int_{S_{N-1}}^{\hat{S}} \frac{\nu_N'(s)ds}{\lambda_T(s)}\right]\right\}} \tag{3.22}$$

where r_i is given by equation (3.9). We also have

$$\frac{dx\left(\hat{S},\hat{t}\right)}{dt} = u_T\left(\hat{t}\right)\frac{v_N\left(S\right)}{\phi}. \tag{3.23}$$

Combining equation (3.22) with equation (3.23), we get

$$x(S,\hat{t})\frac{dx}{dt} = \frac{\Delta p \nu_N(S)}{\phi\left\{\sum_{i=1}^{N} r_i + \frac{1}{\nu_N(S)}\left[\sum_{i=1}^{N-1} I_i + \int_{S_{N-1}}^{\hat{S}} \frac{\nu_N'(s)ds}{\lambda_T(s)}\right]\right\}} \tag{3.24}$$

which, when integrated between $t_{BT,N}$ and $\hat{t}$ letting $\hat{t} \to t_s$ can be written as

$$\phi\left[x(S,t_{BT,N})^2 - L^2\right] = \frac{2\Delta p \nu_N(S)^2\left[t_S - t_{BT,N}\right]}{\sum_{i=1}^{N} r_i \cdot \nu_N(S) + \sum_{i=1}^{N-1} I_i + \int_{S_{N-1}}^{\hat{S}} \frac{\nu_N'(s)ds}{\lambda_T(s)}}. \tag{3.25}$$

Here, $t_{BT,N}$ is known from equation (3.17) and

$$x(S,t_{BT,N}) = \frac{\nu_N(S)}{\phi}\Psi(t_{BT,N}). \tag{3.26}$$

Hence, t_S can be calculated from

$$t_S = t_{BT,N} + \frac{\phi\left[x(S,t_{BT,N})^2 - L^2\right]}{2\Delta p \nu_N(S)^2}\left\{\sum_{i=1}^{N} r_i \cdot \nu_N(S) + \sum_{i=1}^{N-1} I_i + \int_{S_{N-1}}^{S} \frac{\nu_N'(s)ds}{\lambda_T(s)}\right\}. \tag{3.27}$$

The corresponding value for $u_T(t_S)$ is given by

$$u_T(t_S) = \frac{\phi[x(S,t_{BT,N})^2 - L^2]}{2L\nu_N(S)(t_S - t_{BT,N})} \tag{3.28}$$

for $t_S > t_{BT,N}$. For $t = t_{BT,N}$ it is easy to see that u_T in equation (3.28) approaches the value of u_T given by equation (3.10), i.e. u_T is continuous , however, not differentiable at $t = t_{BT,N}$.

The procedure then can be summarized as follows: We can calculate the time t_S when S breaks through at $x = L$ from equation (3.27) for any S on the rarefaction

wave ν_N. Once this time is known, the corresponding value of $u_T(t_S)$ is given by equation (3.28).

3.3. The Case $t > t_{BT,N-1}$

When the entire leading wave ν_N has passed $x = L$, as described in sections 3.1 and 3.2, the procedure can be repeated by removing ν_N from the wave train and starting over again with $S_R = S_{N-1}$. The computational procedure is, therefore, complete for the case when Δp is fixed.

The special case when u_T is constant in both x and t (as in the classical fractional flow theory) can be treated by using

$$x_N = \frac{u_T}{\phi} \nu_N(S_R) t \tag{3.29}$$

in equation (3.11), i.e.

$$\Delta p(t) = u_T[A^* t + B]\,;\; A^* = A\frac{u_T}{\phi}\nu_N(S_R)\,. \tag{3.30}$$

Equation (3.30), of course, reduces to

$$u_T = \lambda_T \frac{\Delta p(0)}{L}\,. \tag{3.31}$$

The procedure for calculating $\Delta p(t)$ for the other cases is straightforward.

3.4. Generalisation

The above derivation for a fixed Δp can easily be generalized to the situation where $\Delta p(t)$ is given as a function of time. Denoting

$$D(t) = \int_0^t \Delta p(\tau) d\tau\,, \tag{3.32}$$

it is easily seen that (as in section 3.2), we get

$$x_N(t) = \frac{-B + \sqrt{B^2 + 4ACD(t)}}{A} \tag{3.33}$$

and

$$u_T(t) = \frac{\Delta p(t)}{Ax_N(t) + B} \tag{3.34}$$

The time to break through of $v_N(S_R)$ is then found from

$$D(t_{BT,N}) = \frac{AL^2 + 2BL}{C} \tag{3.35}$$

and similarly for other cases.

4. Constant Pressure Boundary Case Studies

Two case studies are developed in this section illustrating the use and effectiveness of the generalized constant pressure fixed boundary Reimann problem. The first illustration is a simple waterflooding case where in a) the viscosity of the water is greater than that of oil, with $\mu_o/\mu_w = 0.2$ and in b) the oil viscosity is greater than the water viscosity with $\mu_o/\mu_w = 20$. The second case is a polymer flooding case where the viscosity of the water phase in linearly dependent on the concentration of polymer added. The parameters used in the case studies are outlined in the following table. The core is one meter long with 18% porosity and a permeability of one Darcy. There is a 500 psi pressure drop across the core that is initially 25% water saturation as connate water and 75% oil saturation. The displacing water saturates to 70% leaving 30% residual oil saturation. We use normalized saturations, i.e.

$$S = \frac{S_w - S_{wc}}{1 - S_{or} - S_{wc}}. \tag{4.1}$$

Table 1 Parameters used in the Constant Pressure Boundary Cases

Parameter	Waterflooding		Polymer Flooding
	Case 1a $\mu_w >> \mu_o$	Case 1b $\mu_w << \mu_o$	Case 2 $\mu_w^o = 1$
μ_w (cP)	10	1	$\mu_w(c) = \mu_w^o + 200c$
μ_o (cP)	2	20	8
μ_o/μ_w	0.2	20	
ϕ	0.18		
L (m)	1		
P_{in}	2.1×10^7 Pa (3000 psi)		
P_{wf}	1.7×10^7 Pa (2500 psi)		
S_{or}	0.30		
S_{wc}	0.25		
K (m^2)	1×10^{-12}		
k_{ro}	$k_{ro} = 0.8\left(\frac{1-S_w-S_{or}}{1-S_{wc}-S_{or}}\right)^2 = a_o(1-S)^2$		
k_{rw}	$k_{rw} = 0.2\left(\frac{S_w-S_{wc}}{1-S_{wc}-S_{or}}\right)^2 = a_w S^2$		

4.1. Waterflooding

The Riemann problem for waterflooding is defined as follows for the simple system illustrated in Fig. 1 where either in case 1a) a more viscous water displaces a less viscous oil or in case 1b) a less viscous water displaces a more viscous oil. The viscosity ratio of oil to water varies 100x between the two cases.

The Riemann problem is

$$\frac{\partial S}{\partial t} + \frac{\mu_T}{\phi}\frac{\partial f(s)}{\partial x} = 0 \tag{4.2}$$

$$S^L = 1 - S_{or} = 0.7 \tag{4.3}$$

$$S^R = S_{wc} = 0.25 \tag{4.4}$$

The fractional flow of a phase is defined from the mobility of the phase (λ) with respect to the total mobility as:

$$f(s) = \frac{\lambda_w}{\lambda_o + \lambda_w} \tag{4.5}$$

$$\lambda = \frac{Kk_r}{\mu} \tag{4.6}$$

We use the illustration in Fig. 4 to depict two waves (N=2)

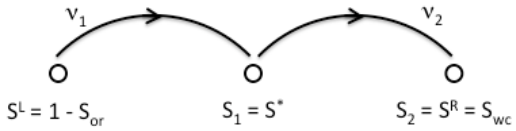

Fig. 4 Depiction of a two wave Reimann problem

The rarefaction wave is denoted by ν_1 and the shock wave, ν_2. The propagation velocities are denoted V_1 and V_2 for the rarefaction and shock waves, respectively.

Table 2 Wave Descriptions

Wave			Propagation Velocity	
Rarefaction	$\nu_1 = f'(S)$	(4.7)	$V_1 = \frac{\mu_T}{\phi}\nu_1$	(4.8)
Shock	$\nu_2 = \frac{f(S^*) - f(S^R)}{S^* - S^R}$	(4.9)	$V_2 = \frac{\mu_T}{\phi}\nu_2$	(4.10)

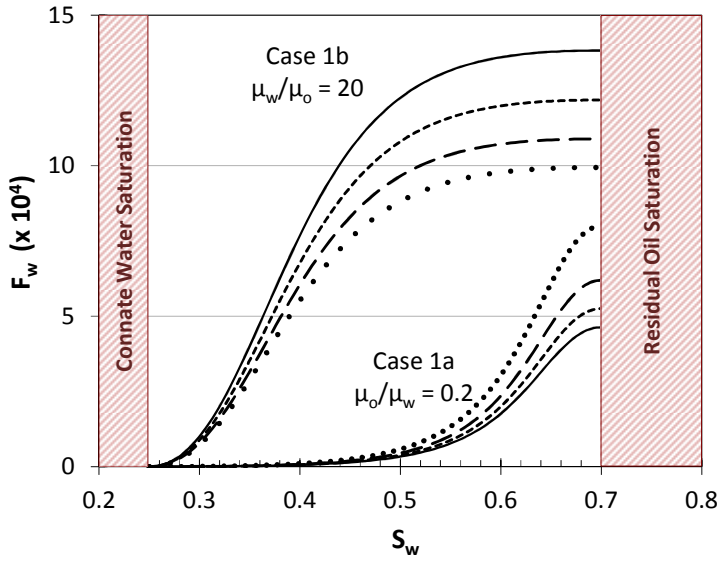

Fig. 5 Fractional Flow Functions for the Waterflooding Cases 1a) $\mu_o/\mu_w = 0.2$ and 1b) $\mu_o/\mu_w = 20$ at Breakthrough Times 0.3 (·····), 0.5 (— —), 0.7 (- - - - -), and 0.9 (——)

Using the data given above, we get:

$$I_1 = \int_{S_o}^{S^*} \frac{f'(S)}{\lambda_T(S)} dS = 1.1763x10^{11} \tag{4.11}$$

$$I_2 = 0 \tag{4.12}$$

$$r_1 + r_2 = \frac{\beta_1 - \alpha_o}{\lambda_T(S_o)} + \frac{\beta_1 - \alpha_1}{\lambda_T(S_1)} = \frac{\nu_1(S_o)}{\lambda_T(S_o)} + \frac{\nu_2 - \nu_2}{\lambda_T(S_o)} = 0 \tag{4.13}$$

$$C = \frac{2\Delta p}{\phi}\nu_2 \quad ; \quad \Delta p = 500\ psi \tag{4.14}$$

$$B = \frac{L}{\lambda_T(S_R)} \tag{4.15}$$

$$A = \frac{1}{\nu_2} I_1 - \frac{1}{\lambda_T(S_R)} \tag{4.16}$$

The corresponding water saturation profiles are shown in Figure 6. The high water saturation for case 1a is physically realistic where a much lower mobility ratio (represented by μ_o/μ_w) will result in better sweep efficiency, i.e. higher water saturation behind the flood front.

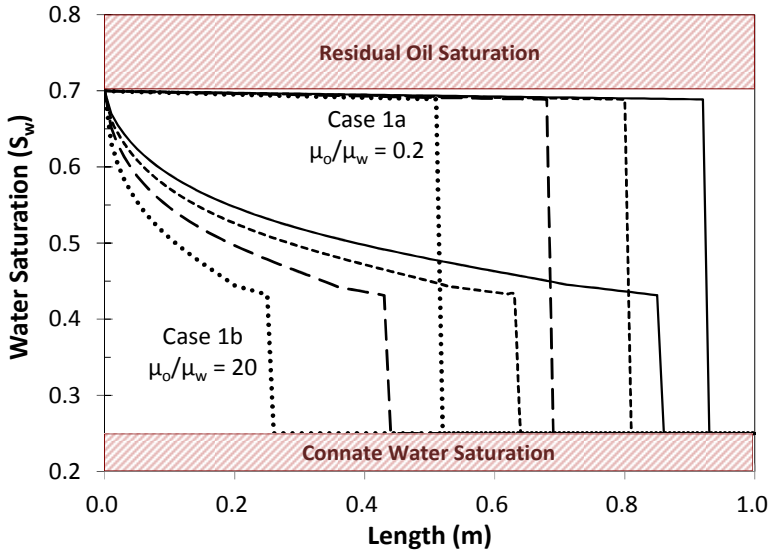

Fig. 6 Saturation Profiles for the Waterflooding Cases 1a) $\mu_o/\mu_w = 0.2$ and 1b) $\mu_o/\mu_w = 20$ at Breakthrough Times 0.3 (·····), 0.5 (— —), 0.7 (- - - - -), and 0.9 (——)

Likewise, the time to breakthrough can be determined from equation (3.35). The time for water to breakthrough in the mobility controlled case 1a, is 523 s whereas it is only 228 s for the mobility unstable case 1b where the water (displacing) viscosity is much less than the oil viscosity (displaced).

First, calculate the integral numerically using $u_T(t)$ before breakthrough, using eqtn. (3.2). The time after breakthrough and the volumetric flux or total velocity can be then calculated from the following equations:

$$t_{si} = t_{BT} + \frac{\phi\left[L^2 - x\left(S_i, t_{BT}\right)^2\right]}{2\Delta p v_2^2} \int_{s^*}^{s_i} \frac{f'(S)dS}{\lambda_T(S)} \tag{4.17}$$

$$u_T(t_{si}) = \left[t_{si} - t_{BT}\right] = \frac{\phi\left[L^2 - x\left(s_i, t_{BT}\right)^2\right]}{2\Delta f'(s_i)} \tag{4.18}$$

The total velocity profiles are shown for both waterflooding cases in Fig. 7 (the following explanation also makes reference to the water saturation profiles depicted in Fig. 6). The total velocity decreases non-linearly for case 1a as expected due to the increasing high viscosity water saturation. After breakthrough, the total velocity is almost constant owing to the uniform 70% water saturation. The opposite is observed for case 1b where the much lower viscosity displacing water saturates less pore volume at breakthrough. As the low viscosity water saturation does continue to increase after breakthrough so does the total velocity.

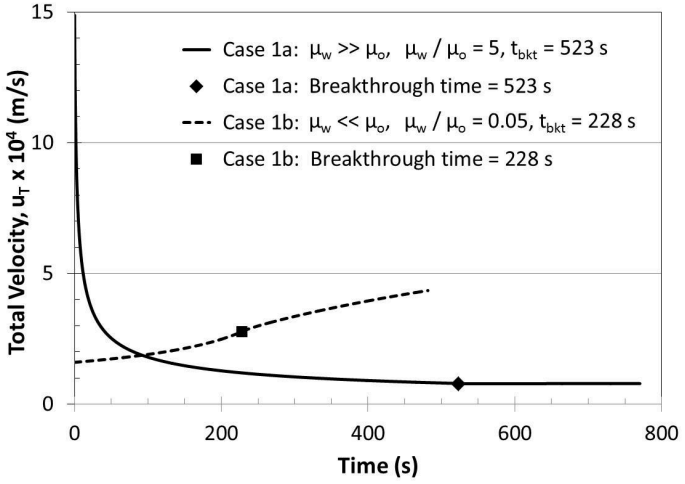

Fig. 7 Total Velocities for Waterflooding Cases 1a) $\mu_o/\mu_w = 0.2$ (——) & 1b) $\mu_o/\mu_w = 20$ (- - -)

The front velocity, in general, does not advance linearly as a function of time, with the application of constant pressure boundaries. It is calculated using equation (3.34) knowing the front position. Before breakthrough, the front position is calculated using equation (3.19) or more explicitly, as shown in the following equation and is shown in Figure 8 for both waterflooding cases.

$$x(S_i, t_{BT}) = \frac{v_2}{\phi} \int_0^{t_{BT}} u_T(t)dt \tag{4.19}$$

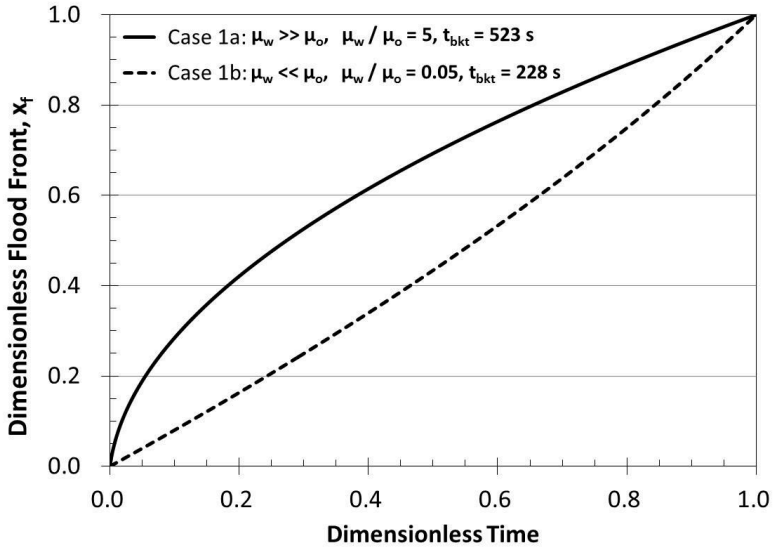

Fig. 8 Position of the Flood Front (Shock Wave) before Breakthrough for Waterflooding Cases 1a) $\mu_o/\mu_w = 0.2$ (——) and 1b) $\mu_o/\mu_w = 20$ (- - - - -)

4.2. Polymer Flooding

The polymer flooding case illustrates the fact that the constant pressure boundary solution works for multi-components, i.e. multiple waves. Physically, polymer may be added to the water to increase its viscosity to overcome an adverse mobility ratio with respect to the more viscous oil. The parameters used for the polymer case are shown in Table 1.

If c is polymer concentration in water, we choose a linear dependence of water solution viscosity on polymer concentration,

$$\mu_w(c) = \mu_w^o + 200c \tag{4.20}$$

which gives,

$$f(S,c)=\frac{S^2}{S^2+\frac{\mu_w}{\mu_o}.\frac{a_o}{a_w}(1-S)^2} \tag{4.21}$$

i.e.,

$$f(S,c)=\frac{S^2}{S^2+(0.5+100c)(1-S)^2} \tag{4.22}$$

For the Riemann problem, we choose:

$$S^L = S_o = 1.0 \quad ; \quad S^R = 0.0$$
$$c^L = 0.01 \quad ; \quad c^R = 0.0$$

An adsorption isotherm of the form shown in equation (4.23), is used to describe the effect of the polymer concentration. The addition of the polymer results in the creation of two shocks and a rarefaction as shown in Fig. 10. This Riemann problem was analysed by Johansen and Winther (1988).

$$a(c)=\frac{0.2c}{1+100c} \tag{4.23}$$

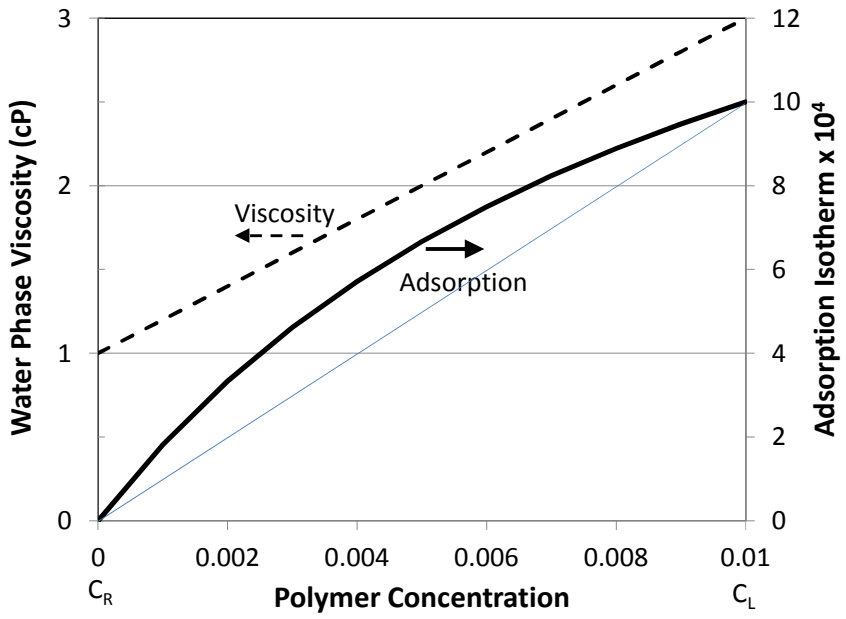

Fig. 9 Water Phase Viscosity (- - -) and Adsorption Isotherm (——) as a Function of Polymer Concentration

Calculated using Newton-Raphson, the constant saturations of the shocks are found to be $S_1 = 0.693$ and $S_2 = 0.514$, and are shown in Figure 10. The fractional flow function is shown

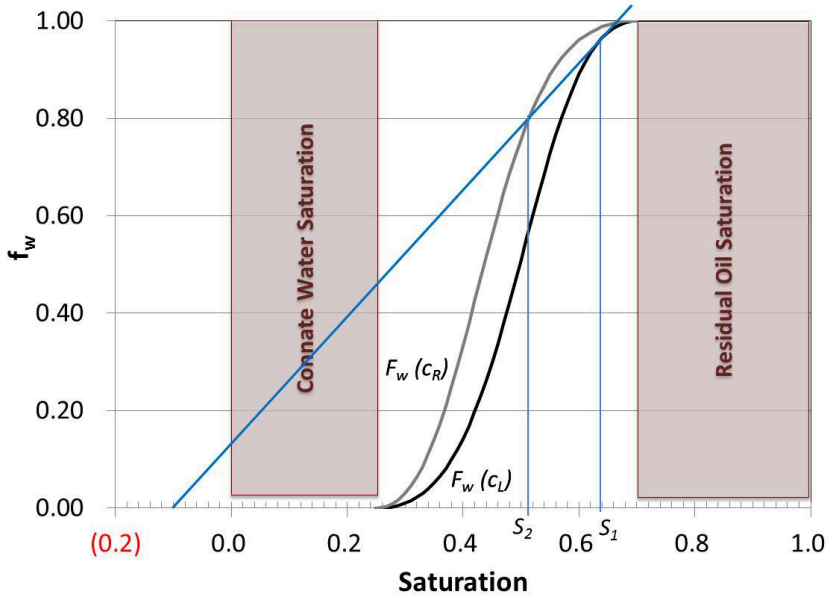

Fig. 10 Fractional Flow Function for the Polymer Case 2

The saturation profiles are shown in Figure 11 showing the two shocks and the rarefaction waves.

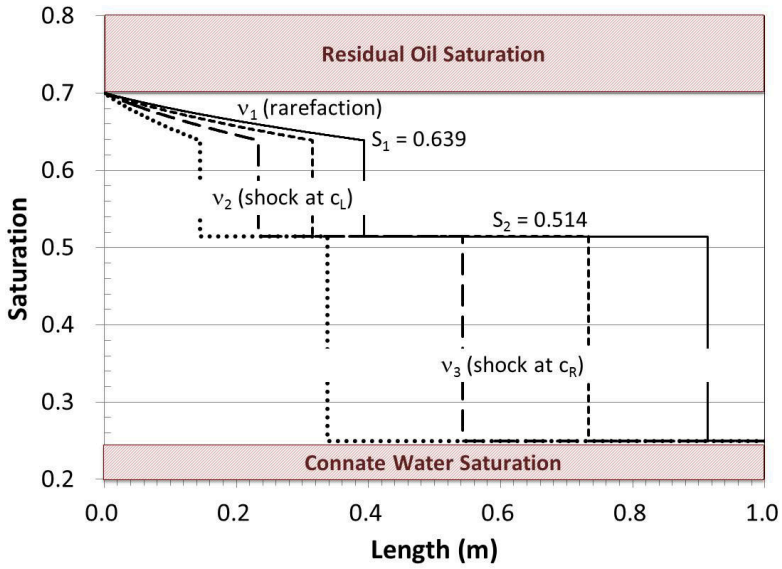

Fig. 11 Saturation Profiles for the Polymer Case 2) at Breakthrough Times 0.3 (·····), 0.5 (— —), 0.7 (– – – –), and 0.9 (——)

The fractional flow functions shown in Figure 12 are functions of the polymer concentration and saturation as shown in equations (4.24) to (4.26).

$$\nu_1 = \frac{df}{dS}(S, c_L) \qquad \text{(rarefaction)} \qquad (4.24)$$

$$\nu_2 = \frac{f(S_1, c_L)}{S_1 + h_{LR}} = 1.01 \qquad \text{(shock)} \qquad (4.25)$$

$$\nu_3 = \frac{f(S_2, c_R)}{S_2} = 1.37 \qquad \text{(shock)} \qquad (4.26)$$

Comparing the right and left fractional flow curves and the slope of the tangents at the point of inflection for the shock waves in Figure 12, we see that the right shock is travelling more quickly than the left shock, i.e. the water-oil shock is advancing through the porous media faster than the increased viscosity polymer water. This is confirmed when compared to the initial higher total flux shown in Figure 13 that decreases as the water-oil interface advances through the porous media. Both, shock wave ν_3 and shock wave ν_2 decelerate as they move through the porous medium (Figure 12) as does the total flux (Figure 13). The total flux profile (in Figure 13) shows that there is a discrete change in shock velocity from shock ν_3 to shock ν_2.

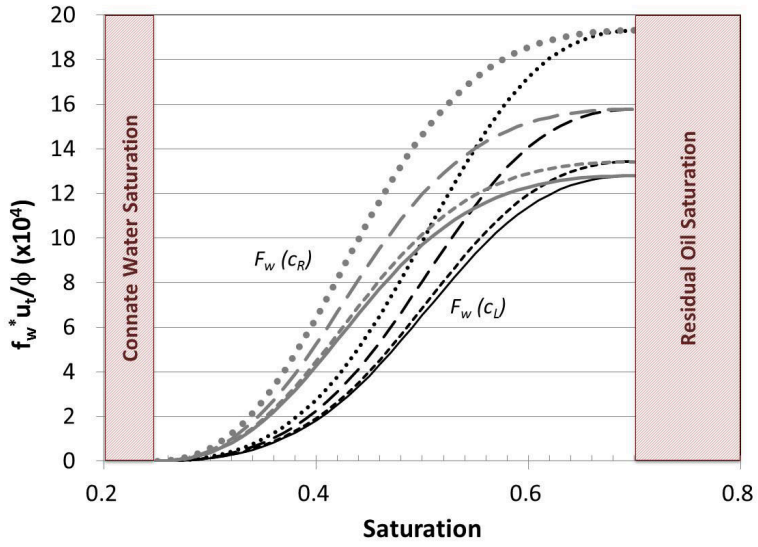

Fig. 12 Fractional Flow Functions for the Polymer Case 2) at Saturation Profiles for the Polymer Case 2) at Breakthrough Times 0.3 (·····), 0.5 (— —), 0.7 (- - - - -), and 0.9 (——) for c_L = 0.01 and c_R = 0

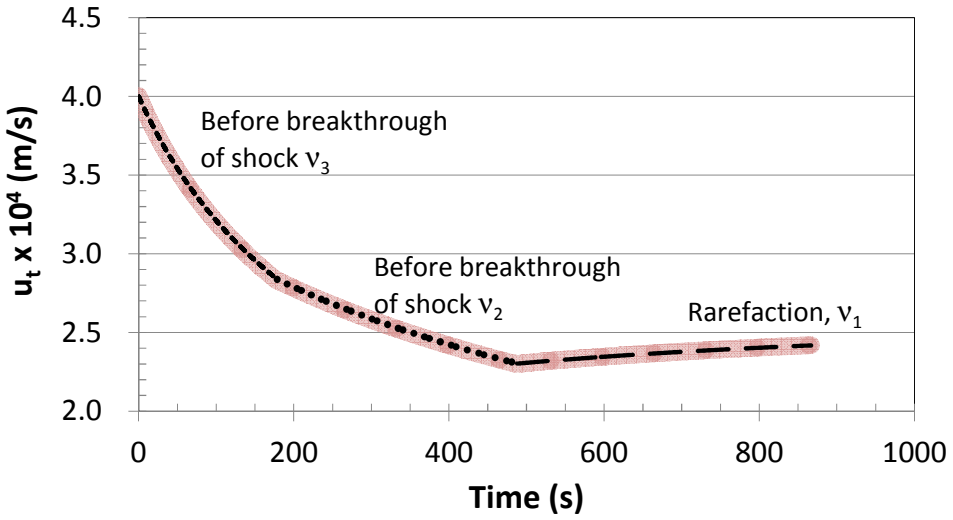

Fig. 13 Total Volumetric Flux: Before ν_3 the Polymer-Oil Shock (- - -); Before ν_2 the Polymer-Water Shock (• • • •); and After ν_2 the Polymer-Water Shock (— —) including the numerical solution ( ) for Case 2

Figure 13 shows the numerical and analytical solutions for the multicomponent system with constant pressure boundaries. The numerical solution matches the analytical solution but the time to run this simple case was 63.1 s compared to 2.9 s for the analytical solution and required 600 grids to match the analytical solution. Having used the IMPES method for the numerical solution, the numerical method needed to calculate the pressure and saturation at every step up to breakthrough unlike the analytical solution which can calculate the time to breakthrough directly.

The integral values are: $I_3 = I_2 = 0$ and $I_1 = 2.27x10^{10}$. The time to breakthrough of shock ν_3 is found to be 179 s and the position of the flood front can be calculated and is shown in Figure 14. One can observe the non-linear curve showing the deceleration of the shock.

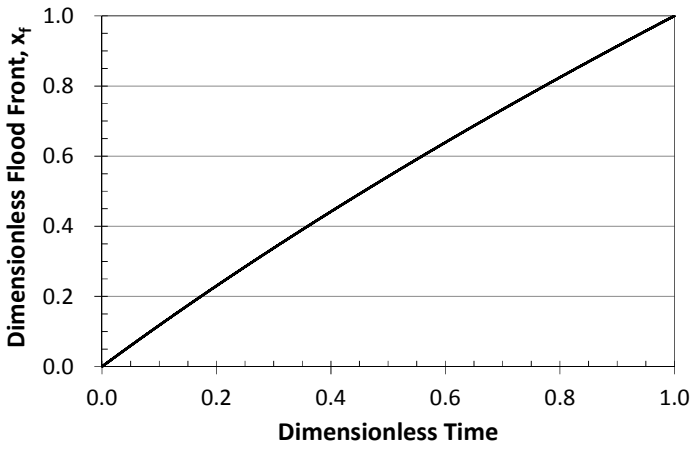

Fig. 14 Position of the Flood Front (Shock Wave ν_3) before Breakthrough for the Polymer Case 2

One can also calculate and plot the pressure profile from injection to production end at any time. Figure 15 shows the pressure profile for 0.3, 0.5 and 0.9 breakthrough times for wave ν_3. As expected, the pressure profile changes at the shock front as it progresses through the porous medium.

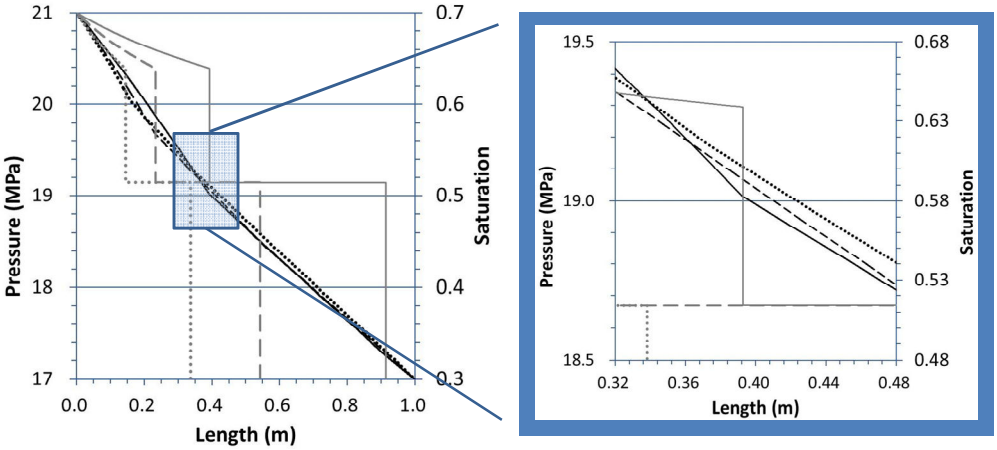

Fig. 15 Pressure Profiles for the Polymer Case 2 (including saturation profiles for reference) at Breakthrough Times 0.3 (·····), 0.5 (— —), and 0.9 (——) Breakthrough Times of wave ν_3

5. Conclusions

The classical Buckley-Leverett fractional flow theory has been extended to constant pressure boundaries with variable flux for multi-component problems. The derivation mathematically describes the explicit behaviour before the first wave breaks through, between waves and post breakthrough of the trailing wave.

Expressions for the position of any wave in the porous media, the overall flux and time for that specific wave to break through are generalised accordingly. The application of the constant pressure boundary solution is illustrated with three examples to fully explore the fact that meaningful results can be obtained for a non-constant flux condition. This is especially significant for describing behaviour under constant injection and well flowing conditions as more often used in industry.

Acknowledgements

We would like to acknowledge the support of NSERC for the financial support. We gratefully appreciate the contributions of Mr. Xiaolong Liu and Ms. Huan Yang.

References

Buckley, S.E., and Leverett, M.C. 1941. Mechanism of Fluid Displacement in Sands, Petrol. Trans. AIME **146**, 107.

Johansen, T. and Winther, R. 1988. The Solution of the Reimann Problem for a Hyperbolic System of Conservation Laws Modelling Polymer Flooding, SIAM Journal of Mathematical Analysis, **19**(3), 451-566.

Welge, H.G. 1952. A Simplified Method for Computing Oil Recovery by Gas or Water Drive, Petrol. Trans AIME **195**, 91.